Strong interactions in the high-energy limit

LLR seminar

Cristian Baldenegro Barrera (c.baldenegro@cern.ch)

December 6, 2021

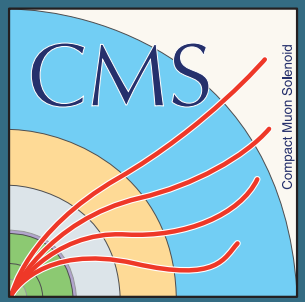

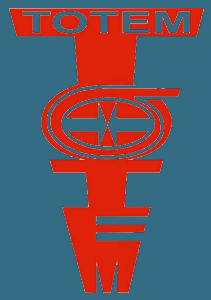

Some background

- B.S. in Physics at Universidad de Sonora in Mexico.

- Ph.D. at the University of Kansas in the U.S.:
  - **Jet measurements with CMS and CMS-TOTEM.**
  - Particle physics phenomenology (physics beyond the standard model in $\gamma\gamma \to X$).

- Postdoc with CMS-LLR heavy-ion group:
  - Jet substructure measurements in pp and PbPb collisions.

Outline

- Quantum chromodynamics.
- The Large Hadron Collider (LHC) and the Compact Muon Solenoid (CMS) detector.
- Jets and perturbation theory.
- High-energy limit of strong interactions (a.k.a. small-x physics).
- Some standard probes of small-x physics.
- Measurement of hard color-singlet exchange dijets at $\sqrt{s} = 13$ TeV with CMS and TOTEM.
- Summary.

Quantum chromodynamics (QCD): the quantum theory of strong interactions

Quarks and gluons (partons), carry color charge (red, green, blue) and are thus sensitive to the strong interaction.

Two key characteristics of QCD:

- **Color confinement:** Only color-neutral particles made of quark & gluons (hadrons), are observed in isolation.
- **Asymptotic freedom:** The interaction strength decreases at short distances (high energies)

QCD is central to modern colliders

...and QCD is what we are made of

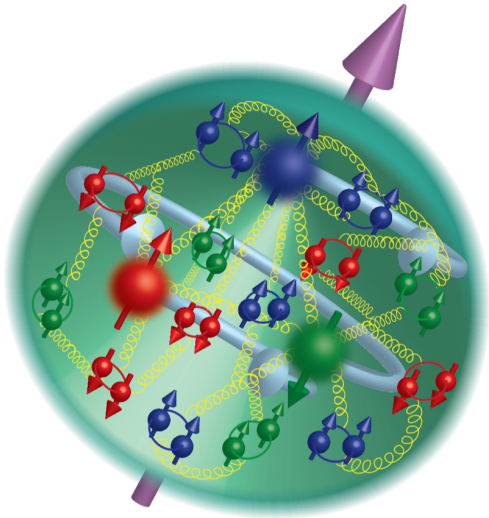

$\approx$ 98% of the mass of the proton comes from QCD binding energy.

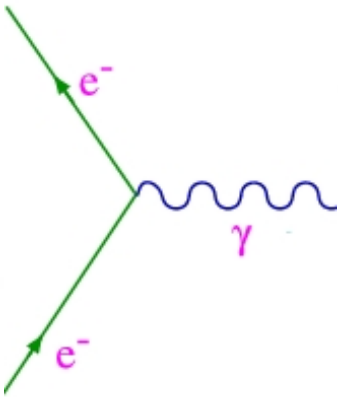

Quantum electrodynamics (QED)

- Electrically charged particles interact via exchange of photons.
- Single interaction vertex (abelian **U(1)** gauge symmetry)

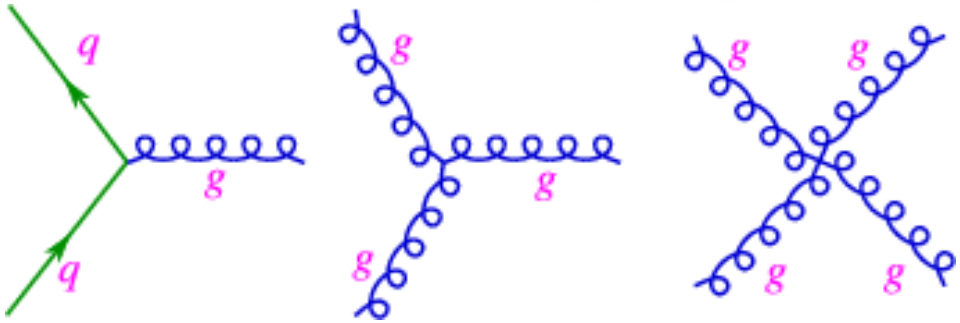

QCD

- Color-charged particles interact via exchange of gluons.
- **Key difference with QED:** self-interacting gauge bosons (gluons) → Makes QCD special!!!
  ...*Consequence of non-abelian* ***SU(3)*** *gauge symmetry of QCD*

A strong coupling, α_s, that gets smaller with shorter distances (higher energies),

$$\alpha_s \propto \frac{1}{\ln(Q^2/\Lambda^2_{QCD})}$$

Theory becomes strongly coupled at $\Lambda_{QCD} \approx 200$ MeV (partons $\rightarrow$ hadrons)

α_s plays a similar role as $\alpha_{em} = e^2/4\pi\epsilon_0 \approx 1/137$ of QED.

Nobel Prize in Physics in 2004 to D. Gross, D. Politzer, F. Wilczek for the discovery of asymptotic freedom.

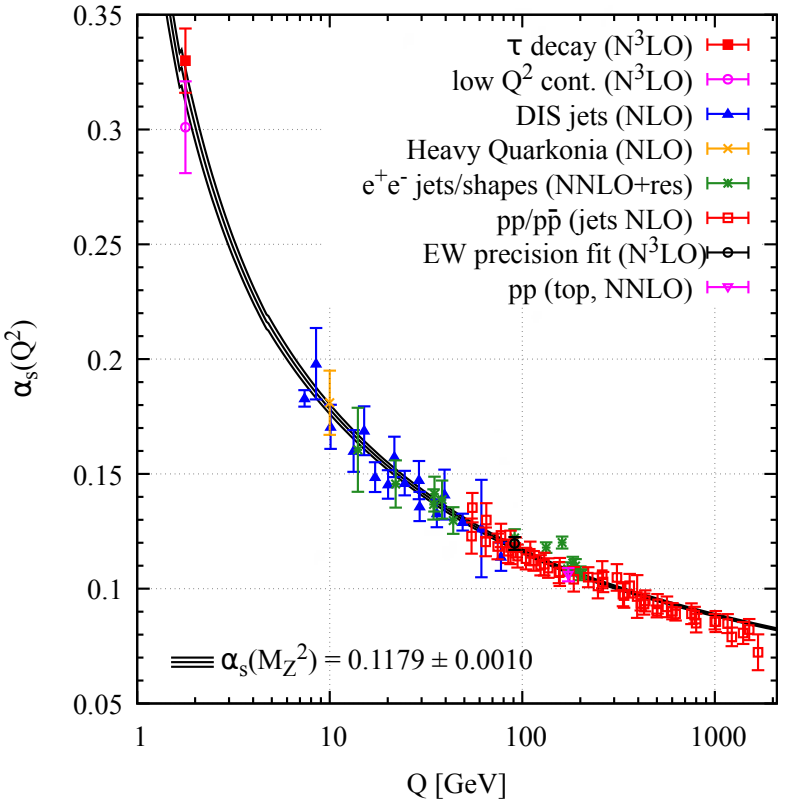

Particle Data Group, Phys. Rev. D 98, 030001 (2018)

Plenty of open problems and questions in QCD

- How are hadrons formed starting from the fundamental degrees of freedom of QCD? How is the "glue" distributed in the proton/nucleus?
- What are the properties of the quark-gluon plasma?
- Do glueballs exist? If so, what are their properties?
- **What is the combined effect of multiple gluon branchings in high energy partonic interactions?**

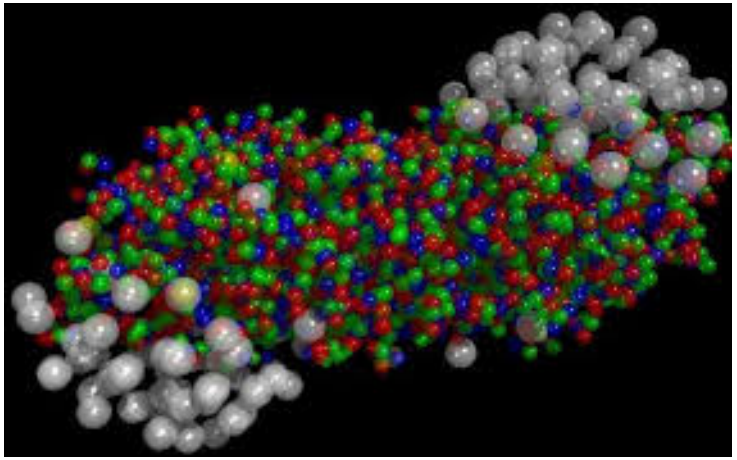

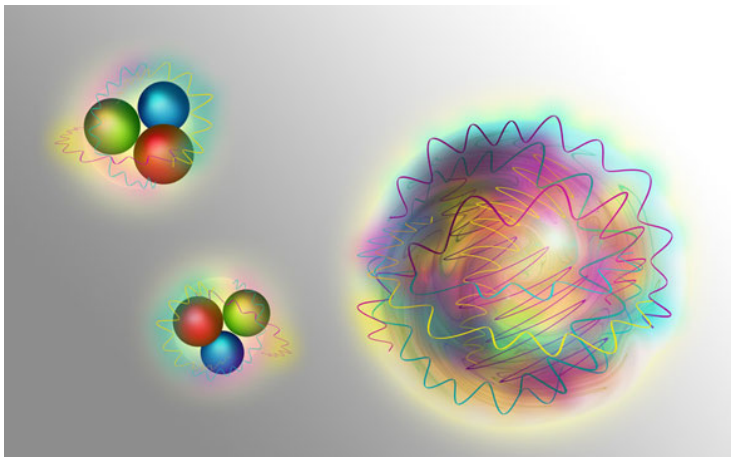

The Large Hadron Collider (LHC)

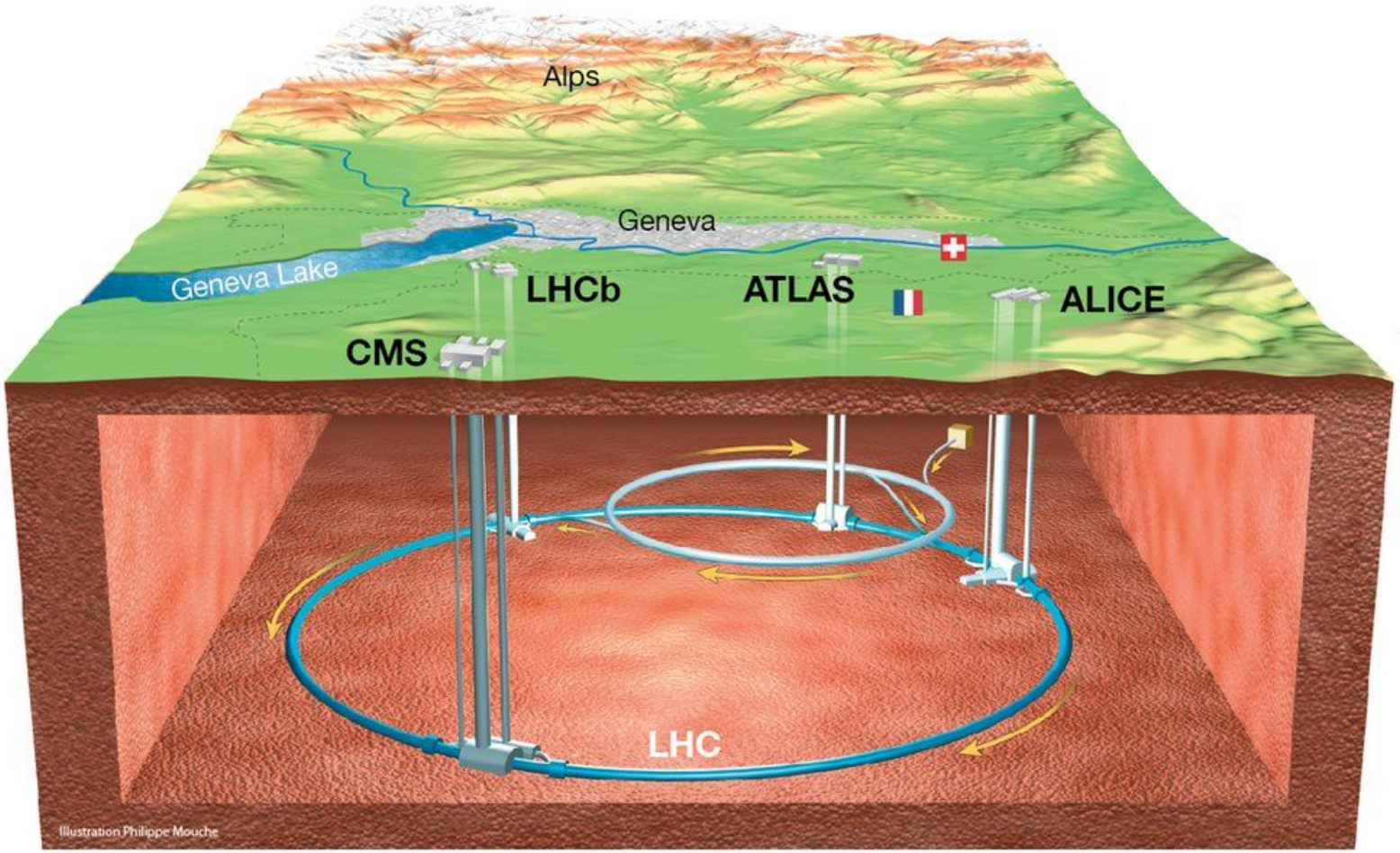

27 km two-ring accelerator ∼100 m underground underneath the border between Switzerland and France.

Protons accelerated at 99.999999% the speed-of-light.

The Compact Muon Solenoid (CMS) experiment

- General purpose particle detector installed at the interaction point 5 at the LHC.
- Several subdetector components dedicated to measure **most of the decay debris in a $\approx 4\pi$ solid angle region of high-energy proton-proton collisions**.

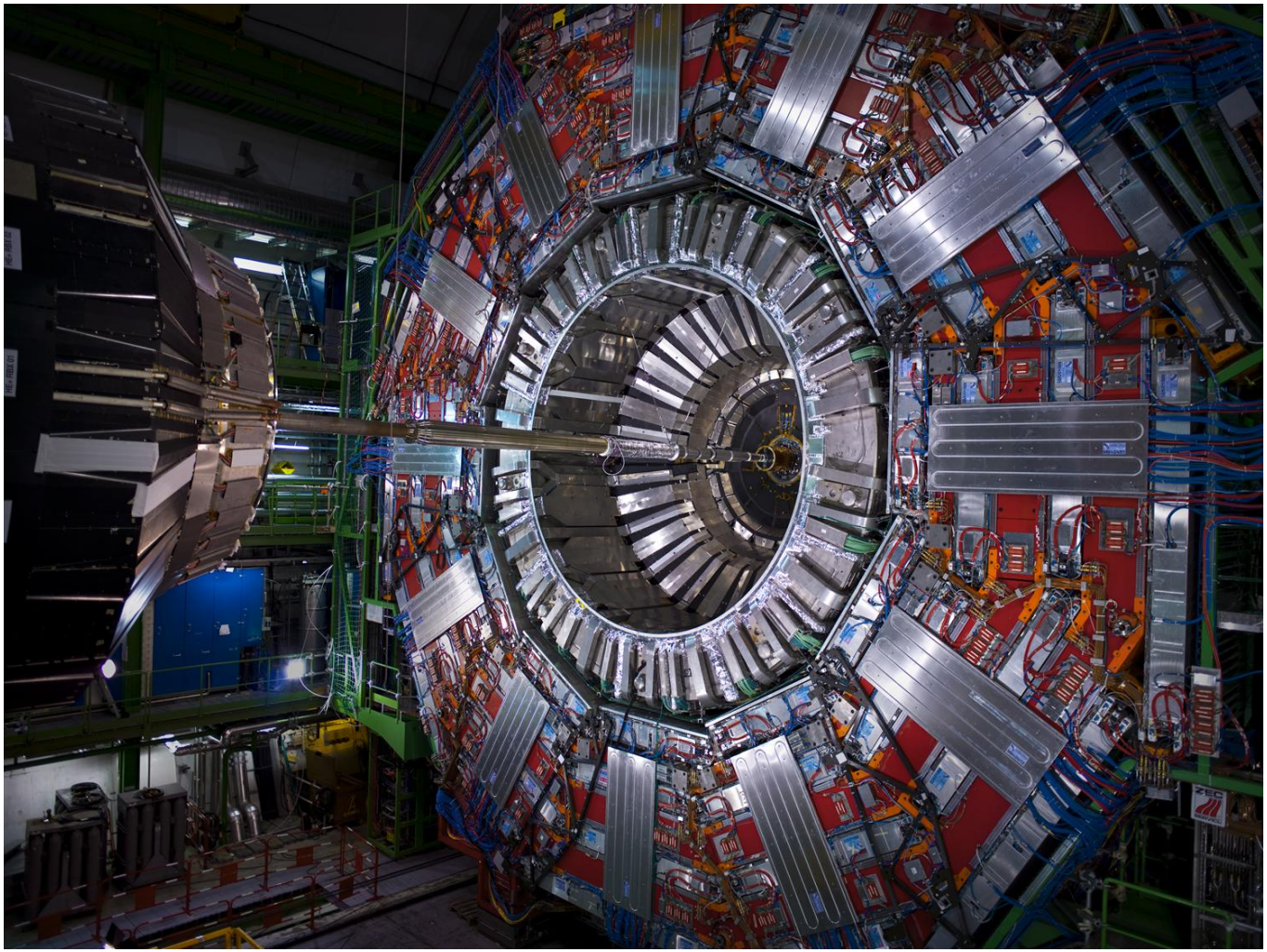

The collimated sprays of particles produced in proton-proton collision are known as "jets."

Jets are used as proxies of the struck quarks and gluons. $\rightarrow$ Consequence of parton shower and hadronization.

Cluster reconstructed particles with sequential algorithms to map $\{p_{i,particles}\} \rightarrow \{p_{i,jets}\}$.

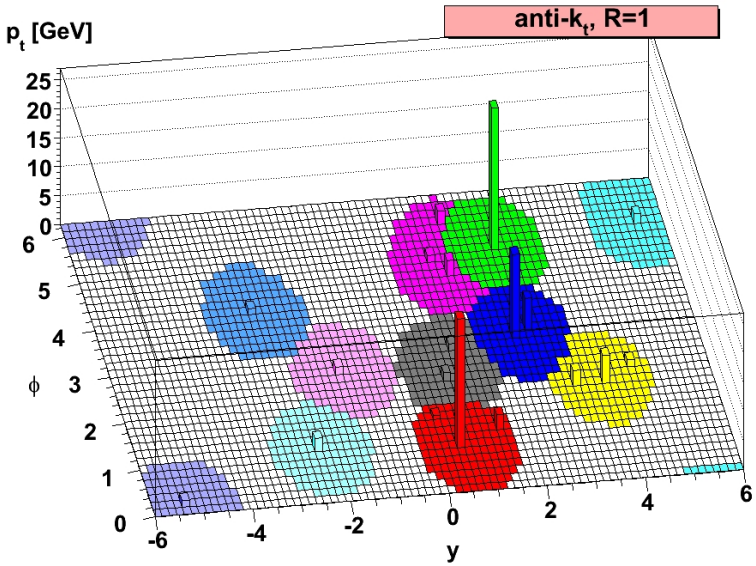

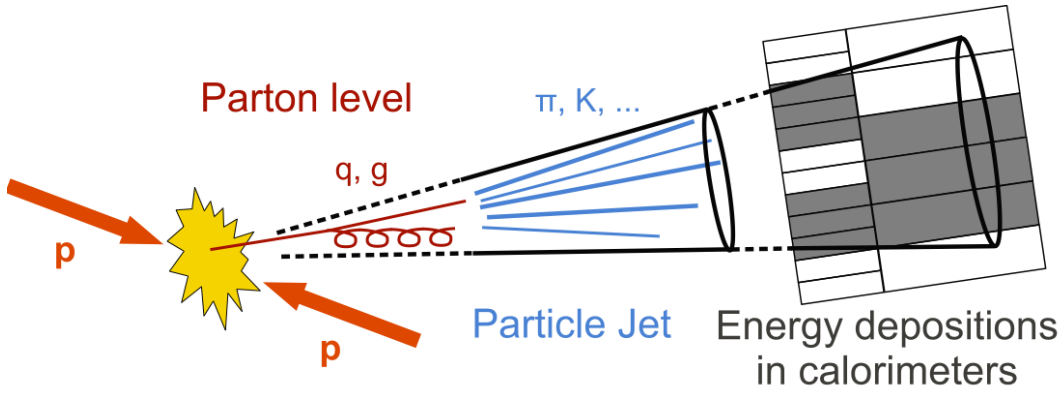

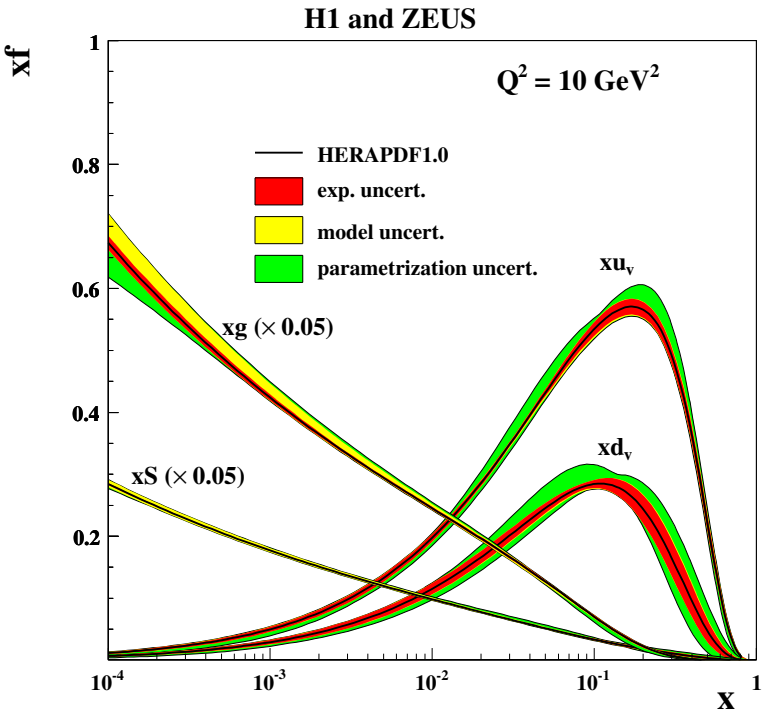

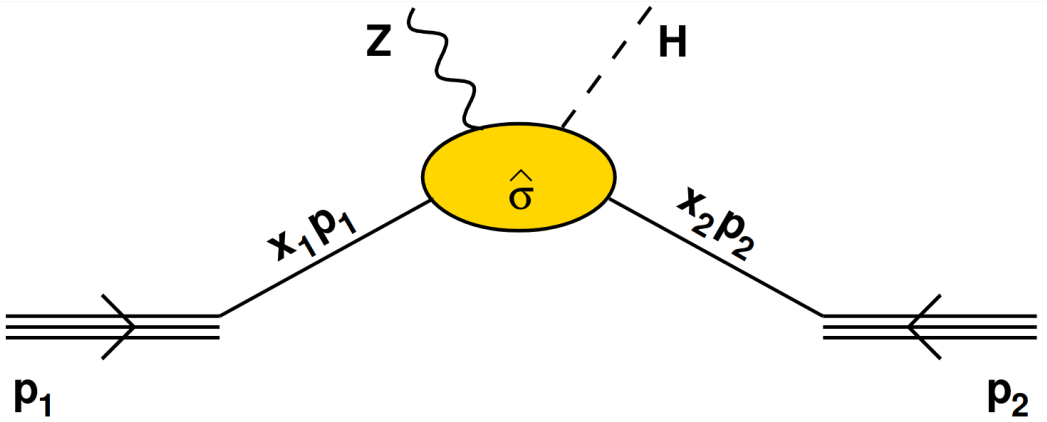

The "hadronic cross section" σ is factorized into a "hard" part $\hat{\sigma}(x_1, x_2, \mu_F^2, \mu_R^2)$ and normalization given by non-perturbative, process-independent parton distribution functions (PDFs), $f_{i/p}$, $f_{j/p}$:

$$\sigma = \sum_{i,j} \int dx_1 f_i(x_1, \mu_F^2) \int dx_2 f_j(x_2, \mu_F^2) \times \hat{\sigma}(x_1, x_2, \mu_F^2, \mu_R^2) + \mathcal{O}(\Lambda_{QCD}^2/Q^2)$$

$\hat{\sigma}(x_1, x_2, \mu_F^2, \mu_R^2)$ is calculated with pQCD techniques.

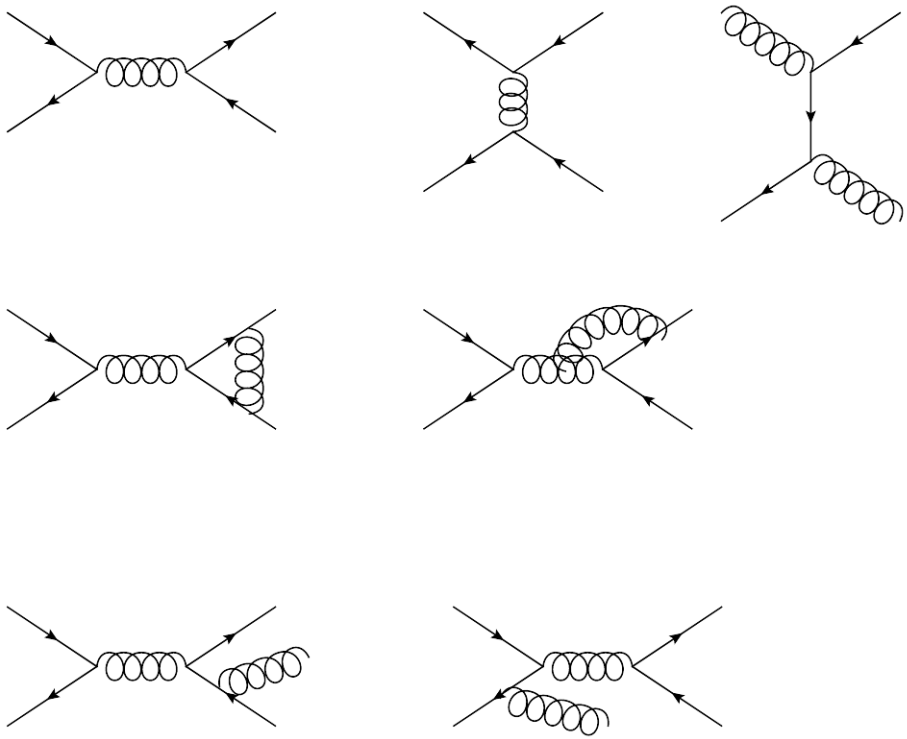

In fixed-order pQCD, we calculate the hard cross sections in powers of $\alpha_s \ll 1$, *symbolically* (ignoring pre-factors) represented by

$$\mathrm{d}\hat{\sigma} \sim \alpha_s^2 + \alpha_s^3 + \alpha_s^4 + \ldots$$

calculations are known at leading order (LO), next-to-LO (NLO), next-to-NLO ($\mathrm{N^2LO}$), and in very few cases for next-to-NNLO ($\mathrm{N^3LO}$).

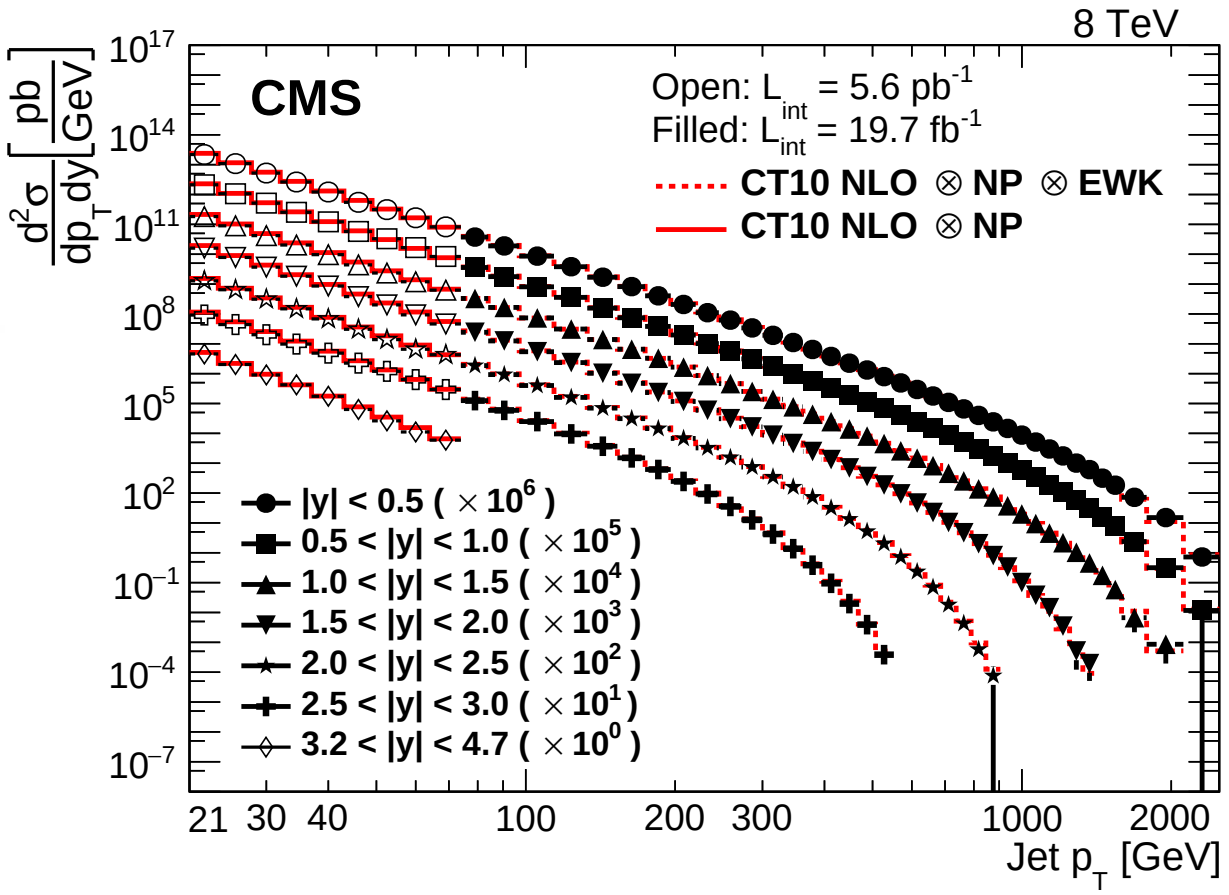

CMS, JHEP 03 (2017) 156, arXiv:1609.05331

pQCD has been rigorously tested in inclusive jet cross section measurements at HERA (ep), the Tevatron ($p\bar{p}$), and the LHC (pp).

Fixed-order pQCD, supplemented with parton shower and non-perturbative QCD effects, is successful at describing data.

Regime of interest: $\hat{s} \gg |\hat{t}| \gg \Lambda^2_{\rm QCD}$, where $\hat{s}$ is the center-of-mass energy squared, $\hat{t}$ is the four-momentum transfer squared.

$\rightarrow$ **Fixed-order pQCD approach breaks down**.

The perturbative expansion should be rearranged (ignoring pre-factors),

$$\mathrm{d}\hat{\sigma} \sim \alpha_s^2 \sum_{n=0}^{\infty} \alpha_s^n \ln^n\left(\frac{\hat{s}}{|\hat{t}|}\right) + \alpha_s^3 \sum_{n=0}^{\infty} \alpha_s^n \ln^n\left(\frac{\hat{s}}{|\hat{t}|}\right) + \alpha_s^4 \sum_{n=0}^{\infty} \alpha_s^n \ln^n\left(\frac{\hat{s}}{|\hat{t}|}\right) + \ldots$$

where $\alpha_s^n \ln^n\left(\hat{s}/|\hat{t}|\right) \lesssim 1$.

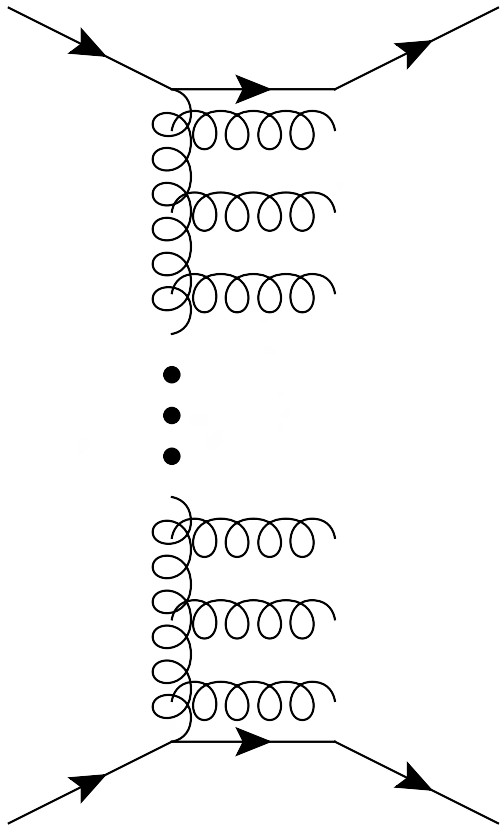

Resummation of large logarithms of $\hat{s}$ to all orders in α_s is done via **Balitsky-Fadin-Kuraev-Lipatov (BFKL)** equation of pQCD.

Very important test of QCD; challenging to isolate experimentally

Onset of BFKL dynamics at large rapidity differences, $\Delta y = \ln(\hat{s}/|\hat{t}|)$.
A notable prediction in BFKL:

$$\hat{\sigma} \propto \hat{s}^{2\lambda}, \qquad 2\lambda = \frac{N_c}{\pi} 8 \ln 2 \alpha_s \approx 0.5 \text{ at leading log}$$

Why is the high energy limit important?

- **Important test of quantum field theory**. Relevant for QCD in particular, and for **Yang-Mills theories in general**.
- **Cosmic ray physics:** cosmic ray interactions with the atmosphere can occur at the multi-TeV scale and beyond. **The strong force dominates.**
- **Gluon saturation effects:** need to understand gluon densities in proton and heavy-ion collisions as a function of x. **An important topic of discussion at the future Electron Ion Collider.**

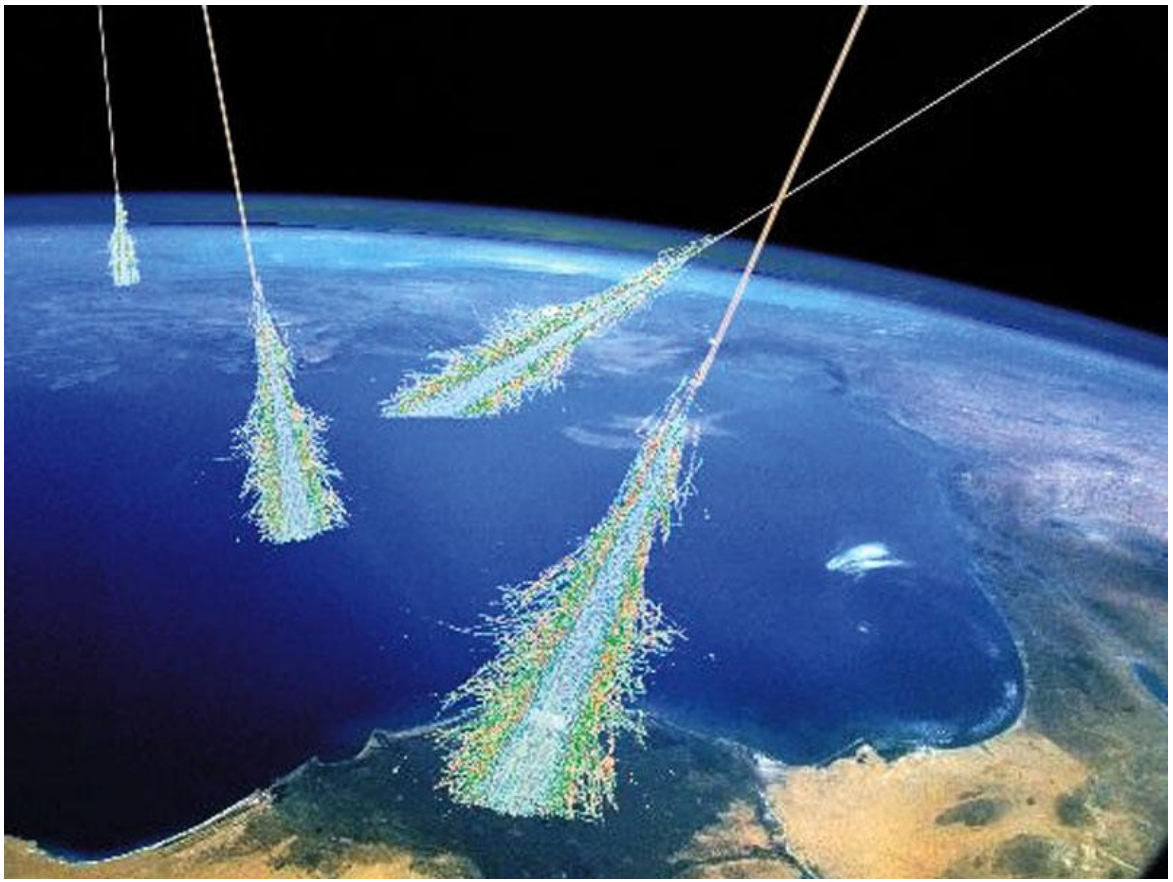

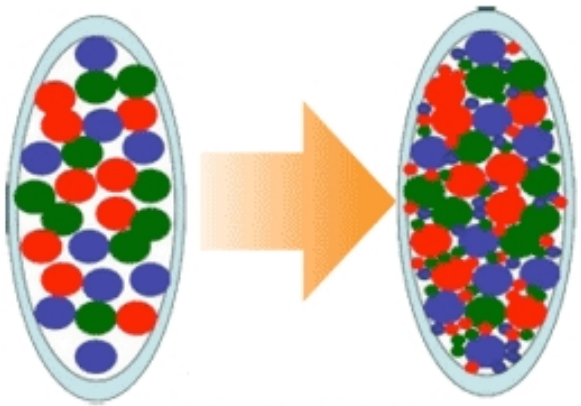

PDF evolution in x and Q^2

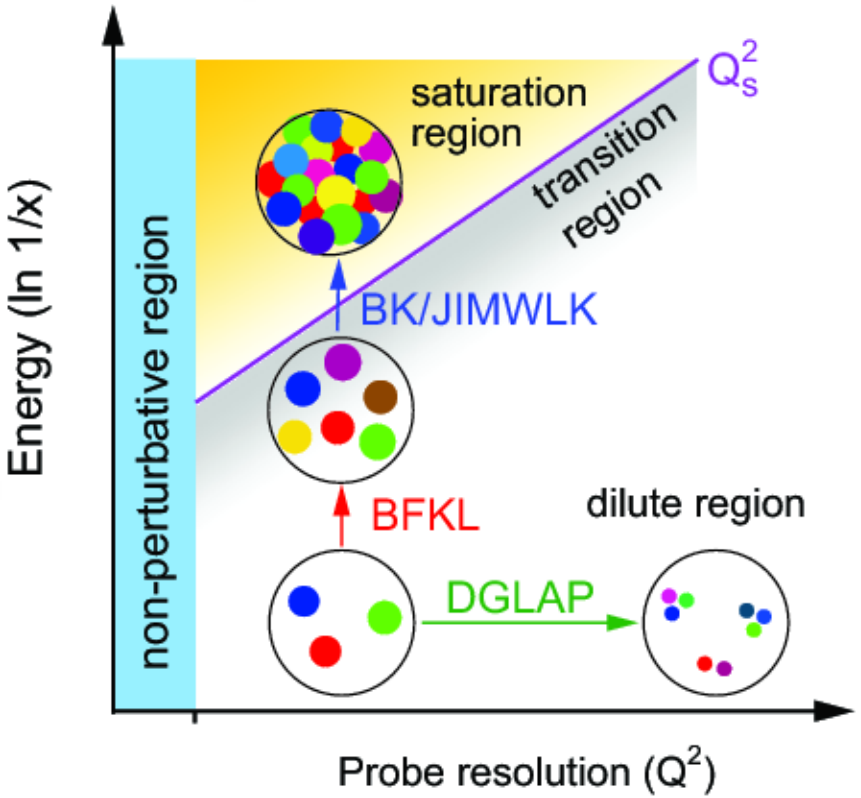

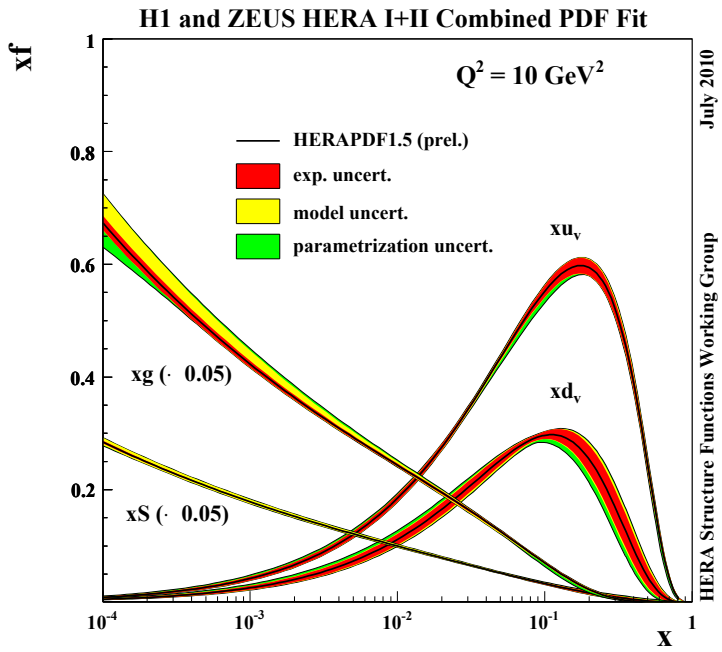

Due to universality of QCD interactions,

high-energy limit of QCD scatterings $\Longleftrightarrow$ **Small-x limit of QCD.**

BFKL: Evolution at small-x driven by $g \to gg$ splitting $\to xg(x, Q^2) \propto x^{-\lambda}$ as $x \to 0$.

Dokshitzer-Gribov-Lipatov-Altarelli-Parisi (DGLAP): evolution in Q^2 (resummation of $\alpha_s^n \ln^n(Q^2/Q_0^2)$). Resolve "smaller" partons with larger Q^2.

Parton saturation is expected at small-x: $g \to gg$ (BFKL) *AND* $gg \to g$ (gluon recombination)

PDFs are determined in global fit analyses + pQCD evolution. ep DIS, fixed target eA DIS, $p\bar{p}$, and pp data are used for the fits.

More than 5000 data points.

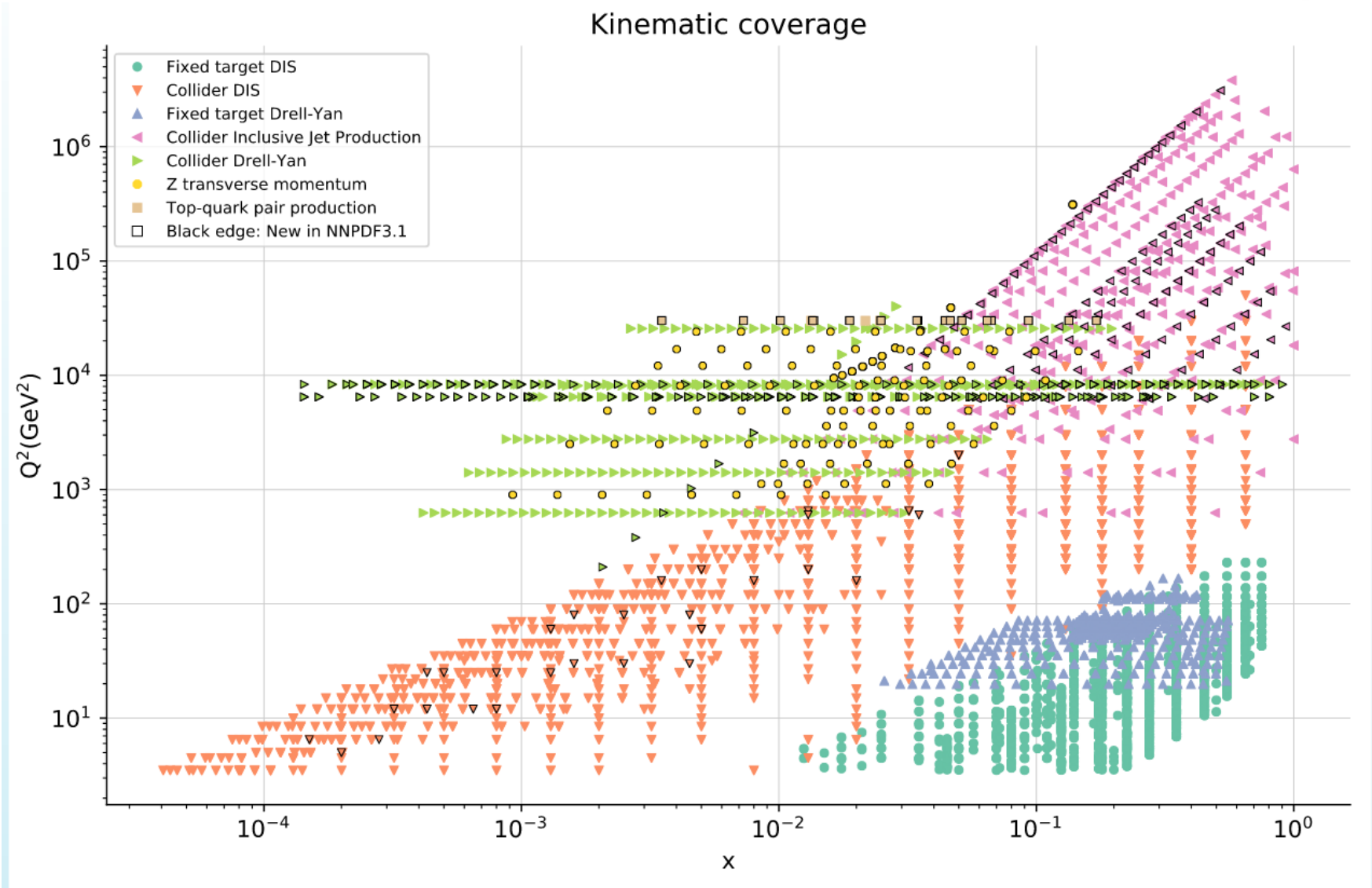

Fig. by J. Rojo

Set of PDFs as a function of x and $Q^2 \gg \Lambda^2_{\mathrm{QCD}}$

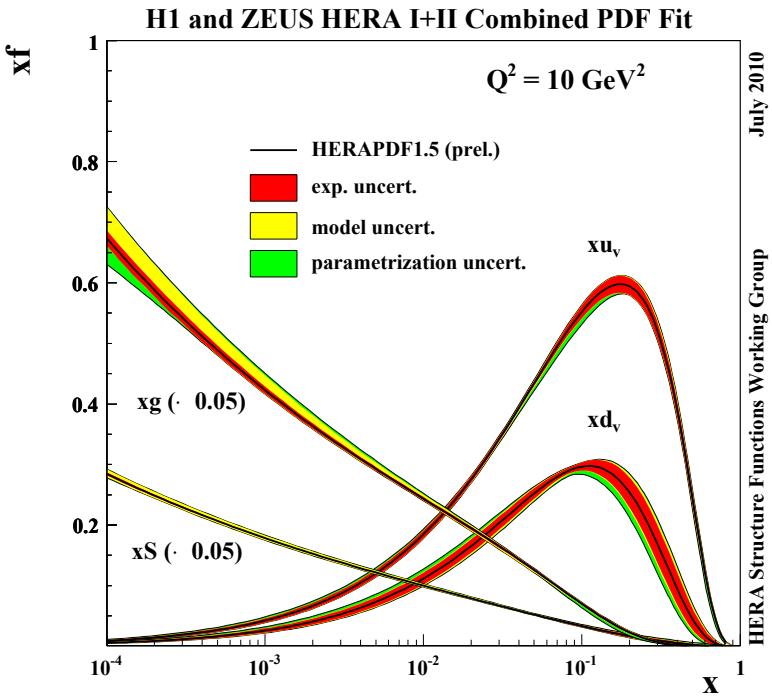

DGLAP

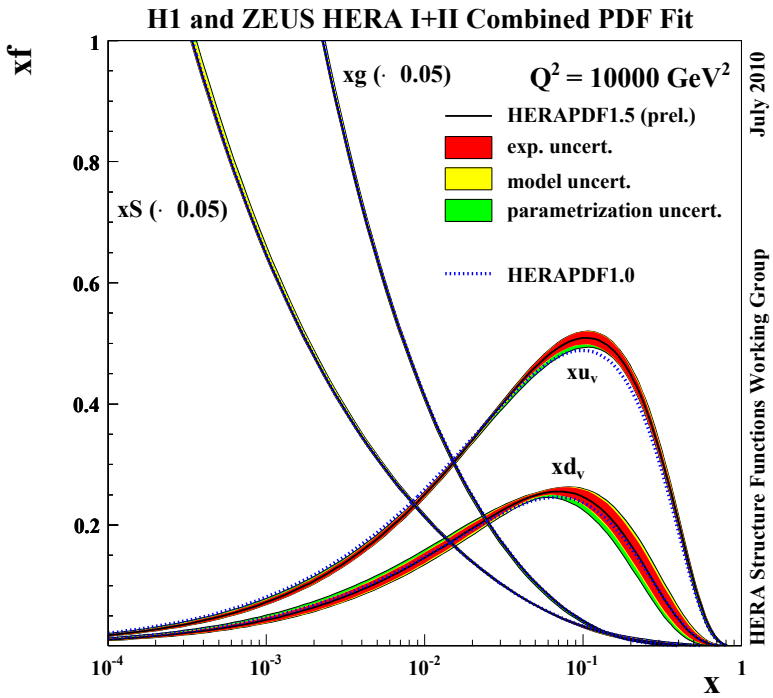

low Q^2 high-Q^2

This is crucial to calculate cross sections for numerous processes at the LHC.

What happens if one includes small-x data?

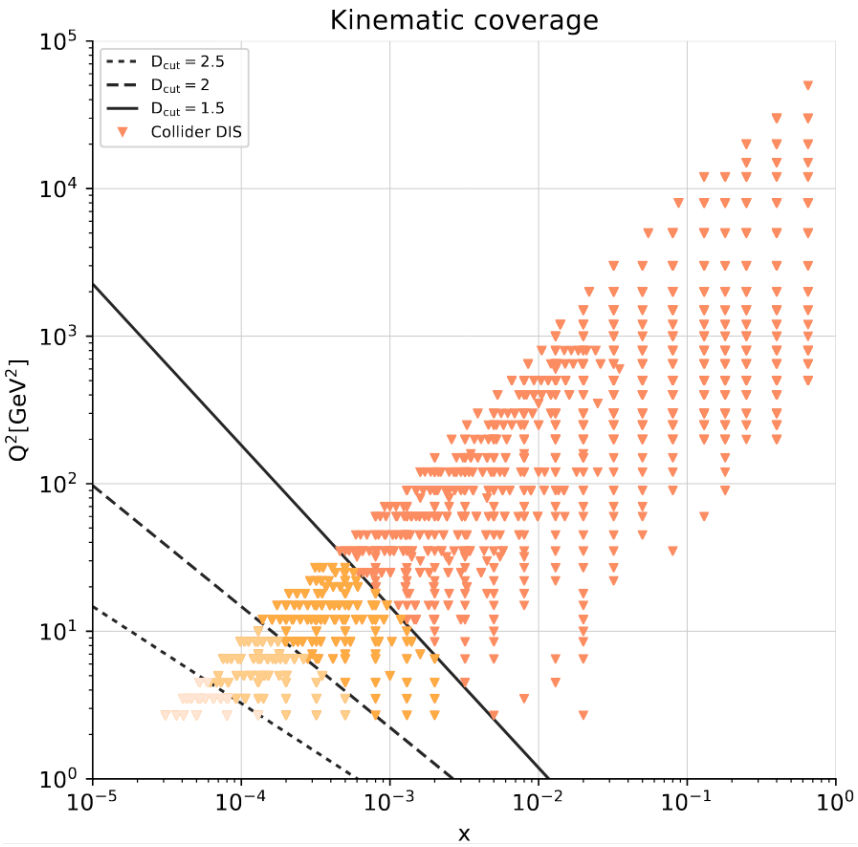

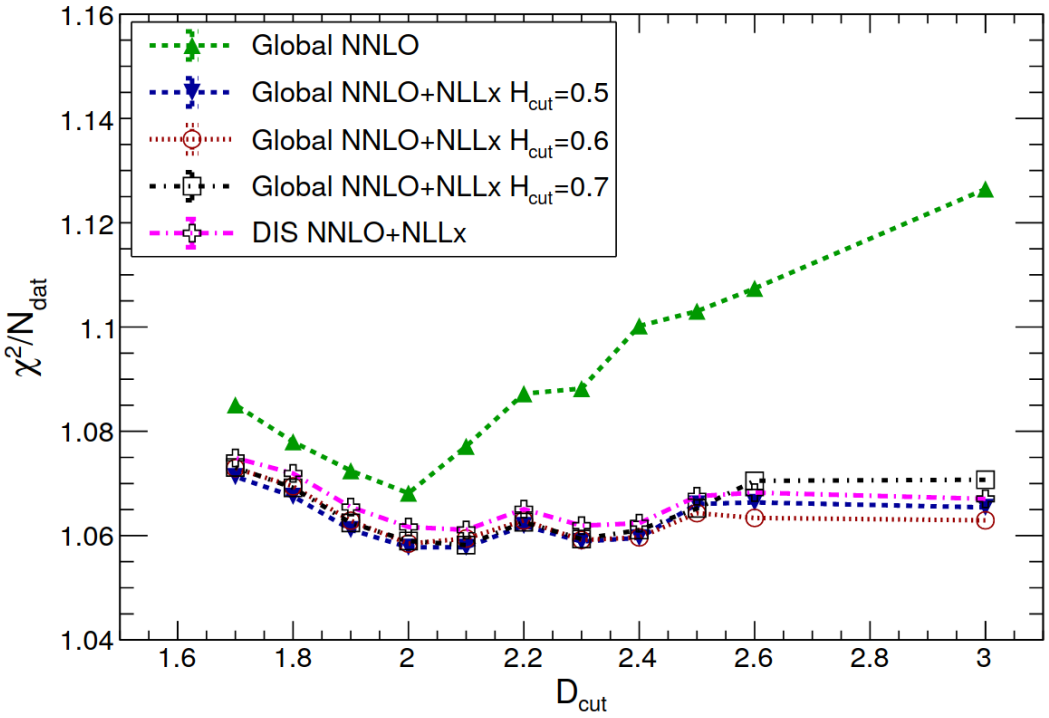

R. D. Ball, V. Bertone, M. Bonvini, S. Marzani, J. Rojo, L. Rottoli, Eur. Phys. J. C (2018) 78:321, arXiv:1710.05935

Tension at small-x, small-Q^2 in global PDF fit analyses with DGLAP at NNLO.

This is cured by matching DGLAP NNLO with BFKL small-x resummation at NLL.

However, perturbativity can be questionnable for some of these points ($Q \gtrsim 1$ GeV).

Exclusive vector boson production ($\gamma^* p \to Vp$)

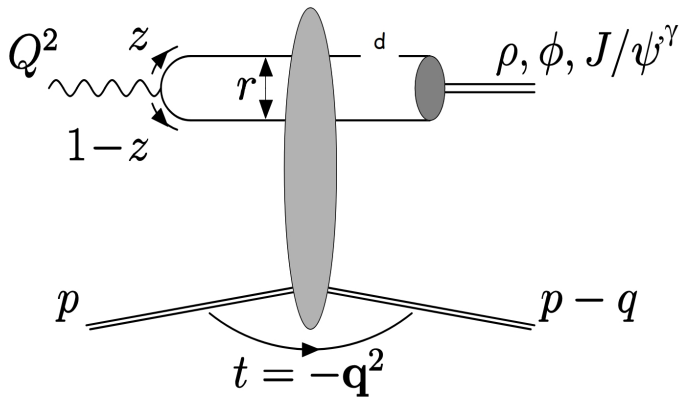

Quasi-real photon fluctuates into a $q\bar{q}$ color dipole that probes the proton structure.

Such an interaction can lead to exclusive production of vector mesons ($V = \rho, \Upsilon, J/\psi$).

Process is very sensitive to gluon densities in the proton. At LO in pQCD,

$$\sigma_{\gamma^* p \to Vp} \propto [xg(x)]^2$$

Small-x limit corresponds to large γ^*-proton masses, $W_{\gamma p}$.

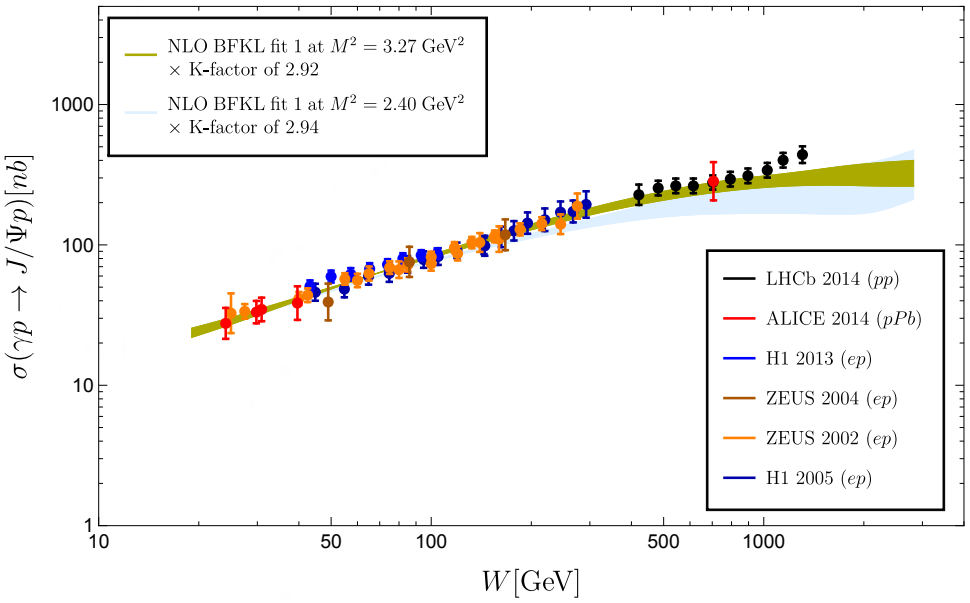

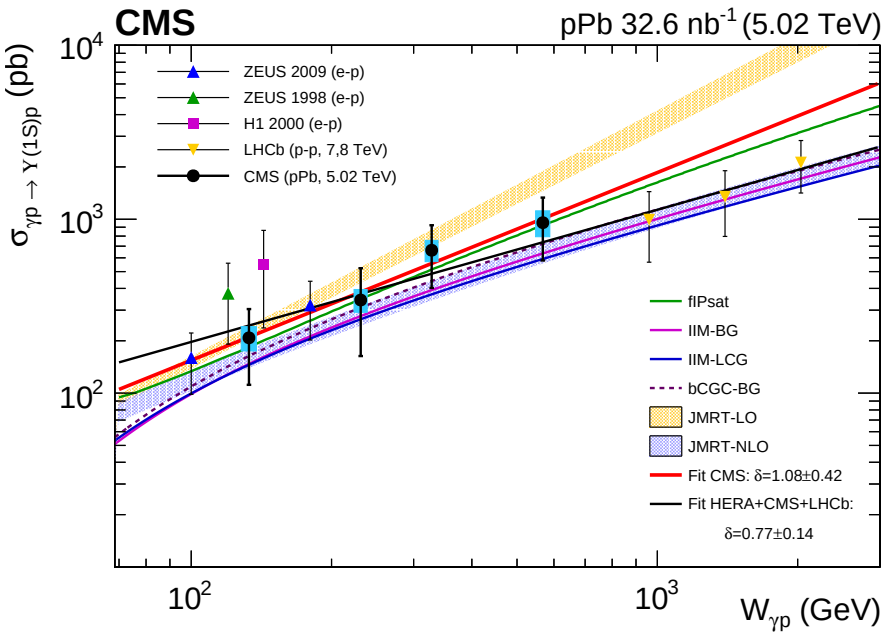

I. Bautista, A. Fernández-Téllez, M. Hentschinski, Phys. Rev. D 94, 054002, arXiv:1607.05203

CMS, Eur. Phys. J. C 79 (2019) 277 arXiv:1809.11080

Predictions based on collinear PDFs give reasonable description of the data, as well as BFKL-based.

Incoming data from LHC experiments on exclusive J/ψ, $\psi(2s)$, Υ, ρ^0, ... at high $W_{\gamma^* p}$ will be crucial.

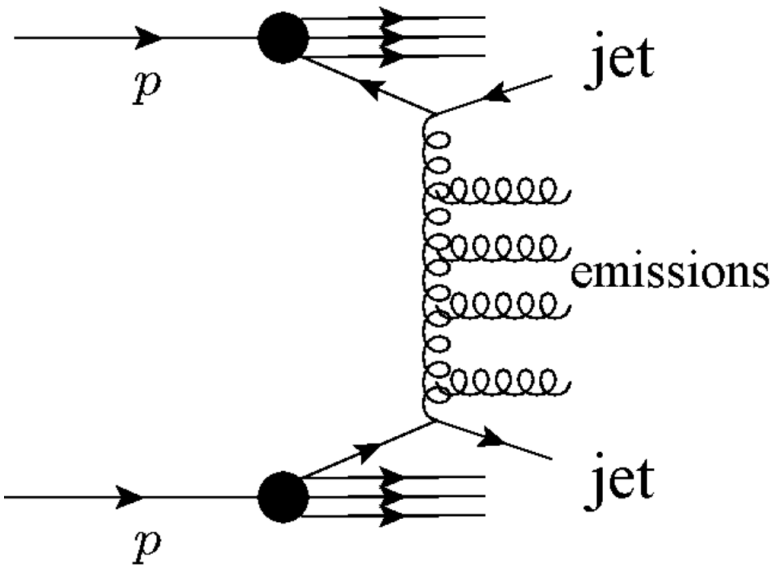

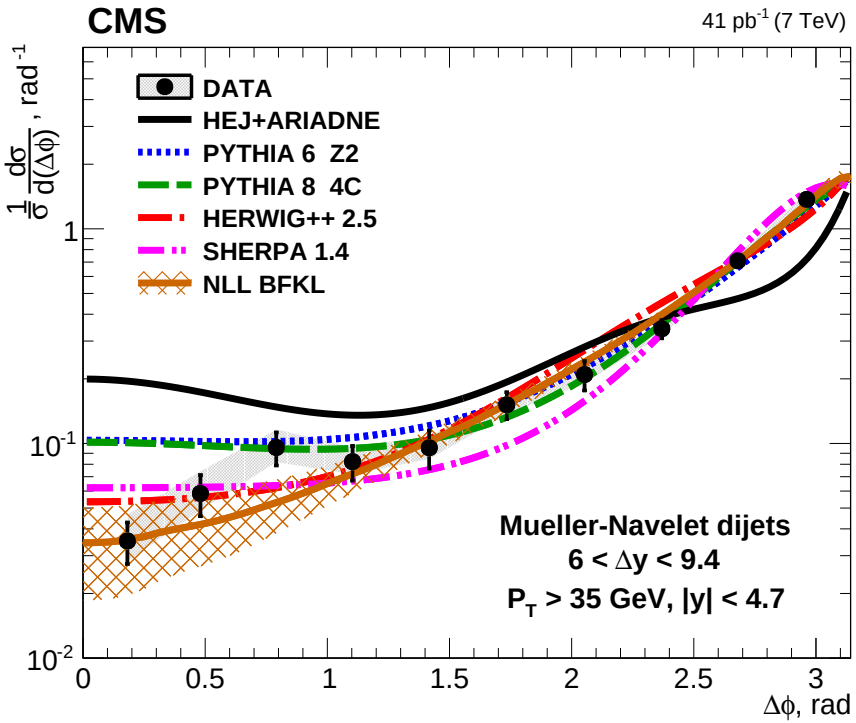

Events where the two outermost jets are largely separated by $\Delta y \equiv |y_{\text{jet1}} - y_{\text{jet2}}| \gg 1$.

At large Δy, the $\Delta\phi$ decorrelations between MN jets are stronger due to increased parton emission with the available phase-space.

$\Delta\phi$ decorrelations are expected to be strong in the BFKL picture.

Average cosine of decorrelation angle vs Δy

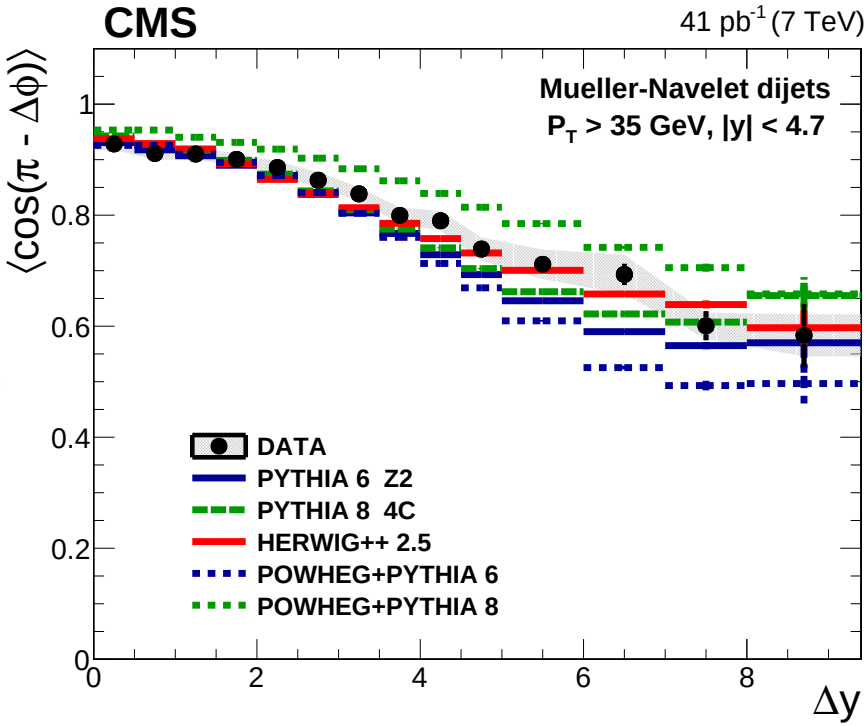

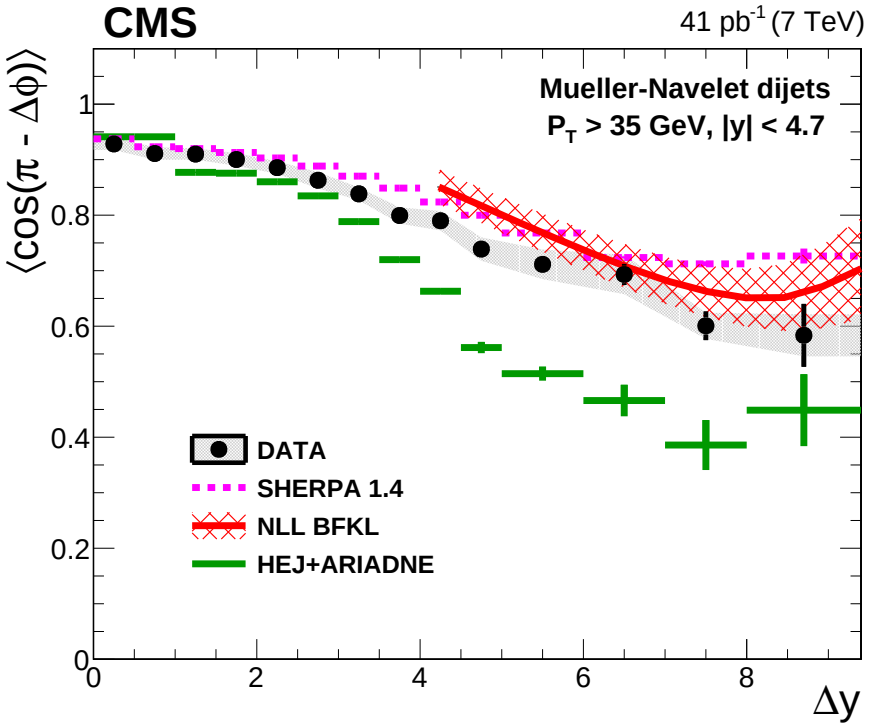

CMS Collaboration, JHEP 08 (2016) 139, arXiv:1601.06713

$$\cos(\pi - \Delta\phi) = 1 \iff \text{back-to-back jets}$$
$$\cos(\pi - \Delta\phi) = 0 \iff \text{collinear jets}$$

The data is consistent with BFKL + NLL calculations, but also with fixed-order (N)LO + parton shower.

We need to explore more processes and/or observables where other higher-order pQCD corrections are suppressed.

Turning to CMS measurement

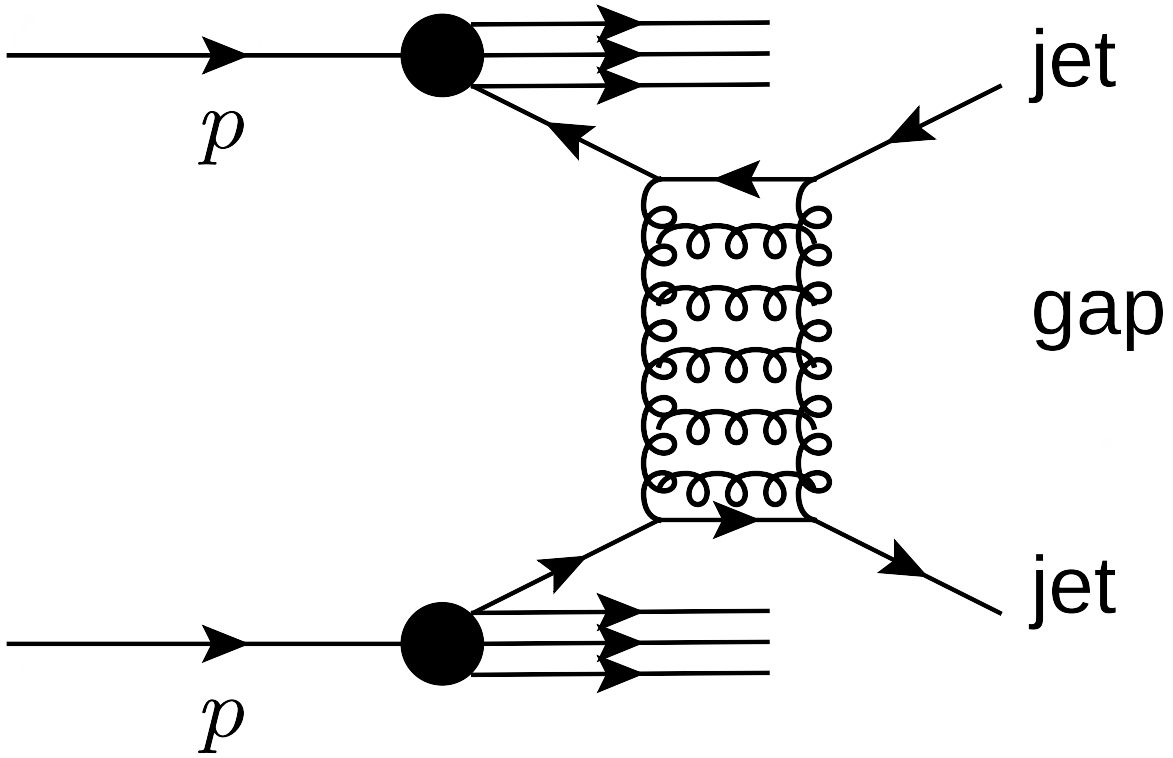

arXiv:2102.06945, *Phys. Rev. D* 104, 032009 (2021)

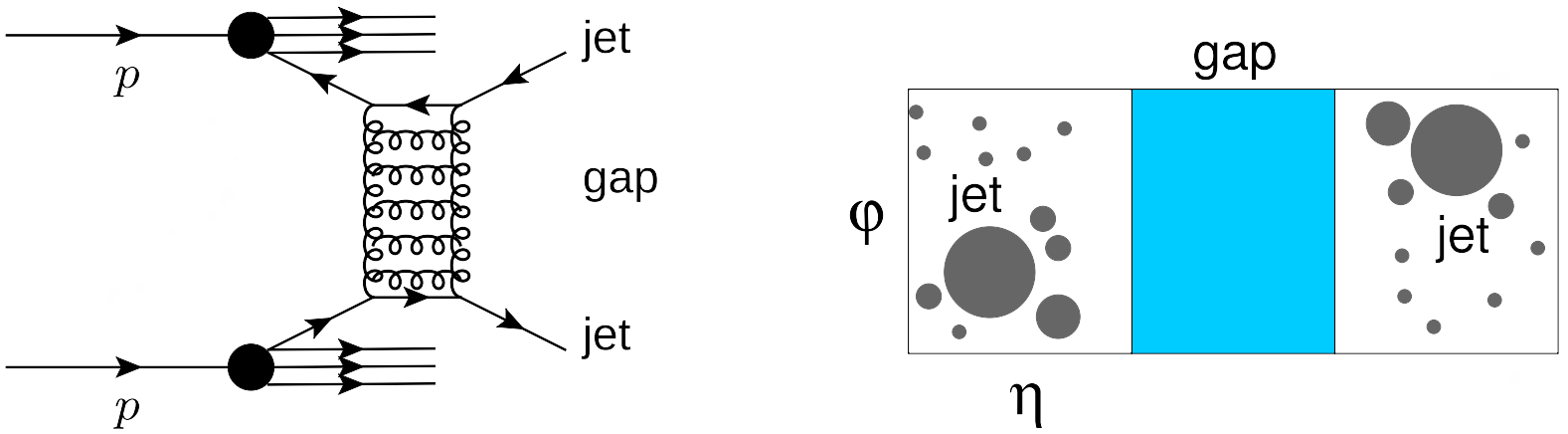

Very clean *jet-gap-jet* experimental signature!

t-channel color-singlet exchange between partons (two-gluon exchange)
$\rightarrow$ **pseudorapidity interval devoid of particle production between jets (pseudorapidity gap)**.

In the high-energy limit, this corresponds to **perturbative pomeron exchange** (BFKL two-gluon ladder exchange). A. Mueller and W-K. Tang, Phys. Lett. B 284 (1992) 123.

DGLAP-like parton splittings are strongly suppressed in events with gaps (Sudakov form factor).

rapidity gaps $\Leftrightarrow$ pomeron exchange $\Leftrightarrow$ diffraction

CMS event displays (single proton-proton collisions)

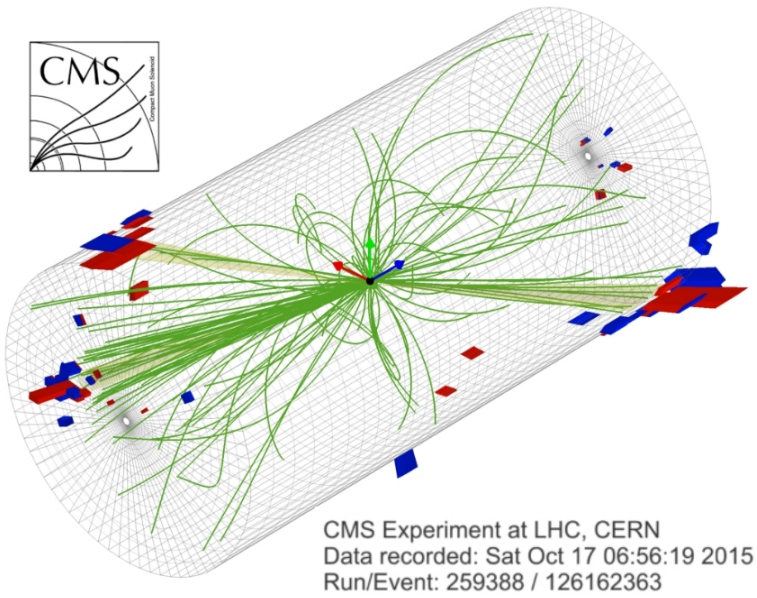

Color-exchange event candidate
(Background-like)

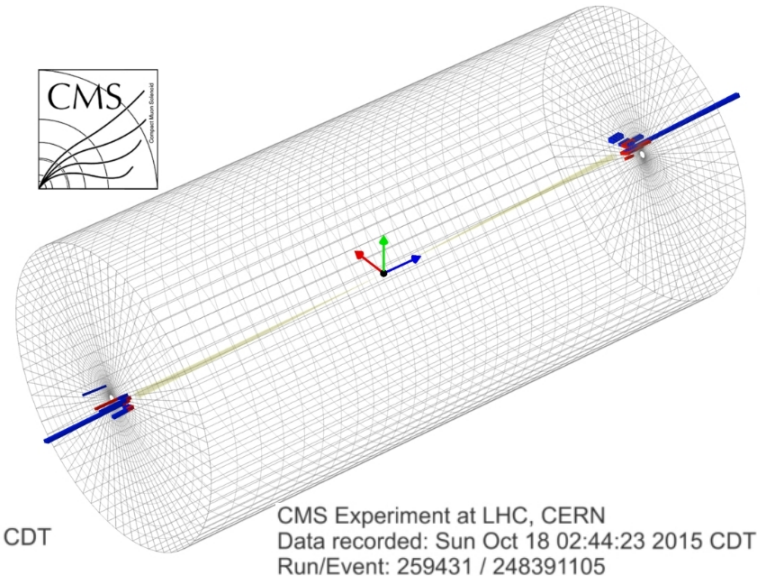

Color-singlet exchange event candidate
(Signal-like)

Leading two jets $p_T > 40$ GeV, all other jets $p_T > 15$ GeV, calorimeter towers with $E > 1$ GeV, charged particles with $p_T > 200$ MeV

Analysis based on special LHC runs with (mostly) single proton-proton collisions per bunch crossing ($\mathcal{L} = 0.66$ pb^{-1}), $\langle pileup \rangle \approx 0.1$
Offline event selection:

- Particle-flow, anti-k_t jets $R = \sqrt{\Delta\eta^2 + \Delta\phi^2} = 0.4$.
- At most one primary vertex.
- **Two highest p_T jets have $p_T > 40$ GeV each.**
- **Leading two jets must have $1.4 < |\eta_{\text{jet}}| < 4.7$ and $\eta^{\text{jet1}}\eta^{\text{jet2}} < 0$**
  $\rightarrow$ Favors t-channel exchanges.

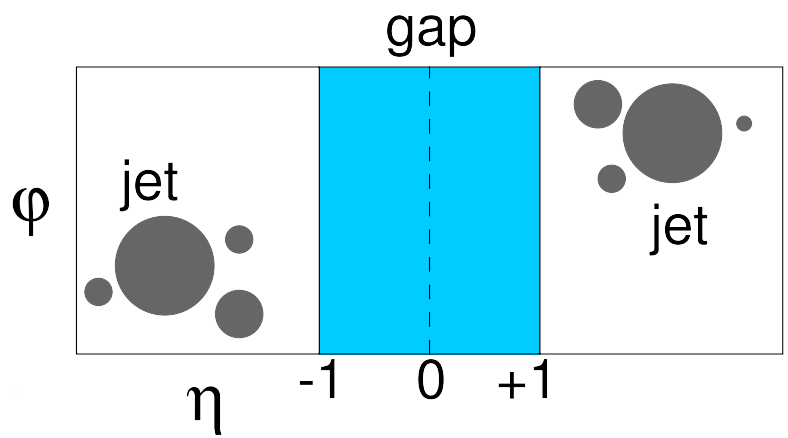

Pseudorapidity gap is defined via the charged particle multiplicity N_{tracks} between the leading two jets. Each charged particle has $p_T > 200$ MeV in $|\eta| < 1$.

Need to distinguish color-exchange from color-singlet exchange contributions

Color-exchange
(single-gluon in
t-channel)

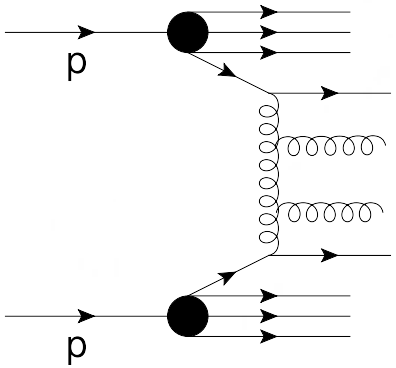

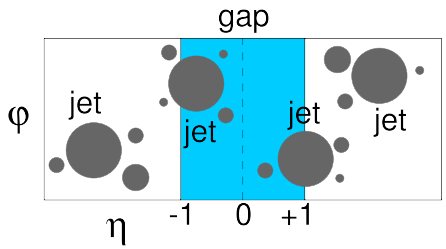

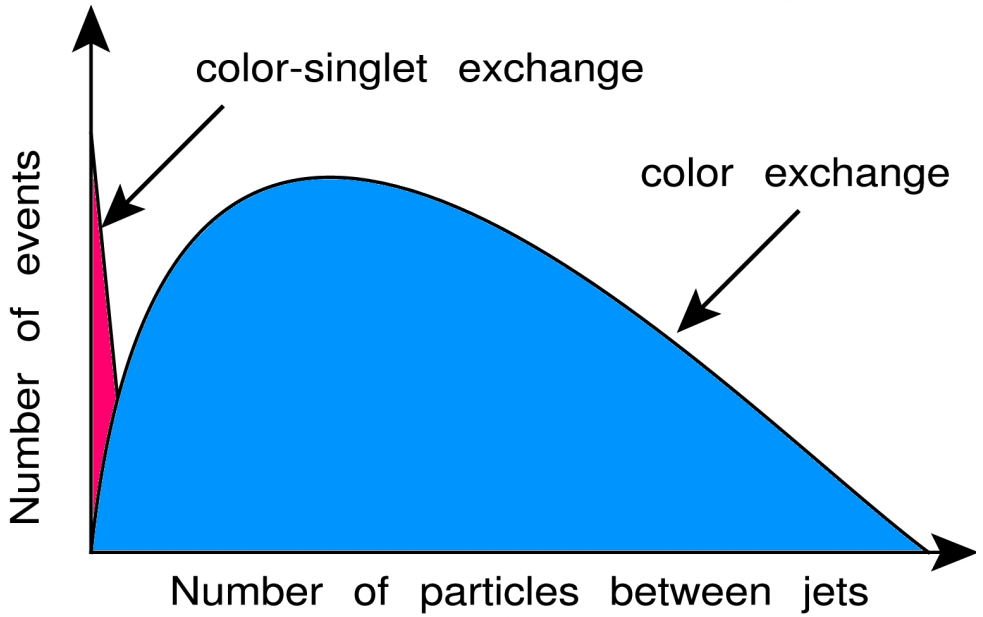

Color-singlet exchange
(two-gluon in t-channel)

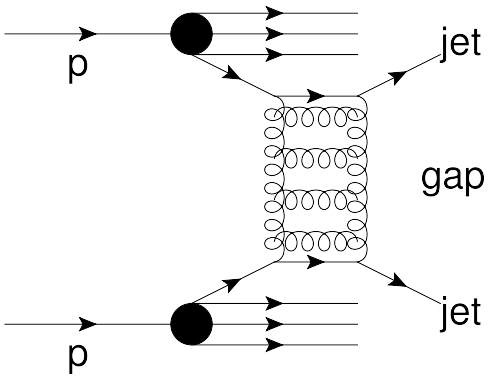

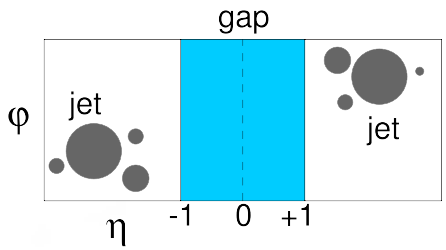

Color-exchange dijet fluctuations at low-multiplicities need to be properly treated.

To avoid model-dependent Monte Carlo predictions, **we used data-based methods to estimate the fluctuations of color-exchange events.**

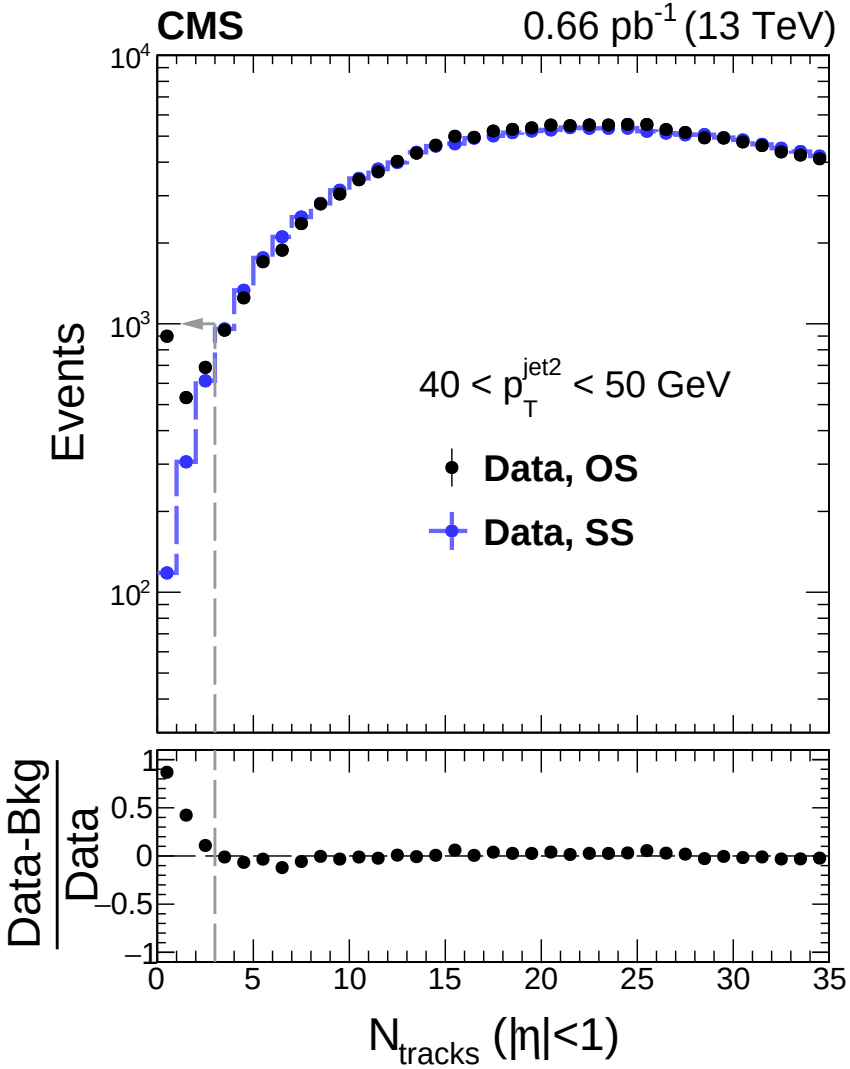

Sharp excess of events at $N_{\text{tracks}} < 3$.

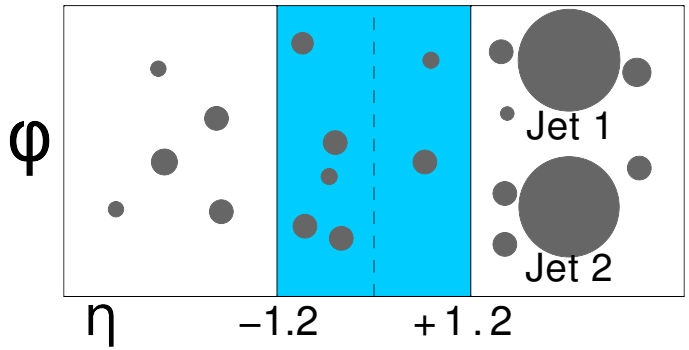

- **Use sample of two jets on the same-side (SS), $\eta^{\text{jet1}}\eta^{\text{jet2}} > 0$.** The resulting N_{tracks} is enriched in color-exchange events.
- Normalize N_{tracks} distribution of SS to the one of opposite-side (OS) jets, $\eta^{\text{jet1}}\eta^{\text{jet2}} < 0$, at large N_{tracks}.
- **The η interval and η_{jet} of the jets in SS are optimized to match the N_{tracks} of the OS sample.**
- Minimum forward particle activity to suppress single-diffractive jet contributions ($3 < |\eta| < 5.2$, $E > 5$ GeV).

Approach 2: negative binomial distribution (NBD) function fit

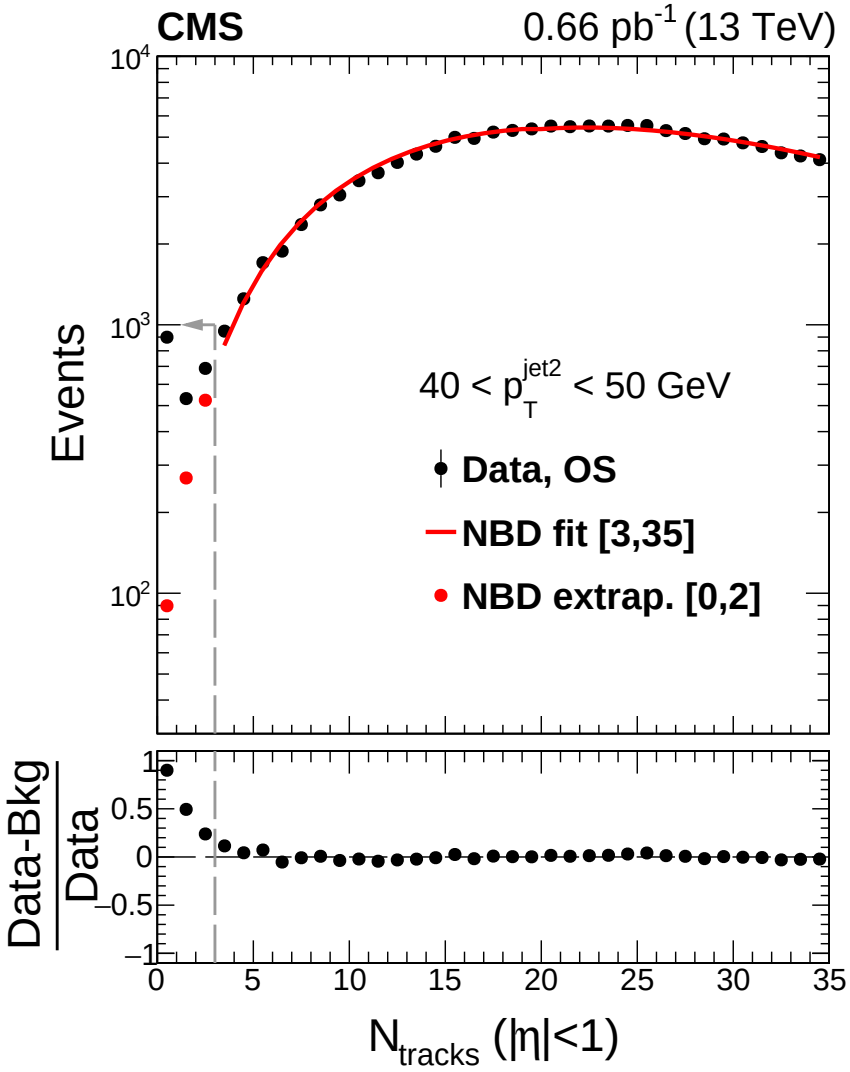

Sharp excess of events at $N_{\text{tracks}} < 3$.

- **Fitted data with NBD in $3 \leq N_{\text{tracks}} \leq 35$, extrapolate down to $N_{\text{tracks}} = 0$.**
- NBDs are good empirical models of N_{ch} distributions in hadron-hadron collisions.
- **Validated the NBD method with trijet data, with SS dijets, and with Monte Carlo events (PYTHIA8 QCD jets).**
- Studied the stability of bkg. when changing fit N_{tracks} interval, other functional forms (eg double NBD), ...

We extract f_{CSE} based on the N_{tracks} analysis between the jets:

$$f_{CSE} \equiv \frac{N(N_{tracks} < 3) - N_{bkg}(N_{tracks} < 3)}{N_{all}} \equiv \frac{\text{color singlet exchange dijet events}}{\text{all dijet events}}$$

f_{CSE} is measured as a function of:

- $\Delta\eta_{jj} \equiv |\eta^{jet1} - \eta^{jet2}|$: Sensitive to expected BFKL dynamics, since it's related to resummation of large logs of s.
- p_T^{jet2}: Sensitive to expected BFKL dynamics.
- $\Delta\phi_{jj} \equiv |\phi^{jet1} - \phi^{jet2}|$: Sensitive to deviations of $2 \to 2$ scattering topology.

Results on color-singlet exchange fraction f_{CSE}

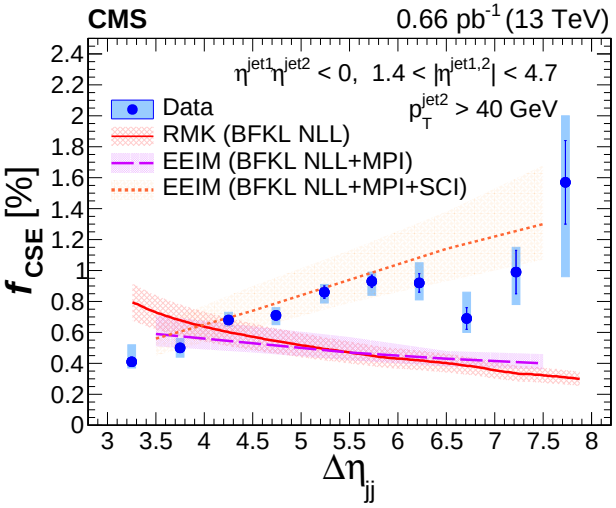

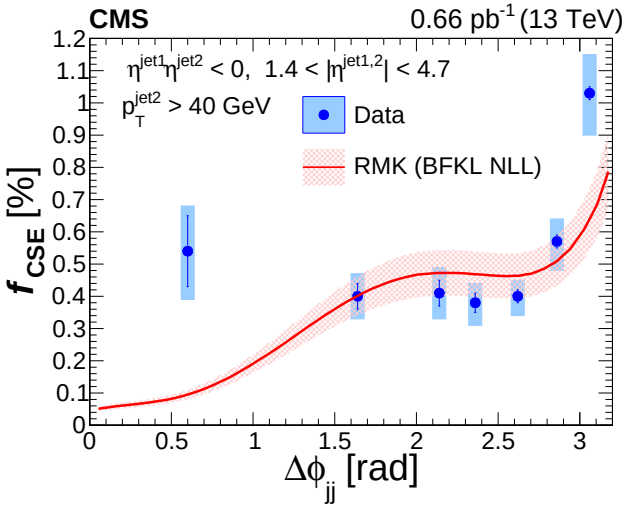

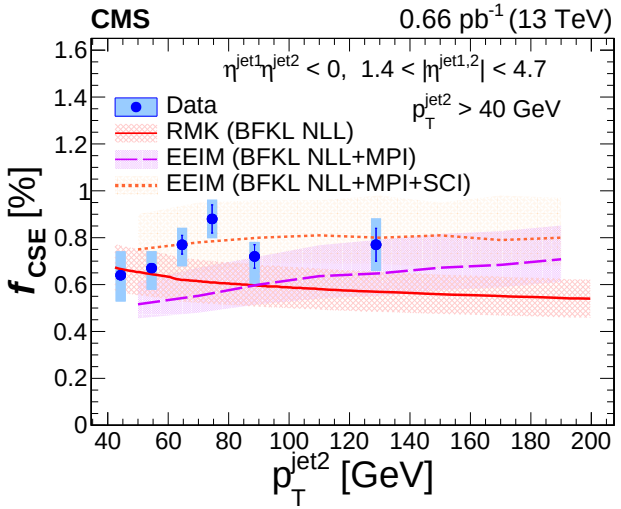

- **Color-singlet exchange represents $\approx 0.6\%$ of the inclusive dijet cross section for the probed phase-space.**
- Clear dependence on $\Delta\eta_{jj}$. First time these events are measured at $\Delta\eta_{jj} > 6$.
- Comparisons to BFKL predictions (resummation at NLL and different modelling of the destruction of the gap):
  - Royon, Marquet, Kepka (**RMK**) predictions and gap survival probability $|S|^2 = 0.1$.
  - Ekstedt, Enberg, Ingelman, Motyka (**EEIM**) predictions with **multiple-parton interactions (MPI)**, also supplemented with **soft-color interactions (SCI)** ($\sim$ Lund string).
- **Challenging to describe theoretically all aspects of the measurement simultaneously.**
- Current predictions are partially NLO; higher-order corrections to impact factors are being done.

Comparison to measurements at lower $\sqrt{s}$

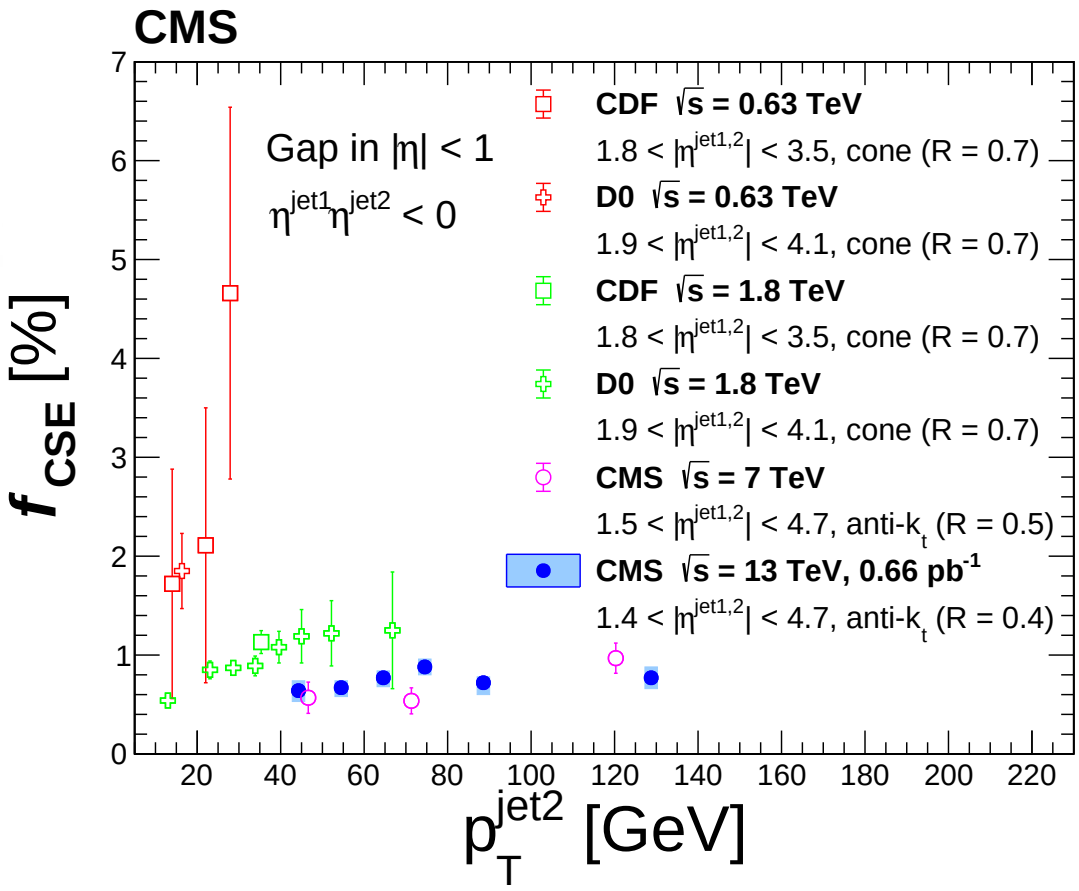

- Jet-gap-jet events at four different energies in $p\bar{p}$ and pp collisions at 0.63 TeV, 1.8 TeV, 7 TeV, and 13 TeV (this measurement).
- Generally, f_{CSE} has been observed (and is expected) to decrease with increasing $\sqrt{s}$, due to an increase in spectator parton activity with $\sqrt{s}$.
- Within the uncertainties, f_{CSE} **stops decreasing with $\sqrt{s}$ at LHC energies**, in contrast to trend observed at lower energies 0.63 TeV $\rightarrow$ 1.8 TeV $\rightarrow$ 7 TeV.

Turning to CMS-TOTEM combined measurement

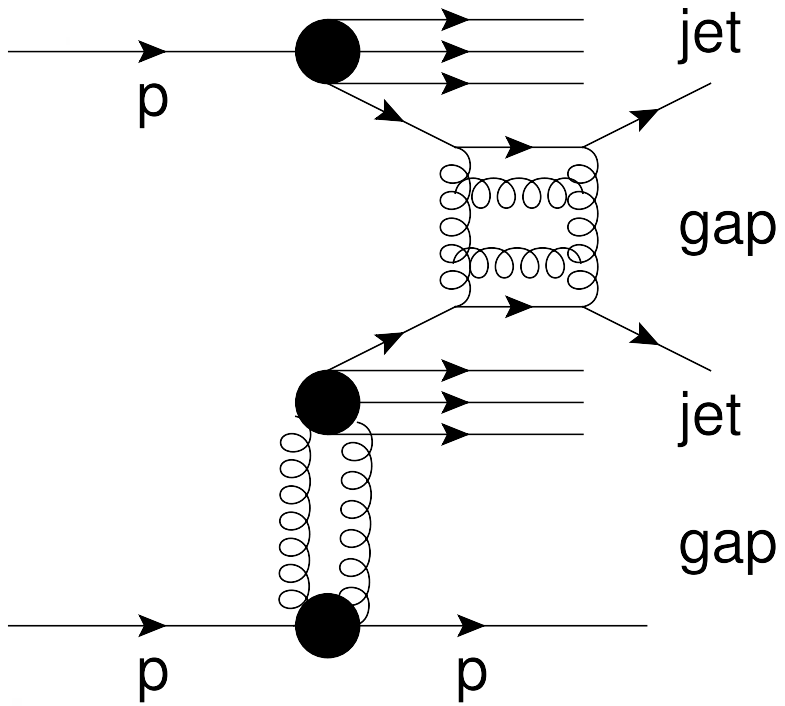

arXiv:2102.06945, *Phys. Rev. D* 104, 032009 (2021)

Process has not been studied before.

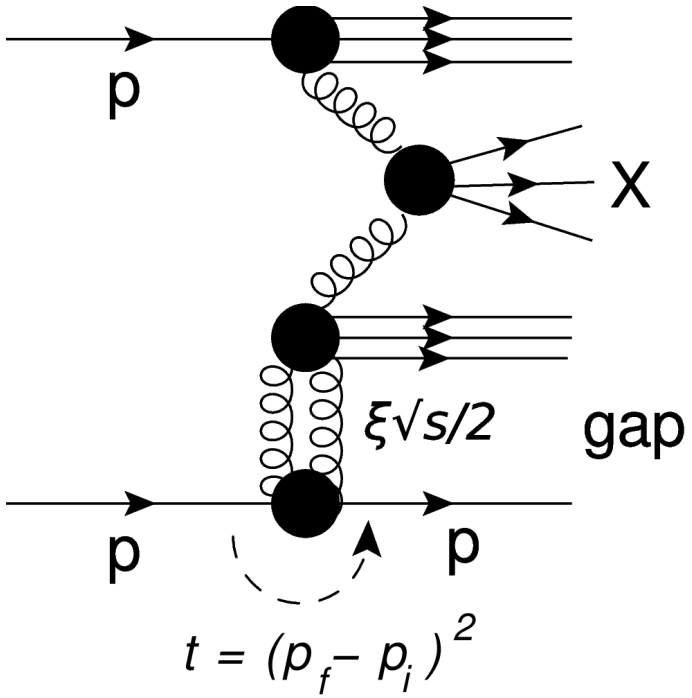

Color-singlet exchange off the proton

Most hard QCD processes are from single parton-parton collisions.

A fraction of the hard QCD processes are mediated by **color-singlet multiparton exchange from the proton** (two-gluons at LO QCD).

The proton may remain **intact** and be detected very far from the interaction point.

Two additional kinematic variables:

- The fraction of beam momentum carried away by the pomeron exchange, $\xi \equiv \Delta p/p$.
- Square of four-momentum transfer at the proton vertex, $t \equiv (p_f - p_i)^2$.

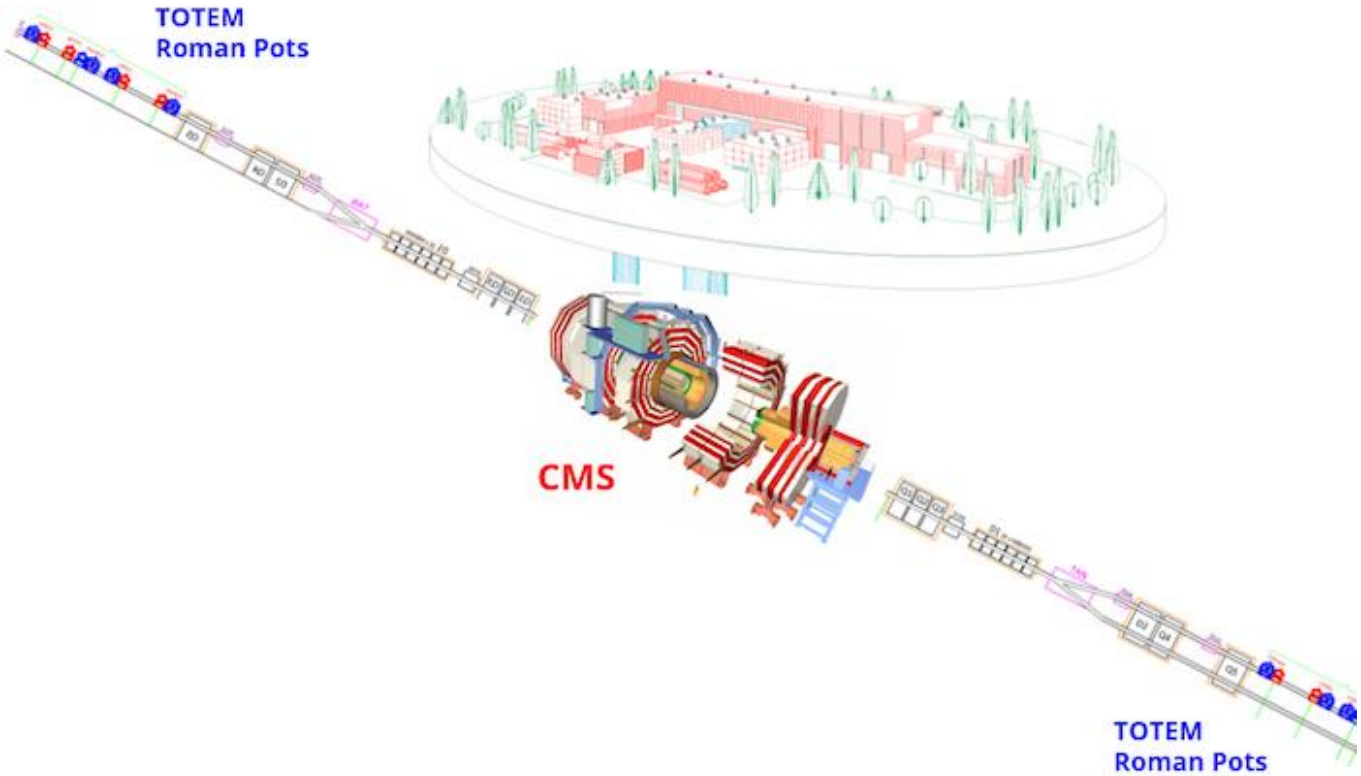

CMS:

- General purpose detector at IP5 of the CERN LHC.
- Jets with $R = 0.4$ reconstructed within $|\eta^{\text{jet}}| < 4.7$.

TOTEM:

- **Roman pots:** Forward tracking detectors at $\approx$ 220m w.r.t. IP5 that measure the protons scattered at small angles w.r.t. the beam.

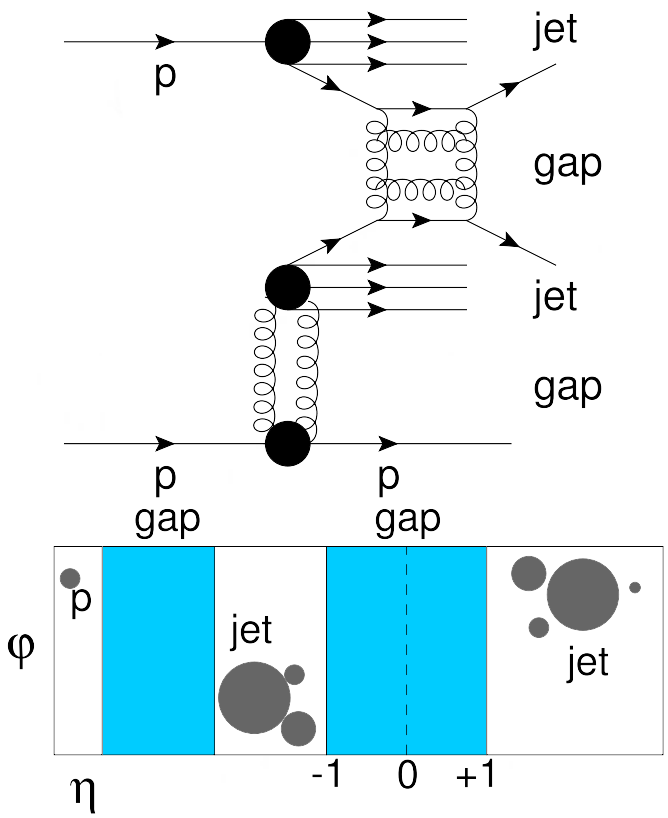

Better understand the role of spectator partons in the destruction of the central gap.

Same dijet and central gap definitions as with CMS-only analysis.

Additional requirements:

- ≥ 1 intact proton.
- $\xi_p(\mathrm{RP}) < 0.2$ and $-4 < t < -0.025$ GeV^2 (+ fiducial RP requirements).
- To suppress beam background, we cut on $\xi_p(\mathrm{PF}) - \xi_p(\mathrm{RP}) < 0$, where $\xi_p(\mathrm{PF}) = (\sum_i E_i \pm p_{z,i})/\sqrt{s}$ is reconstructed with PF candidates of CMS.

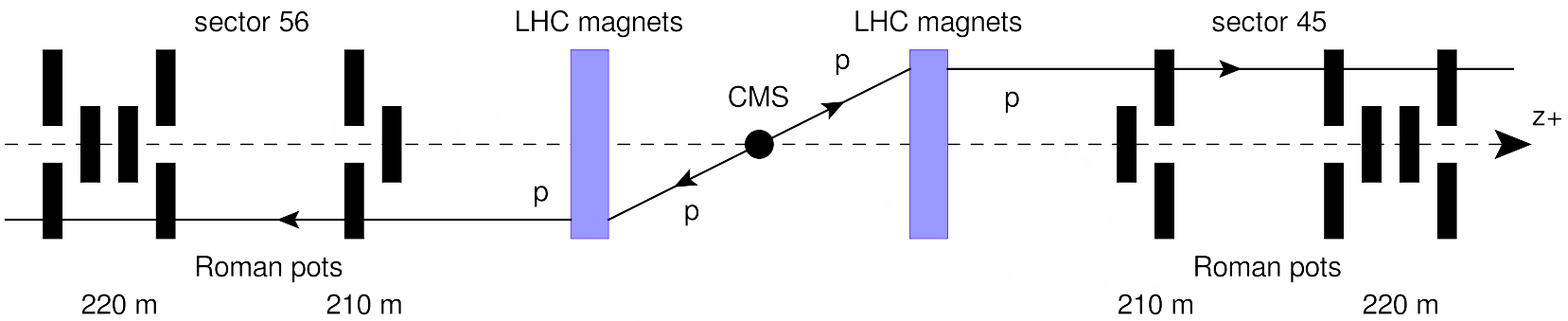

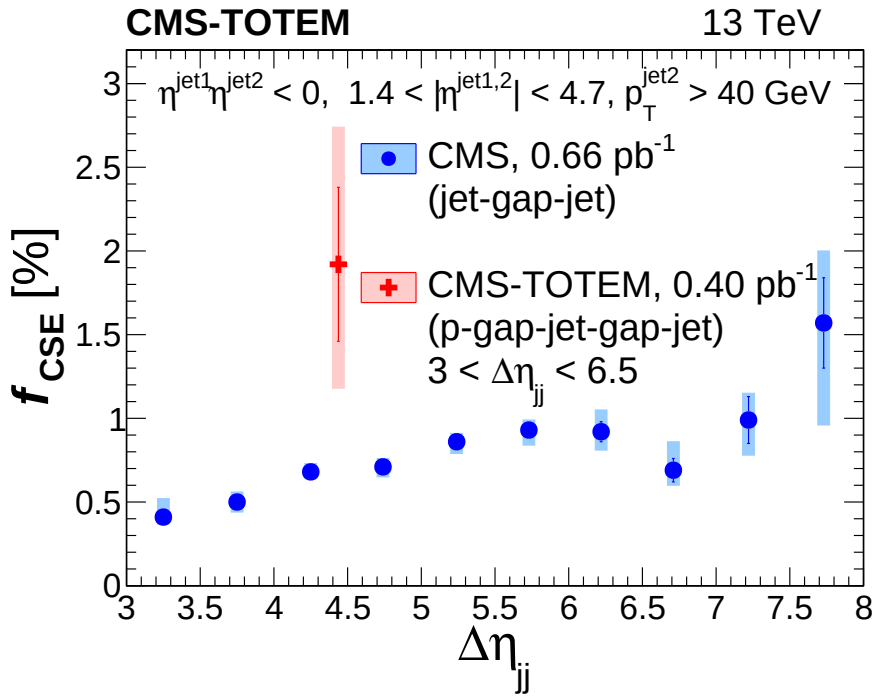

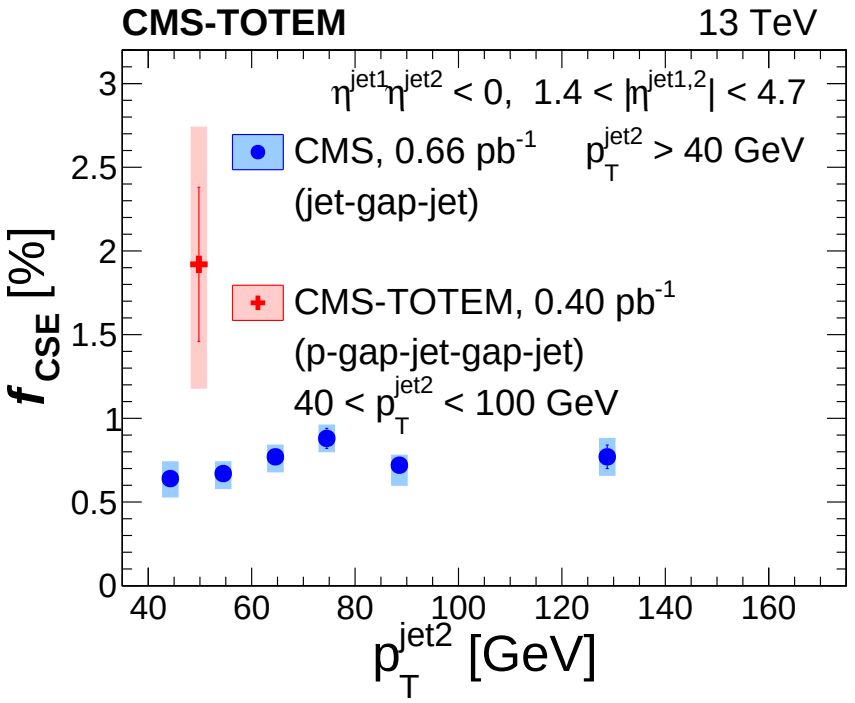

$f_{CSE} \equiv$ p-gap-jet-gap-jet/p-gap-jet-jet is $2.91 \pm 0.70\,\mathbf{(stat)}\,^{+1.08}_{-1.01}\,\mathbf{(syst)}$ times larger than $f_{CSE} \equiv$ jet-gap-jet/inc. dijet, for similar dijet kinematics.

Lower spectator parton activity in events with intact protons $\rightarrow$ **Better chance of central gap surviving the collision.**

Future low-PU runs with dedicated trigger w/ more lumi to study process differentially.

- High-energy limit of QCD is an important test of pQCD and QFTs.
- We measured hard color-singlet exchange dijet events at $\sqrt{s} = 13$ TeV with CMS and TOTEM data (arXiv:2102.06945, *Phys. Rev. D* 104, 032009 (2021)
- About 0.6% of dijet events are produced by t-channel hard color-singlet exchange (subprocess absent in Monte Carlo generators).
- First measurement of jet-gap-jet with protons w/ CMS-TOTEM. f_{CSE} in this sample is larger than in CMS-only.

Thank you!

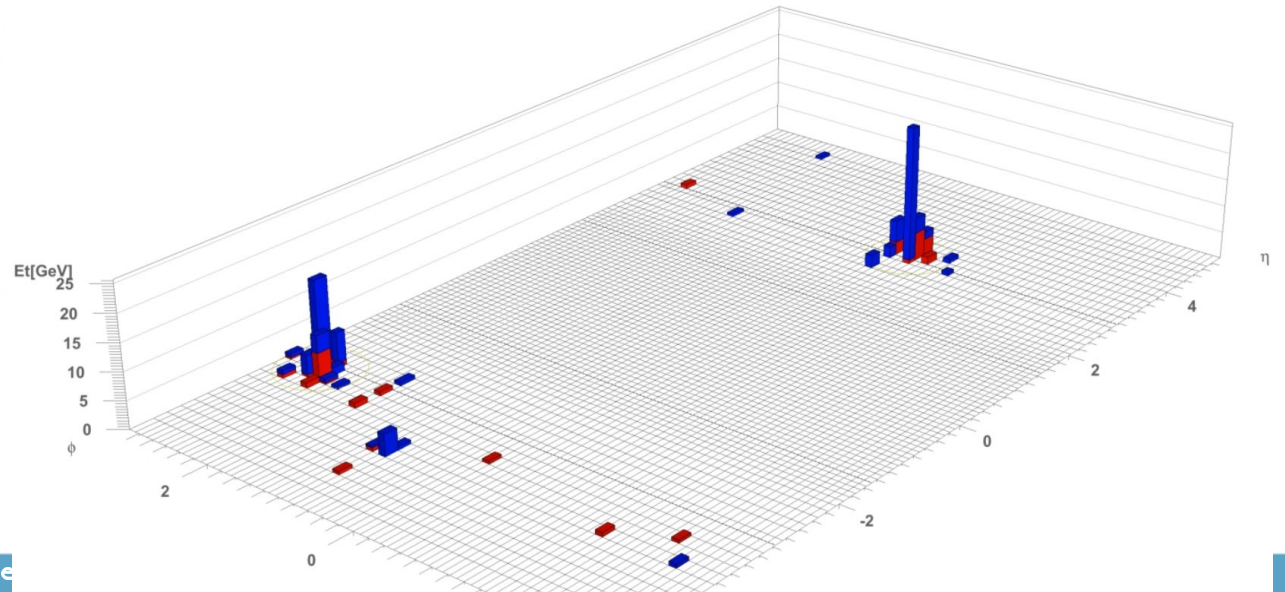

f_{CSE} vs. $\Delta\eta_{jj}$ between 7 and 13 TeV CMS results

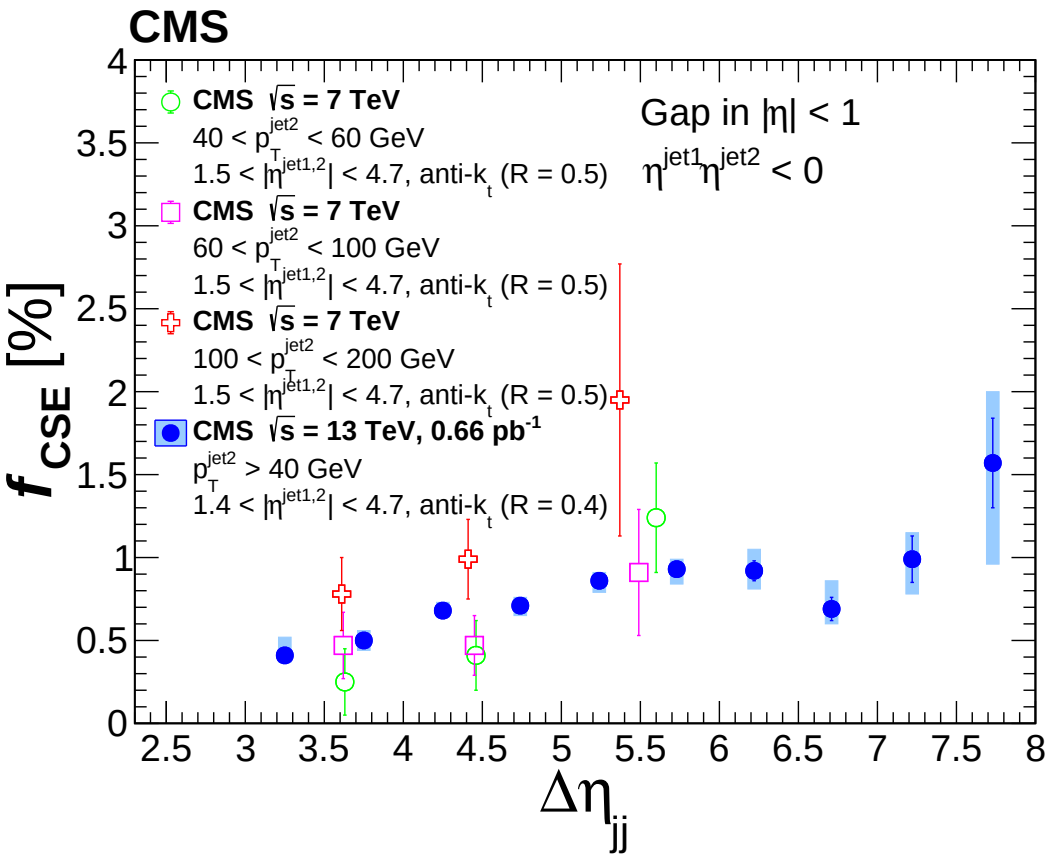

- 7 TeV CMS measurement in three bins of p_T^{jet2} (*EPJC* 78(2018)242, arXiv:1710.02586)
- Trend of increasing f_{CSE} with $\Delta\eta_{jj}$ is confirmed with present 13 TeV results with improved precision.
- New results reach previously unexplored values of $\Delta\eta_{jj}$.

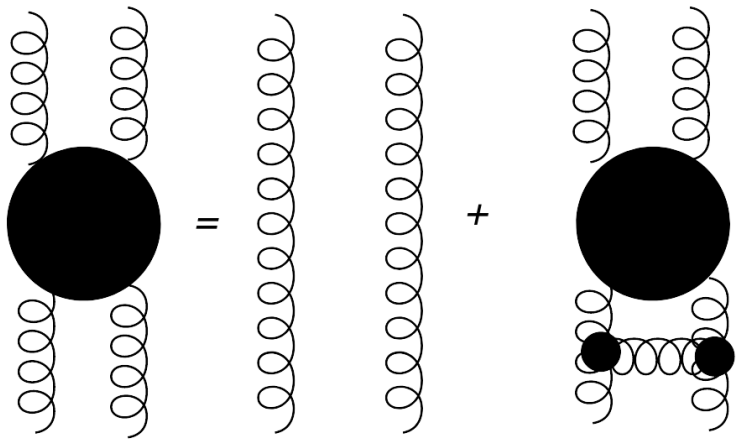

All-orders resummation in α_s is done via the Balitsky–Fadin–Kuraev–Lipatov (BFKL) evolution equations. Resummation is known at leading logarithmic (LL) accuracy ($\alpha_s^n \ln^n(\hat{s}/|\hat{t}|)$ terms) and next-to-LL (NLL) accuracy ($\alpha_s^n \ln^{n-1}(\hat{s}/|\hat{t}|)$ terms).

The BFKL equation (in Mellin space), which emerges upon the resummation of logs, is symbolically represented by:

$$\omega \mathcal{G}_\omega = \mathbb{I} + \mathcal{K} \otimes \mathcal{G}_\omega \tag{1}$$

$\mathcal{G}_\omega$ is known as the BFKL Green's function, and encodes the all-orders resummation of logarithms, ω is a complex angular momentum variable, $\mathcal{K}$ is the BFKL kernel, and $\otimes$ represents a convolution.

By solving for $\mathcal{G}_\omega$ (in terms of the eigenfunctions of $\mathcal{K}$), one can then calculate the corresponding scattering amplitude by means of an **inverse** Mellin transform to momentum space.

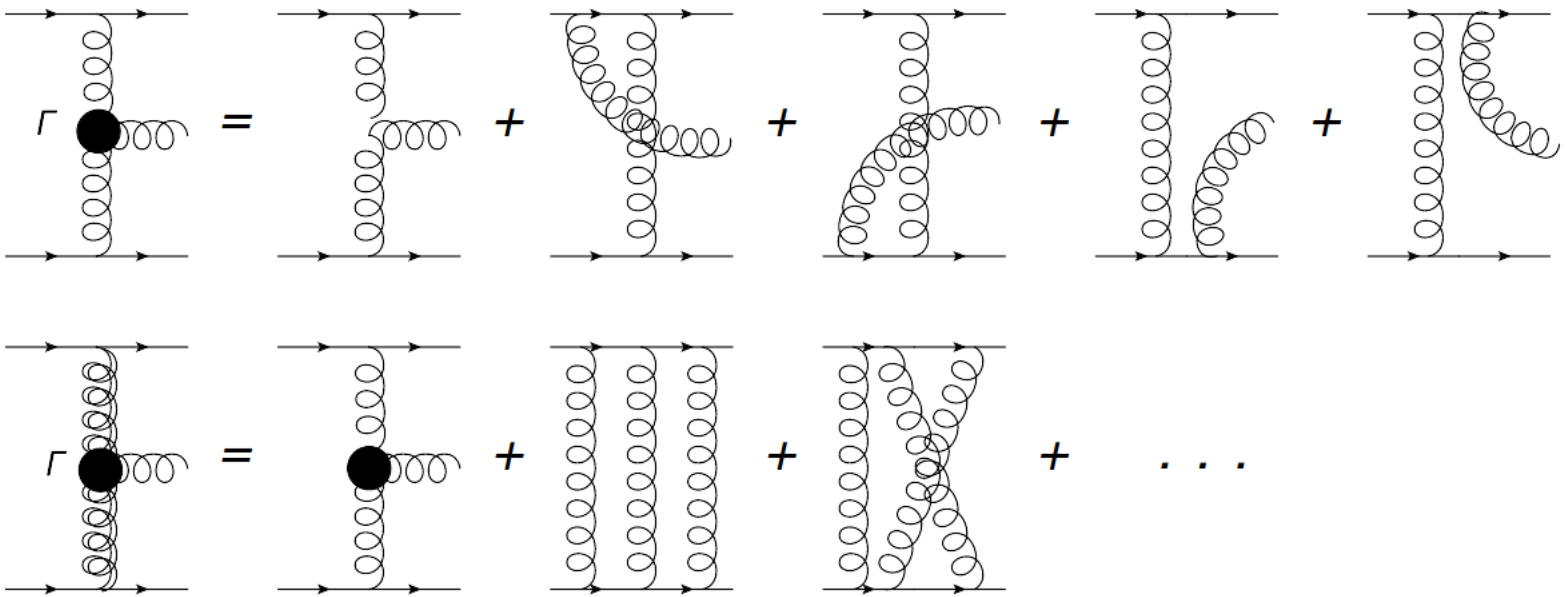

Figure 4.1: Upper diagrams: definition of the Lipatov effective vertex, Γ, which contains the dominant real emission diagrams in the leading-logarithm (LL) approximation. Lower diagrams: reggeization of the gluon obtained by summing up all the virtual gluon emission diagrams in the LL approximation. The double-gluon lines in the lower left diagram represents the *reggeized* t-channel gluons.

CMS slice

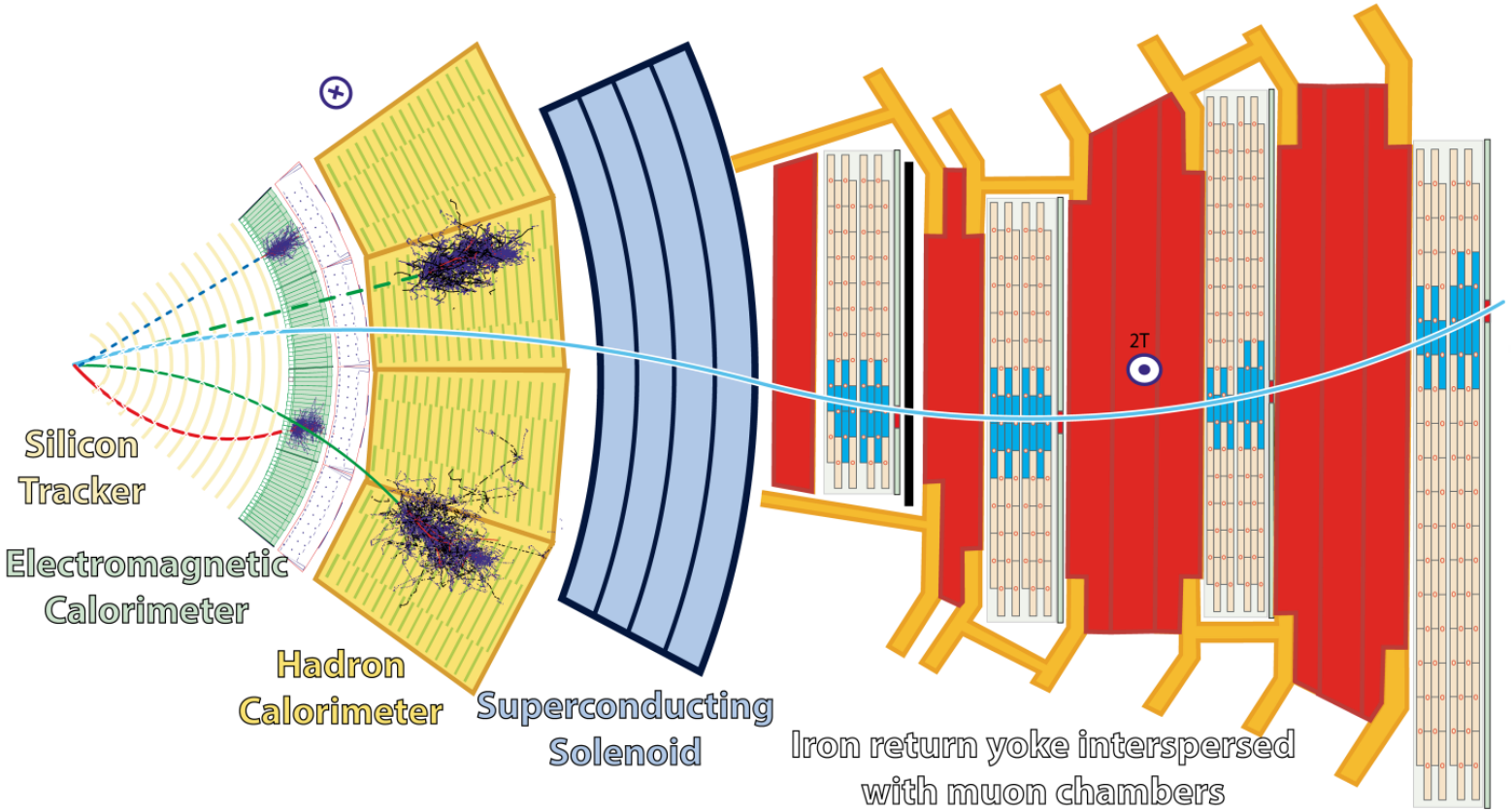
Silicon Tracker
Electromagnetic Calorimeter
Hadron Calorimeter
Superconducting Solenoid
Iron return yoke interspersed with muon chambers
2T
Muon
Electron
Charged hadron (e.g. pion)
Neutral hadron (e.g. neutron)
Photon

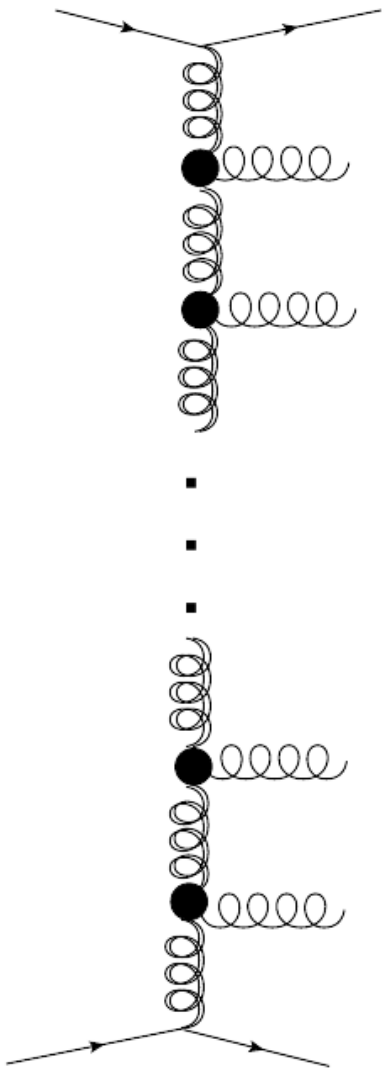

Figure 4.2: Gluon ladder diagram that contributes significantly in the high-energy limit of QCD. The t-channel gluons are "reggeized" gluons. The disks represent the Lipatov effective vertices.

Similar set of resummation techniques are used for square momentum transfer Q^2. This resummation is done via the Dokshitzer-Gribov-Lipatov-Altarelli-Parisi (DGLAP) evolution equations.

DGLAP evolution equations are the bread-and-butter of PDF evolution for the LHC physics program (PDF at low Q_0^2 is "evolved" to another PDF at $Q^2 > Q_0^2$).

DGLAP dynamics are approximated in parton shower algorithms embedded in standard Monte Carlo generators (Pythia8, Herwig, Sherpa, ...) for numerical resummation of collinear parton splittings.

In the DGLAP picture, parton splittings strongly ordered in p_T contribute in the leading logarithm approximation,

$$y_1 < y_2 < y_3 < \cdots < y_{n-2} < y_{n-1} < y_n$$

$$p_{T,1} \gg p_{T,2} \gg p_{T,3} \gg \cdots p_{T,n-2} \gg p_{T,n-1} \gg p_{T,n} \gg \Lambda_{\mathrm{QCD}}$$

The SM is the quantum field theory of elementary interactions.

- It describes the strong, weak, and electromagnetic interactions between particles.
- The matter content consists of quarks and leptons.
- The interactions are mediated by force-carrying particles: gluons, W and Z bosons, photon.
- Higgs boson; consequence of spontaneous symmetry breaking that endows particles with mass.

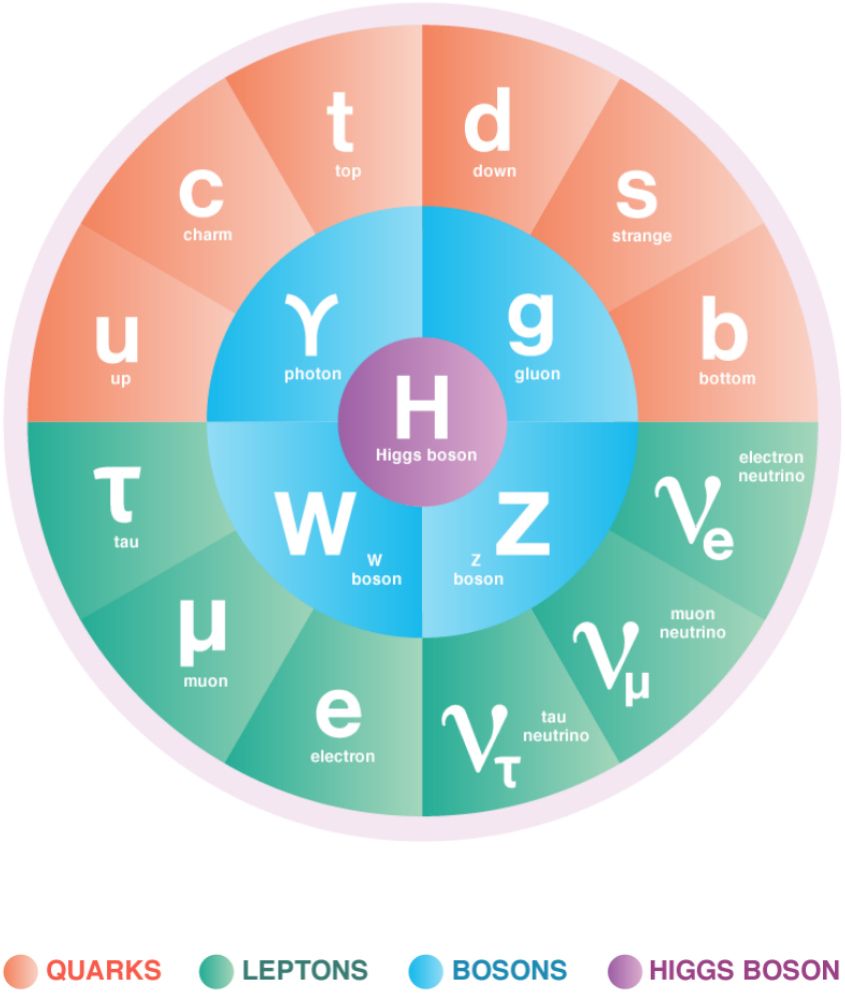

In the experiment, we measure the production rate of a process in terms of the **"cross section"**,

$$\sigma = \frac{N_{\text{events}}}{\epsilon \times \mathcal{A} \times \mathcal{L}} \tag{2}$$

where N_{events} is the number of events, $\mathcal{L}$ the machine luminosity, $\epsilon \times \mathcal{A}$ are the detector-related inefficiencies and acceptance.

σ typically measured in units of $1 barn = 10^{-28}$ m^2.

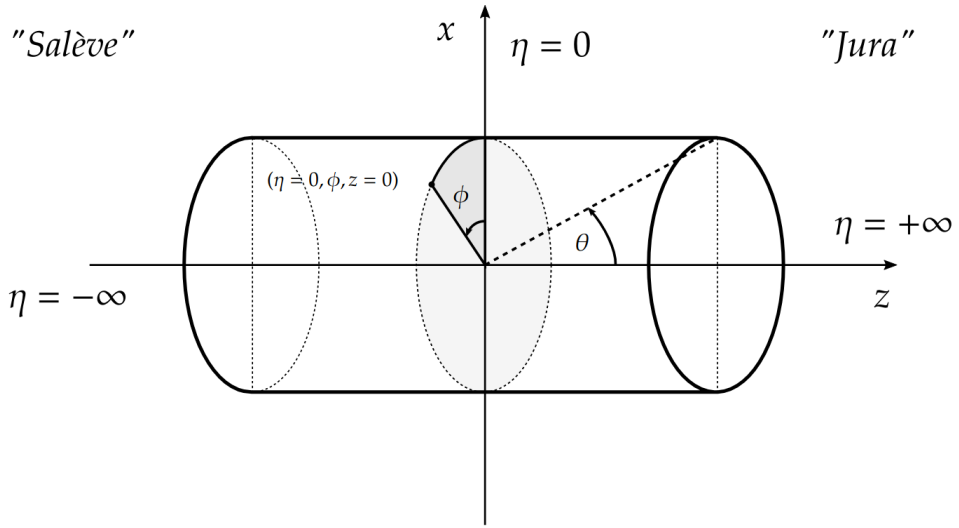

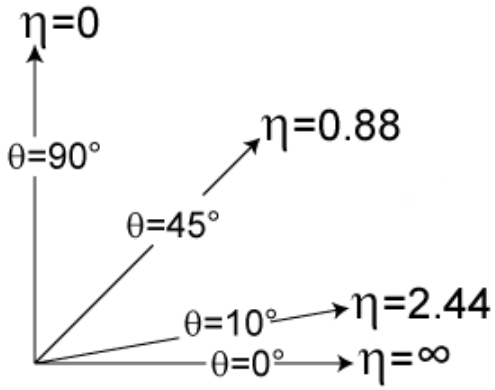

η: Pseudorapidity $\eta \equiv -\ln\left(\tan[\theta/2]\right)$.

ϕ: Azimuthal angle on the plane perpendicular to the beam axis.

p_T: Three-momentum projected on transverse plane (transverse momentum).

y: Rapidity $y \equiv \frac{1}{2}\ln\left(\frac{E+p_z}{E-p_z}\right)$. ($\eta \to y$ in $m \to 0$ limit)

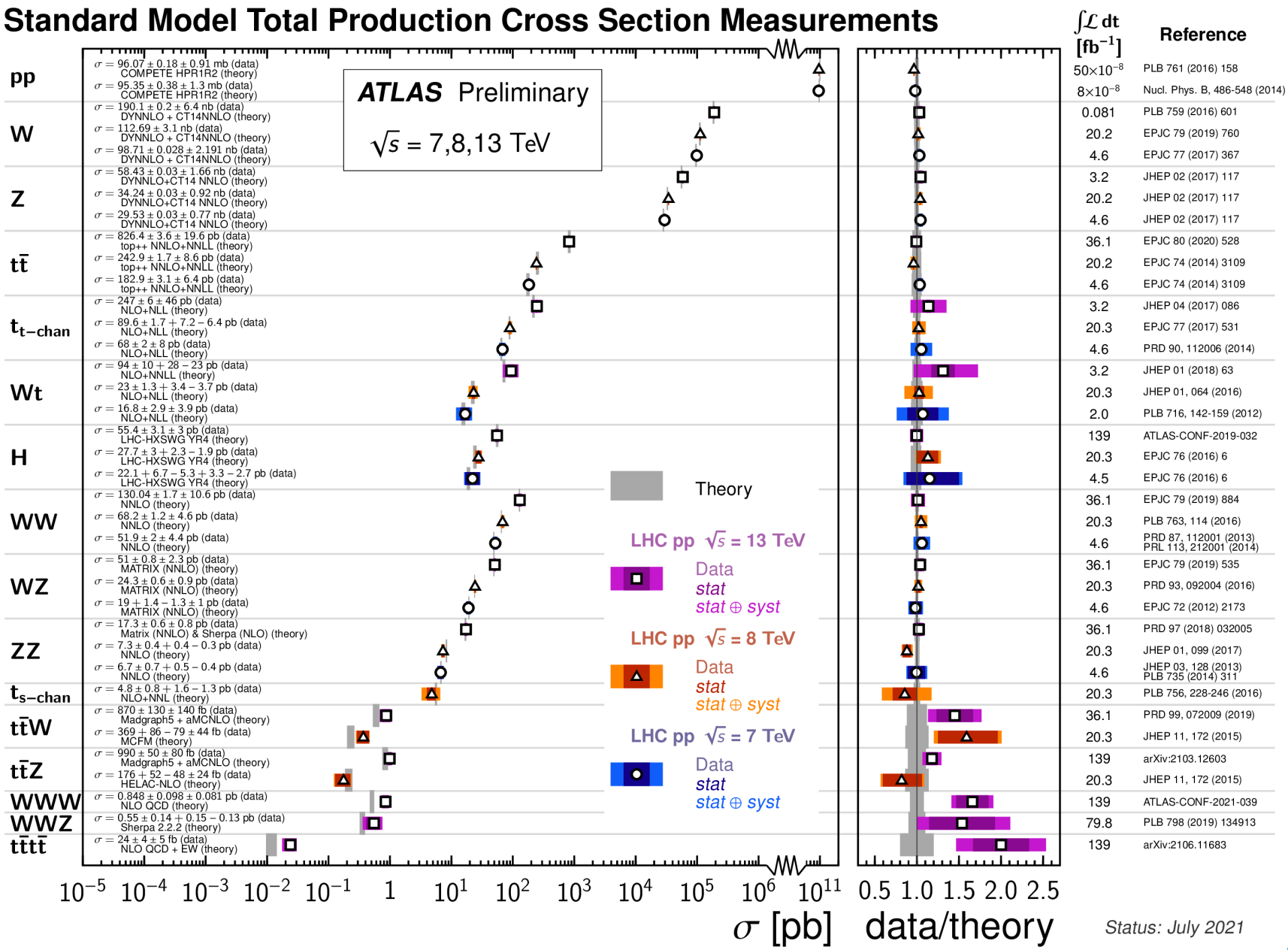
Standard Model Total Production Cross Section Measurements
ATLAS Preliminary
√s = 7,8,13 TeV
Theory
LHC pp √s = 13 TeV
Data
stat
stat ⊕ syst
LHC pp √s = 8 TeV
Data
stat
stat ⊕ syst
LHC pp √s = 7 TeV
Data
stat
stat ⊕ syst
pp
W
Z
tt̄
t_t−chan
Wt
H
WW
WZ
ZZ
t_s−chan
tt̄W
tt̄Z
WWW
WWZ
tt̄tt̄
σ = 96.07 ± 0.18 ± 0.91 mb (data) COMPETE HPR1R2 (theory)
σ = 95.35 ± 0.38 ± 1.3 mb (data) COMPETE HPR1R2 (theory)
σ = 190.1 ± 0.2 ± 6.4 nb (data) DYNNLO + CT14NNLO (theory)
σ = 112.69 ± 3.1 nb (data) DYNNLO + CT14NNLO (theory)
σ = 98.71 ± 0.028 ± 2.191 nb (data) DYNNLO + CT14NNLO (theory)
σ = 58.43 ± 0.03 ± 1.66 nb (data) DYNNLO+CT14 NNLO (theory)
σ = 34.24 ± 0.03 ± 0.92 nb (data) DYNNLO+CT14 NNLO (theory)
σ = 29.53 ± 0.03 ± 0.77 nb (data) DYNNLO+CT14 NNLO (theory)
σ = 826.4 ± 3.6 ± 19.6 pb (data) top++ NNLO+NNLL (theory)
σ = 242.9 ± 1.7 ± 8.6 pb (data) top++ NNLO+NNLL (theory)
σ = 182.9 ± 3.1 ± 6.4 pb (data) top++ NNLO+NNLL (theory)
σ = 247 ± 6 ± 46 pb (data) NLO+NLL (theory)
σ = 89.6 ± 1.7 + 7.2 − 6.4 pb (data) NLO+NLL (theory)
σ = 68 ± 2 ± 8 pb (data) NLO+NLL (theory)
σ = 94 ± 10 + 28 − 23 pb (data) NLO+NNLL (theory)
σ = 23 ± 1.3 + 3.4 − 3.7 pb (data) NLO+NLL (theory)
σ = 16.8 ± 2.9 ± 3.9 pb (data) NLO+NLL (theory)
σ = 55.4 ± 3.1 ± 3 pb (data) LHC-HXSWG YR4 (theory)
σ = 27.7 ± 3 + 2.3 − 1.9 pb (data) LHC-HXSWG YR4 (theory)
σ = 22.1 + 6.7 − 5.3 + 3.3 − 2.7 pb (data) LHC-HXSWG YR4 (theory)
σ = 130.04 ± 1.7 ± 10.6 pb (data) NNLO (theory)
σ = 68.2 ± 1.2 ± 4.6 pb (data) NNLO (theory)
σ = 51.9 ± 2 ± 4.4 pb (data) NNLO (theory)
σ = 51 ± 0.8 ± 2.3 pb (data) MATRIX (NNLO) (theory)
σ = 24.3 ± 0.6 ± 0.9 pb (data) MATRIX (NNLO) (theory)
σ = 19 + 1.4 − 1.3 ± 1 pb (data) MATRIX (NNLO) (theory)
σ = 17.3 ± 0.6 ± 0.8 pb (data) Matrix (NNLO) & Sherpa (NLO) (theory)
σ = 7.3 ± 0.4 + 0.4 − 0.3 pb (data) NNLO (theory)
σ = 6.7 ± 0.7 + 0.5 − 0.4 pb (data) NNLO (theory)
σ = 4.8 ± 0.8 + 1.6 − 1.3 pb (data) NLO+NNL (theory)
σ = 870 ± 130 ± 140 fb (data) Madgraph5 + aMCNLO (theory)
σ = 369 + 86 − 79 ± 44 fb (data) MCFM (theory)
σ = 990 ± 50 ± 80 fb (data) Madgraph5 + aMCNLO (theory)
σ = 176 + 52 − 48 ± 24 fb (data) HELAC-NLO (theory)
σ = 0.848 ± 0.098 ± 0.081 pb (data) NLO QCD (theory)
σ = 0.55 ± 0.14 + 0.15 − 0.13 pb (data) Sherpa 2.2.2 (theory)
σ = 24 ± 4 ± 5 fb (data) NLO QCD + EW (theory)
∫L dt [fb⁻¹]
Reference
50×10⁻⁸ PLB 761 (2016) 158
8×10⁻⁸ Nucl. Phys. B, 486-548 (2014)
0.081 PLB 759 (2016) 601
20.2 EPJC 79 (2019) 760
4.6 EPJC 77 (2017) 367
3.2 JHEP 02 (2017) 117
20.2 JHEP 02 (2017) 117
4.6 JHEP 02 (2017) 117
36.1 EPJC 80 (2020) 528
20.2 EPJC 74 (2014) 3109
4.6 EPJC 74 (2014) 3109
3.2 JHEP 04 (2017) 086
20.3 EPJC 77 (2017) 531
4.6 PRD 90, 112006 (2014)
3.2 JHEP 01 (2018) 63
20.3 JHEP 01, 064 (2016)
2.0 PLB 716, 142-159 (2012)
139 ATLAS-CONF-2019-032
20.3 EPJC 76 (2016) 6
4.5 EPJC 76 (2016) 6
36.1 EPJC 79 (2019) 884
20.3 PLB 763, 114 (2016)
4.6 PRD 87, 112001 (2013) PRL 113, 212001 (2014)
36.1 EPJC 79 (2019) 535
20.3 PRD 93, 092004 (2016)
4.6 EPJC 72 (2012) 2173
36.1 PRD 97 (2018) 032005
20.3 JHEP 01, 099 (2017)
4.6 JHEP 03, 128 (2013) PLB 735 (2014) 311
20.3 PLB 756, 228-246 (2016)
36.1 PRD 99, 072009 (2019)
20.3 JHEP 11, 172 (2015)
139 arXiv:2103.12603
20.3 JHEP 11, 172 (2015)
139 ATLAS-CONF-2021-039
79.8 PLB 798 (2019) 134913
139 arXiv:2106.11683
10⁻⁵ 10⁻⁴ 10⁻³ 10⁻² 10⁻¹ 1 10¹ 10² 10³ 10⁴ 10⁵ 10⁶ 10¹¹
σ [pb]
0.5 1.0 1.5 2.0 2.5
data/theory
Status: July 2021

Beam background
Non-diffractive dijet production + uncorrelated proton from pileup or beam-halo activity. **Needs special treatment.**

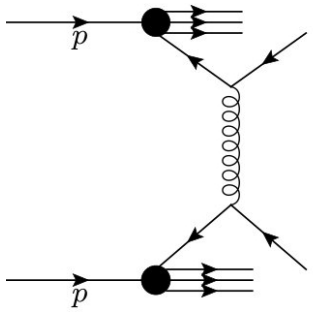

+ uncorrelated forward proton(s)

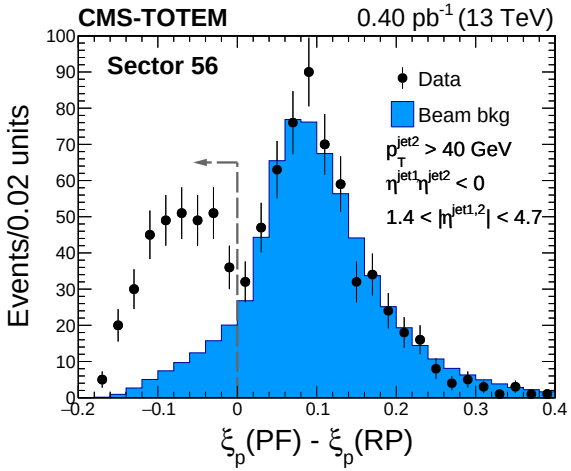

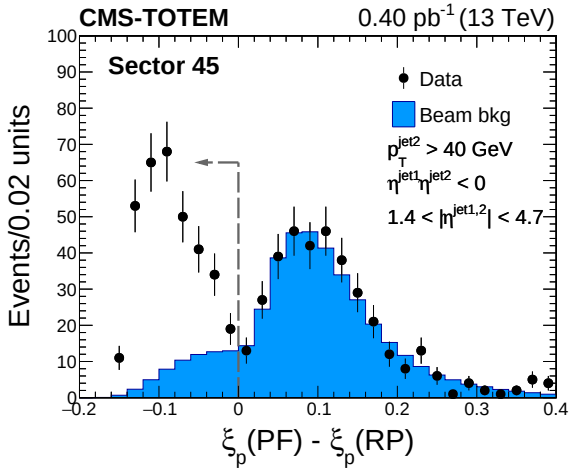

Bkg populates kinematically forbidden region $\xi_p(\mathrm{PF}) - \xi_p(\mathrm{RP}) > 0$, where $\xi_p(\mathrm{PF})$ is the fractional momentum loss calculated with CMS,

$\xi_p(\mathrm{PF}) = (\sum_i E_i \pm p_{z,i})/\sqrt{s}$, summing up **all** PF candidates in $|\eta| < 5.2$.

Beam-background estimated using an event mixing procedure: dijet events from the data paired with protons from zero-bias sample.

Charged particle multiplicity between jets + intact proton

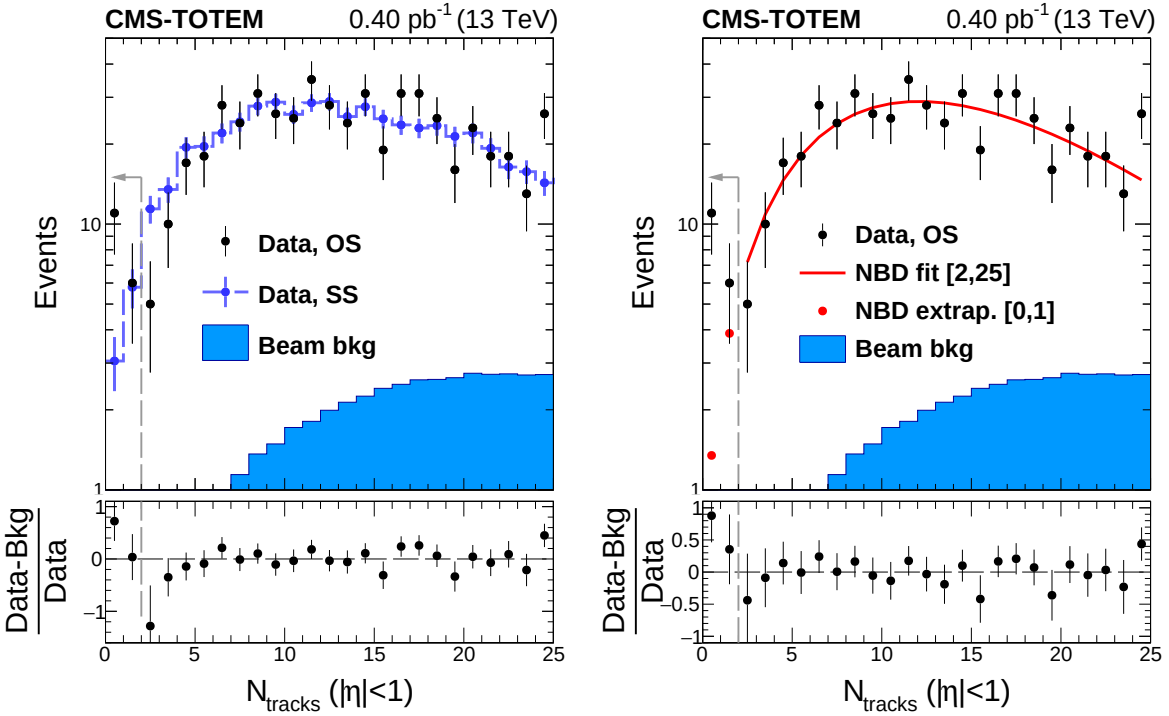

Similar techniques to estimate background from fluctuations in particle multiplicity:

- Orthogonal dijet sample approach: Two jets in same side w.r.t. fixed η region. Interval needs to be adjusted to account for boosts in SD dijet events (0.8 units in η).
- NBD approach: NBD is fit in $2 < N_{\text{tracks}} < 25$, and extrapolated down to $N_{\text{tracks}} = 0$. Different fit range accounts for lower mean N_{tracks} in events with intact protons.

Both approaches lead to an excess of events at low $N_{\text{tracks}} \rightarrow$ For the first time these events are studied!

Hard diffractive dijet production at 13 TeV with CMS and TOTEM

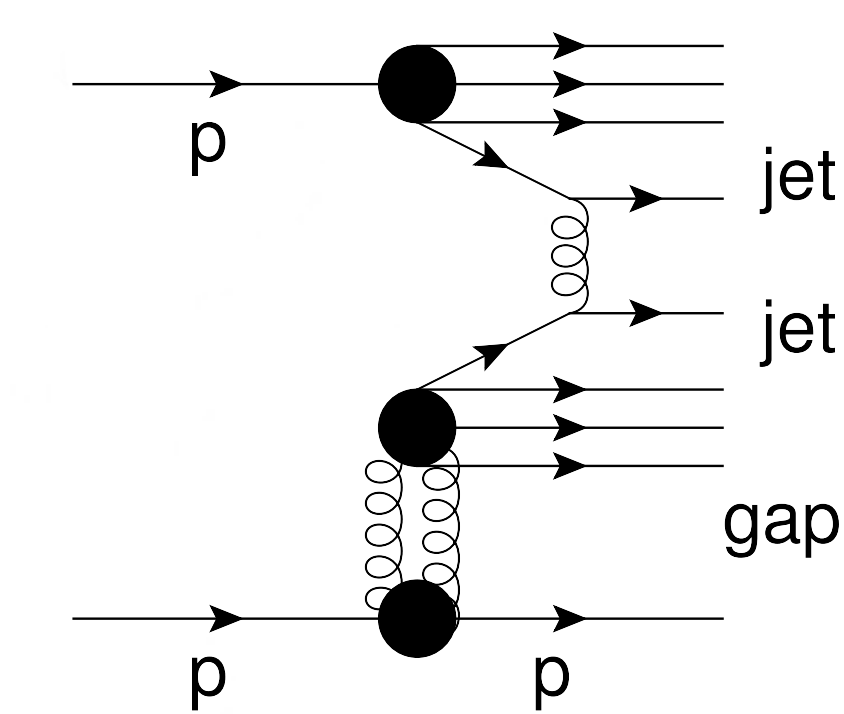

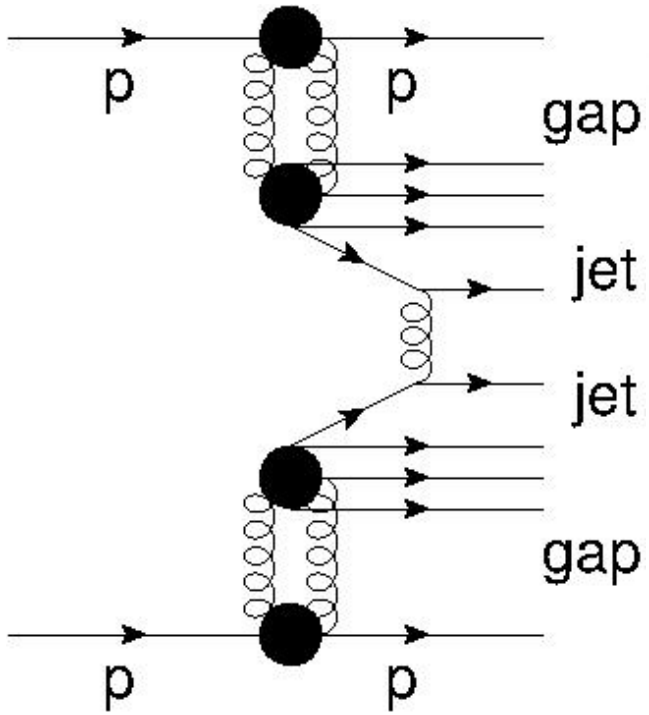

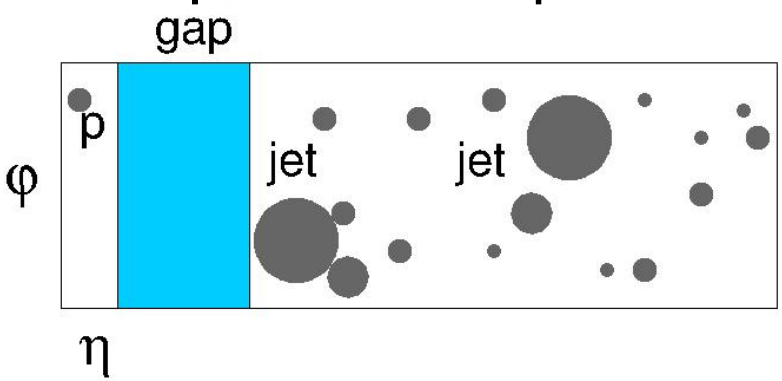

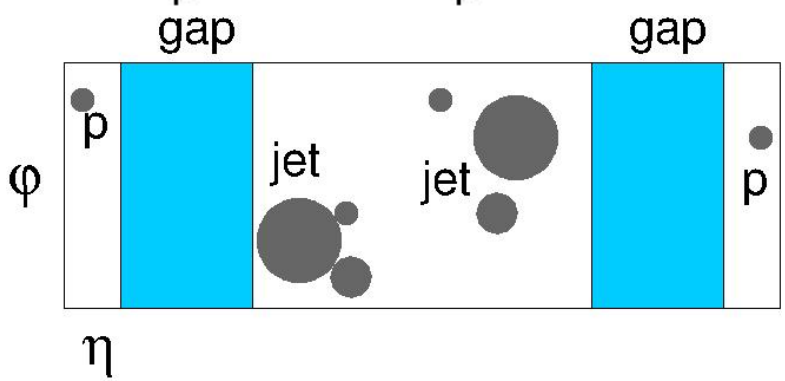

CMS-TOTEM work in progress

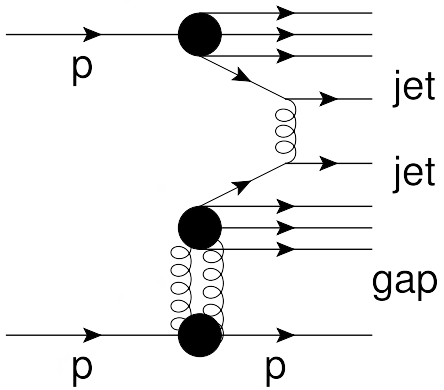

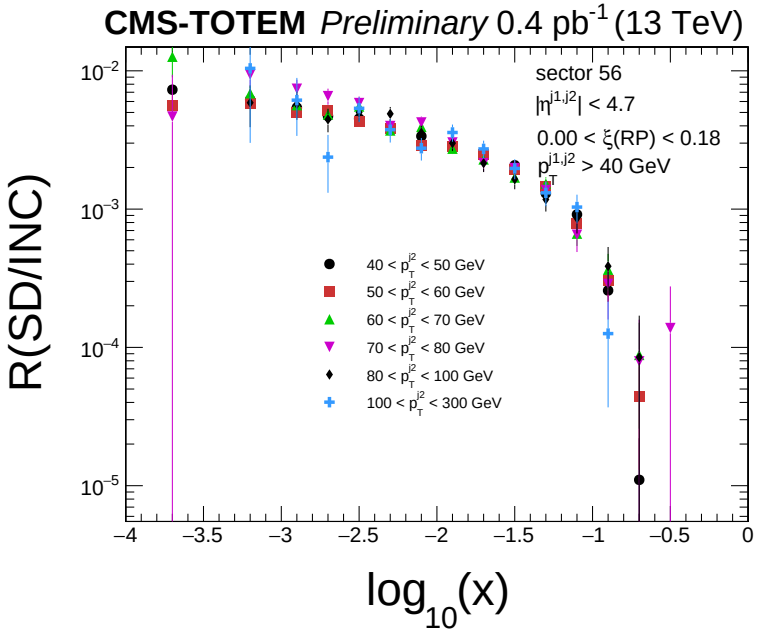

R(SD/INC) vs. x in bins of $p_T^{\mathbf{jet2}}$ (test of DGLAP evolution).

Scientific merit:

- Diffractive structure function of the proton in an extended kinematic range. $\rightarrow$ **Poorly-understood part of the proton gluonic component.**
- Test DGLAP evolution of diffractive PDFs.
- Test Regge factorization hypothesis (separation of "pomeron flux" and "pomeron PDF").
- If Regge factorization holds, constrain quark-gluon densities of the pomeron.

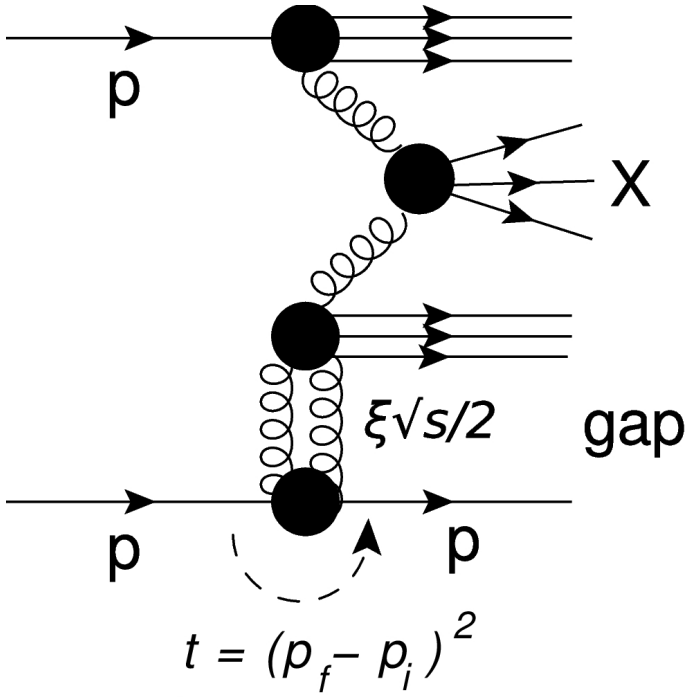

Pomeron exchange

- QCD two-gluon exchange process, larger cross sections.
- Studied in low-luminosity runs.

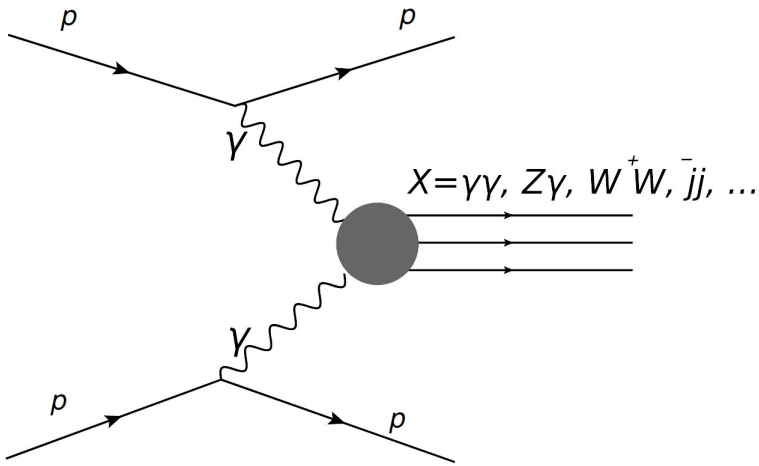

Photon exchange

- **The photon is a color-singlet particle**; protons may remain intact.
- QED process → smaller cross sections.
- Focus on higher invariant masses → **probe of physics beyond the SM.**

Particle physics phenomenology work

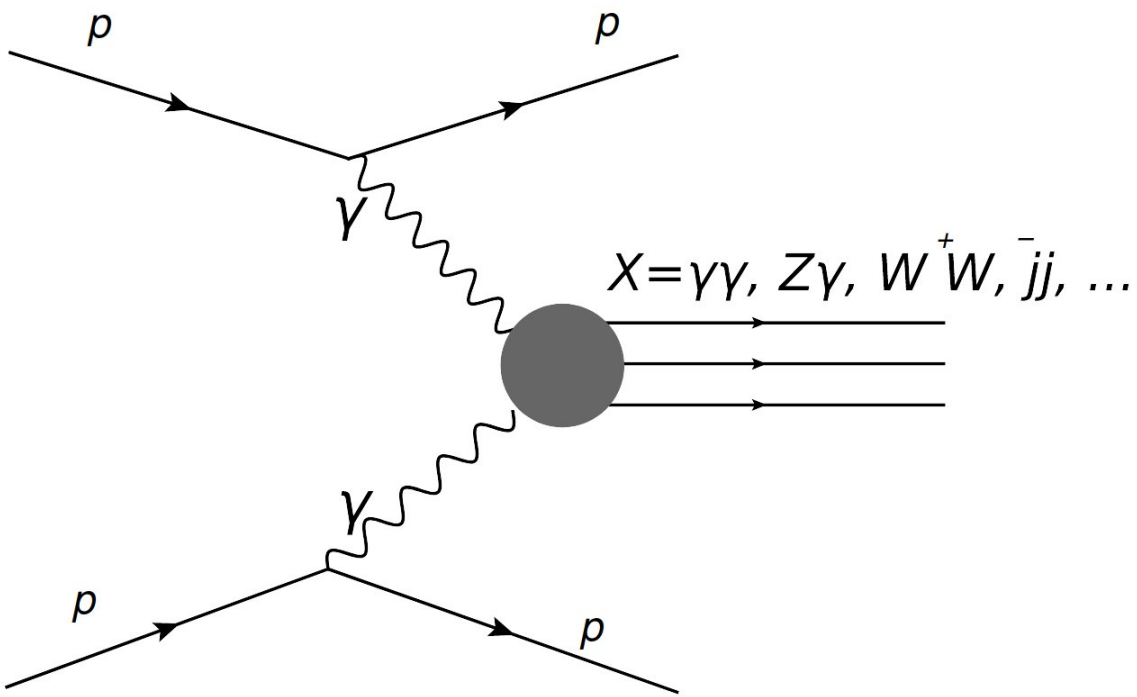

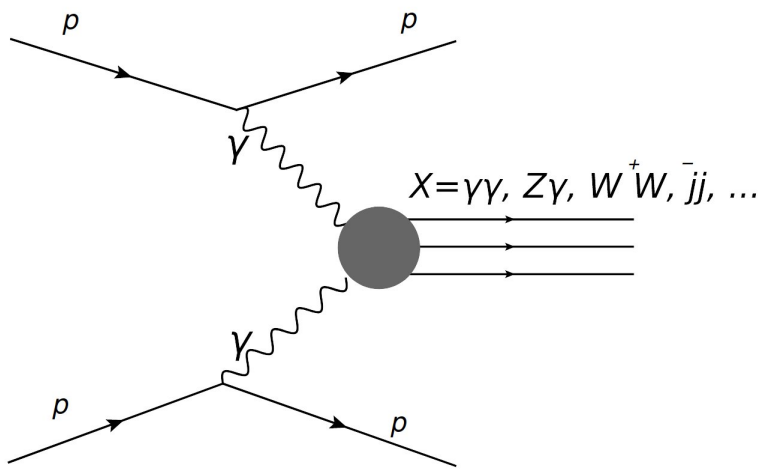

Full reconstruction of final-state!

- Quasi-real photon exchange is well-known theoretically (*equivalent photon approximation*).
- Typical acceptance $0.015 \lesssim \xi \lesssim 0.15$ ($350 \lesssim m_X \lesssim 2000$ GeV).
- The central system and intact protons are kinematically correlated:

$$m_X = m_{pp} \equiv \sqrt{\xi_1 \xi_2 s}, \qquad y_X = y_{pp} \equiv \frac{1}{2} \ln\left(\frac{\xi_1}{\xi_2}\right) \tag{3}$$

- Forward spectrometer systems in operation during Run-2: the CMS-TOTEM Precision Proton Spectrometer (PPS) and ATLAS Forward Proton (AFP).
- **As part of my PhD work, I implemented numerous processes in the Forward Physics Monte Carlo (FPMC) generator.**

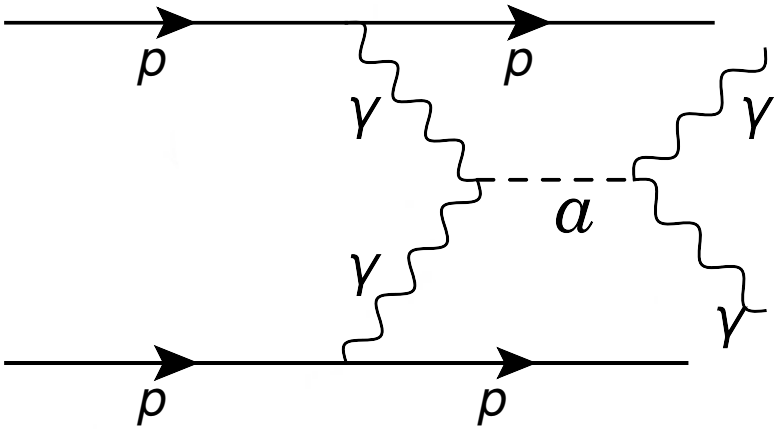

Implemented in the FPMC generator.

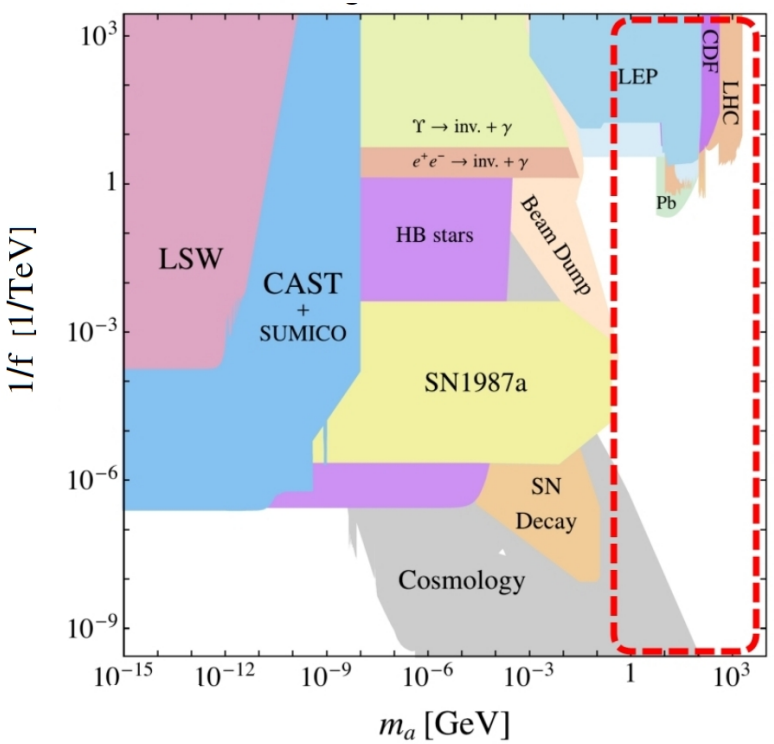

- Pseudoscalars weakly coupled to SM particles are known as ALPs (a).
- ALP–photon interaction modelled with dimension-five operator,

$$\mathcal{L}^{\text{eff}} = \frac{1}{f} a F^{\mu\nu} \tilde{F}_{\mu\nu}$$

- Strongly constrained for $m_a \approx 10^{-15} - 1$ GeV.
- **For ALPs with masses $m_a > 1$ GeV, collider probes are necessary.**
- ALPs would induce anomalous scattering of **light-by-light**.
  $\rightarrow$ **Can search for high-mass ALP in $pp \to p\gamma\gamma p$ scattering.**

Irreducible backgrounds

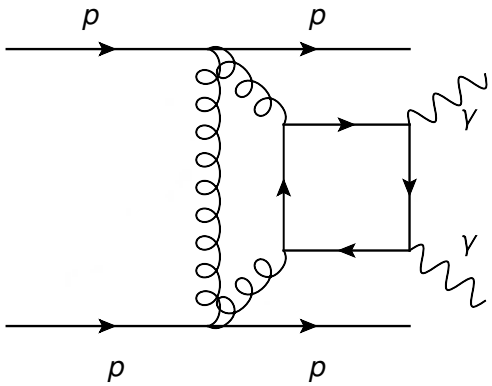

Two-gluon exchange, largely suppressed at $m_{\gamma\gamma} > 600$ GeV (about 10^{-3} fb).

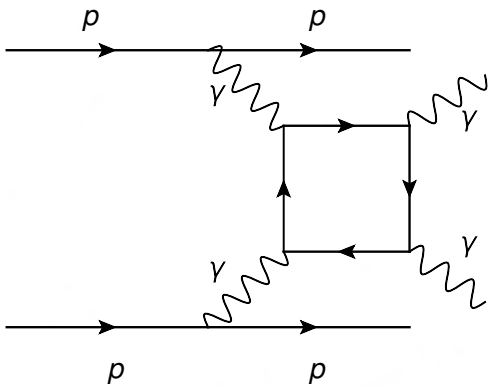

SM light-by-light scattering (10^{-1} fb for $m_{\gamma\gamma} > 600$ GeV).

Reducible backgrounds

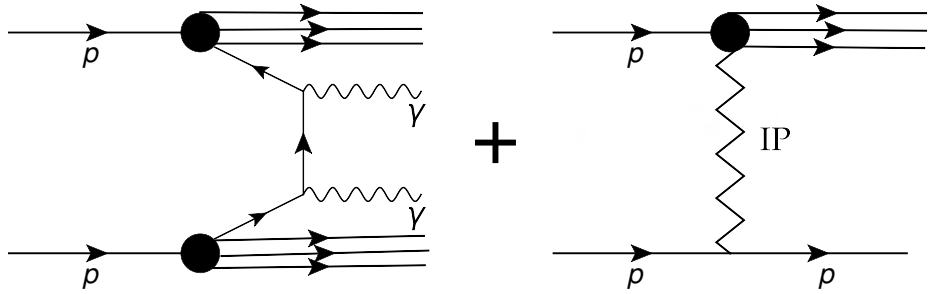

QCD-initiated $\gamma\gamma + X$ with protons from pileup.

Very large background, but reducible with forward-central correlations.

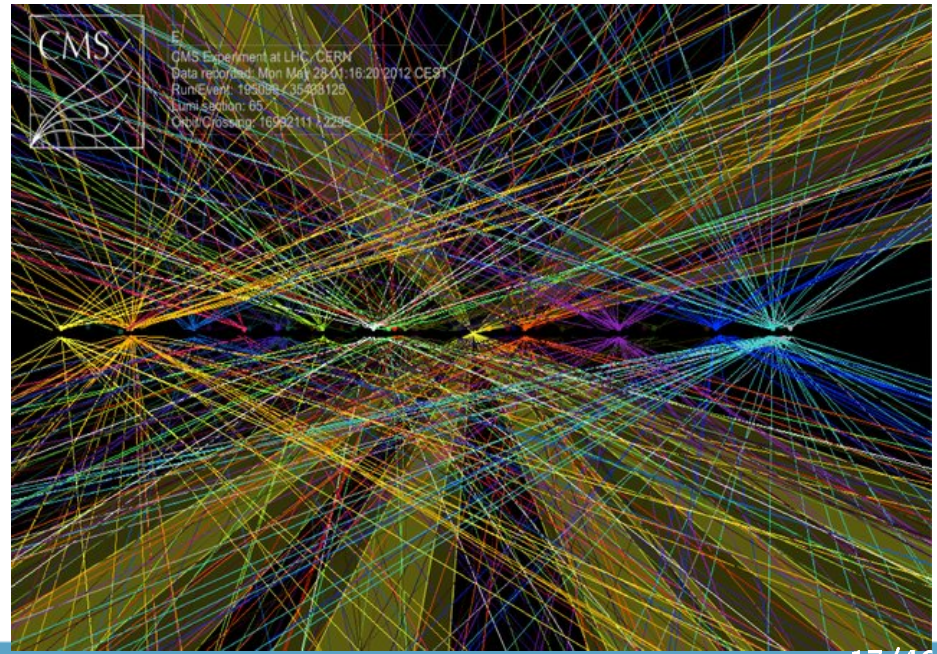

Selection of $pp \to p\gamma\gamma p$ events

Signature:

- Two high p_T, back-to-back isolated photons.
- Two forward intact protons in the RPs.

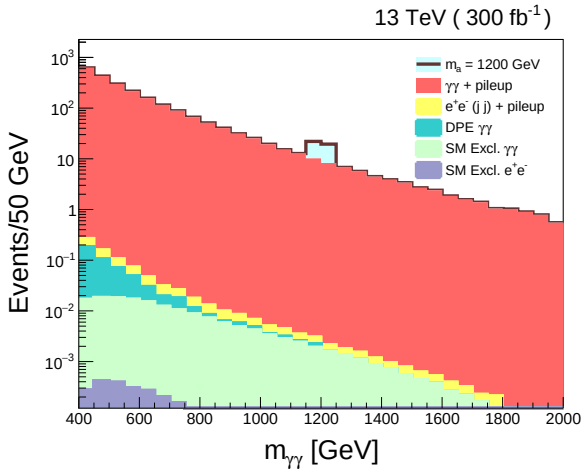

CB, S. Fichet, G. von Gersdorff, C. Royon, *JHEP* **06** (2018) 131, arXiv:1803.10835

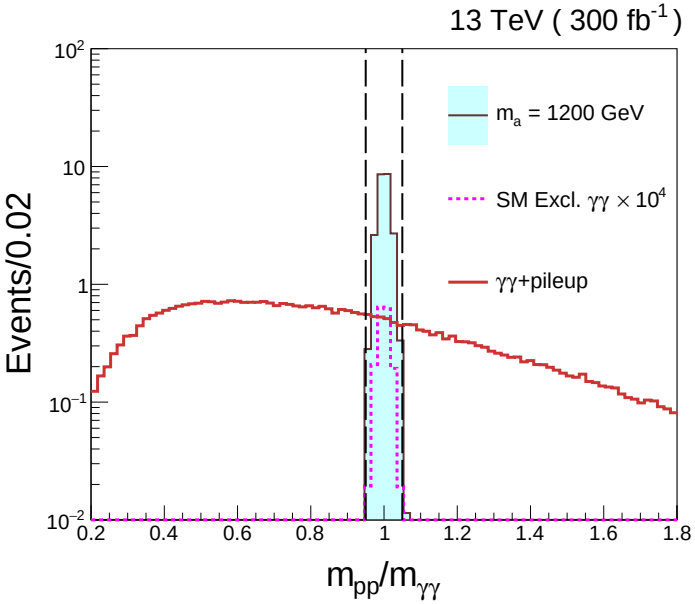

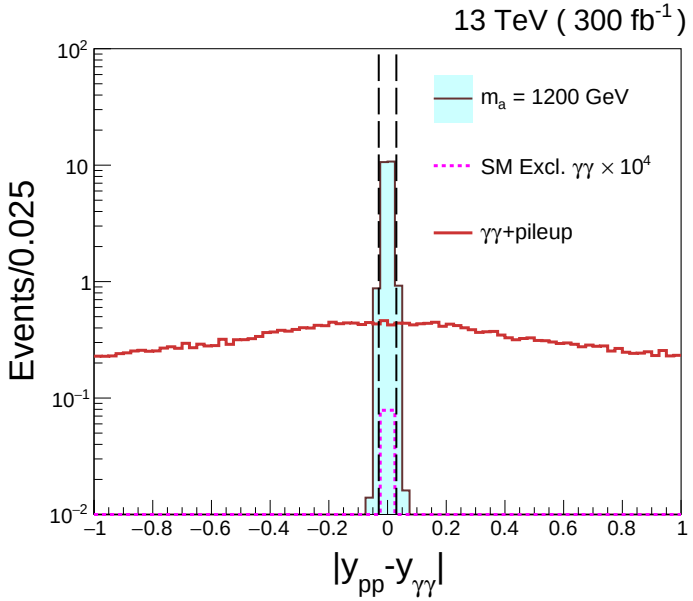

We can isolate signal from **background** by looking at forward-central kinematic correlations.

Projections on mass m_a versus coupling strength $1/f_a$ plane

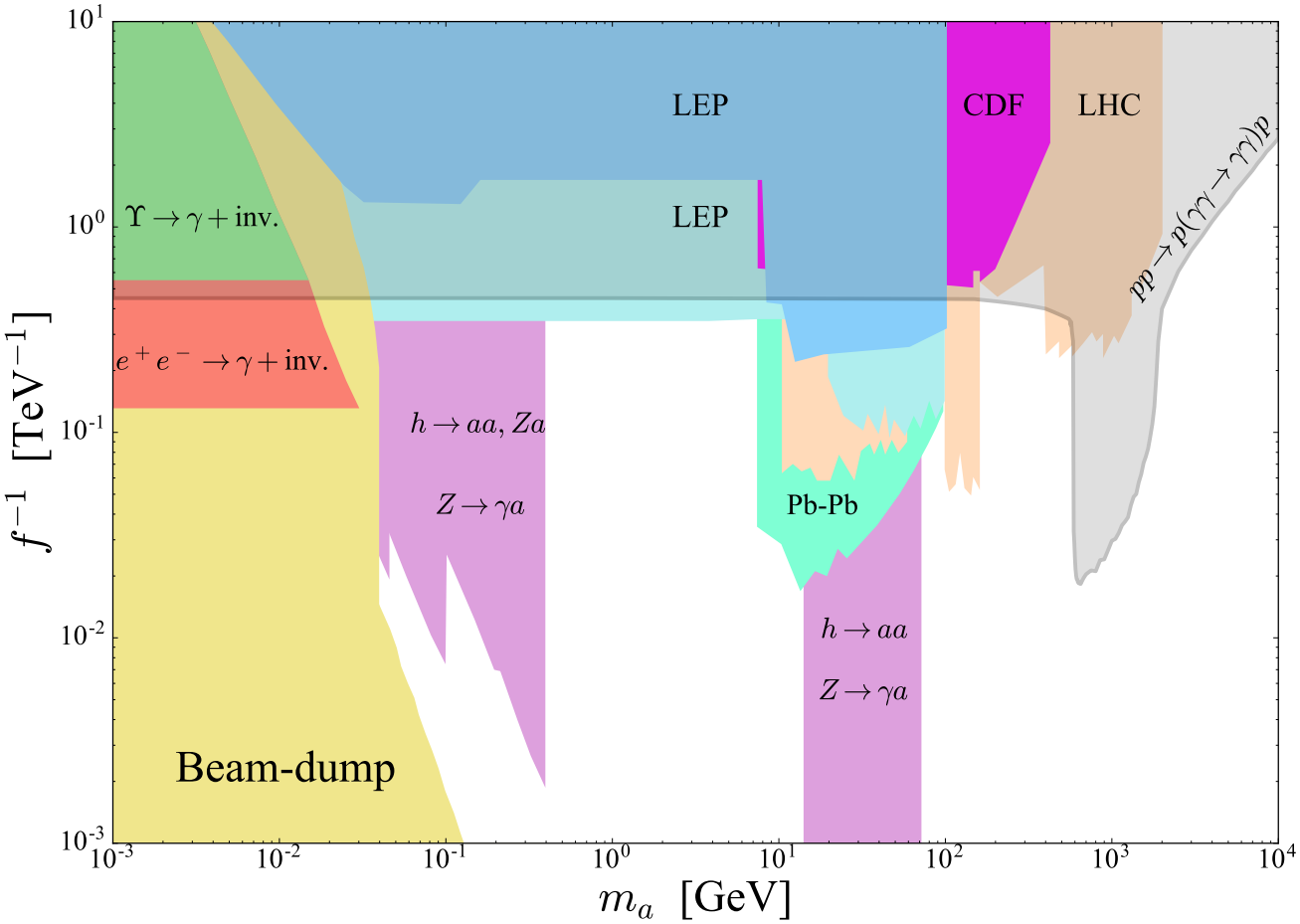

CB, S. Fichet, G. von Gersdorff, C. Royon, *JHEP* **06** (2018) 131, arXiv:1803.10835

Best sensitivity at $600 < m_a < 2000$ GeV, with $1/f = 10^{-2} - 10^{-1}$ TeV^{-1}.

Complements PbPb$\to$ PbPb $\gamma\gamma$ at low masses.

Extension with ultraperipheral ArAr and pPb collisions

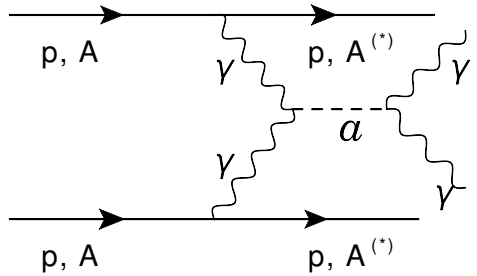

We analyzed ArAr$\to$ Ar$\gamma\gamma$Ar at $\sqrt{s_{\mathrm{NN}}} = 7$ TeV and pPb$\to$p$\gamma\gamma$Pb collisions at 8.16 TeV, where the photons have $E_{T1,2}^{\gamma} > 3$ GeV and $|\eta| < 2.5$.

Complements parameter space covered by pp and PbPb collisions.

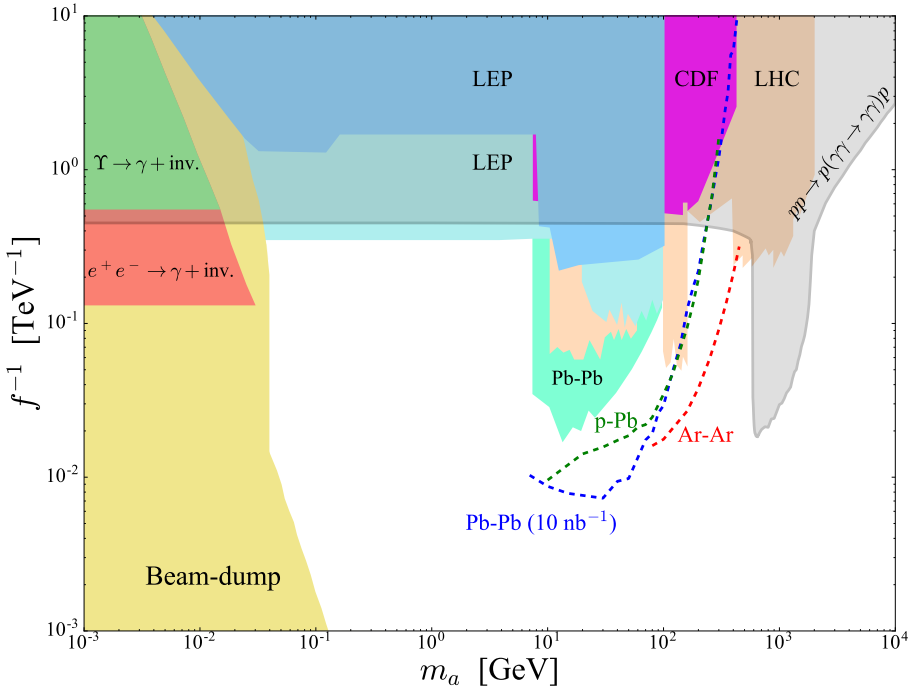

CB, S. Hassani, L. Schoeffel, C. Royon, *Phys. Lett. B* **795** (2019) 339, arXiv:1903.04151

Anomalous $\gamma\gamma\gamma Z$ couplings in exclusive γZ production:

CB, S. Fichet, G. von Gersdorff, C. Royon, *JHEP* **1706** (2017) 142, arXiv:1703.10600

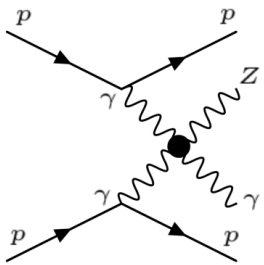

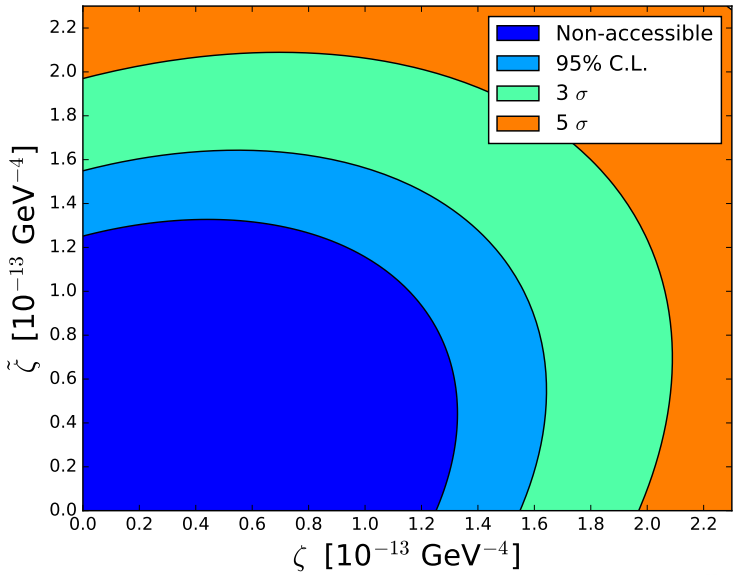

Projected limits on $\gamma\gamma\gamma Z$ coupling coefficients are superior to those based on rare decays of $Z \to \gamma\gamma\gamma$ **by three orders of magnitude.**

$\gamma\gamma \to W^+W^-$ in hadronic and semi-leptonic channels

CB, G. Biagi, G. Legras, C. Royon, *JHEP* 12 (2020) 165, arXiv:2009.08331

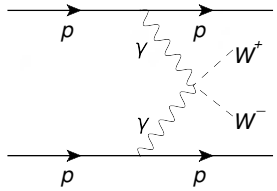

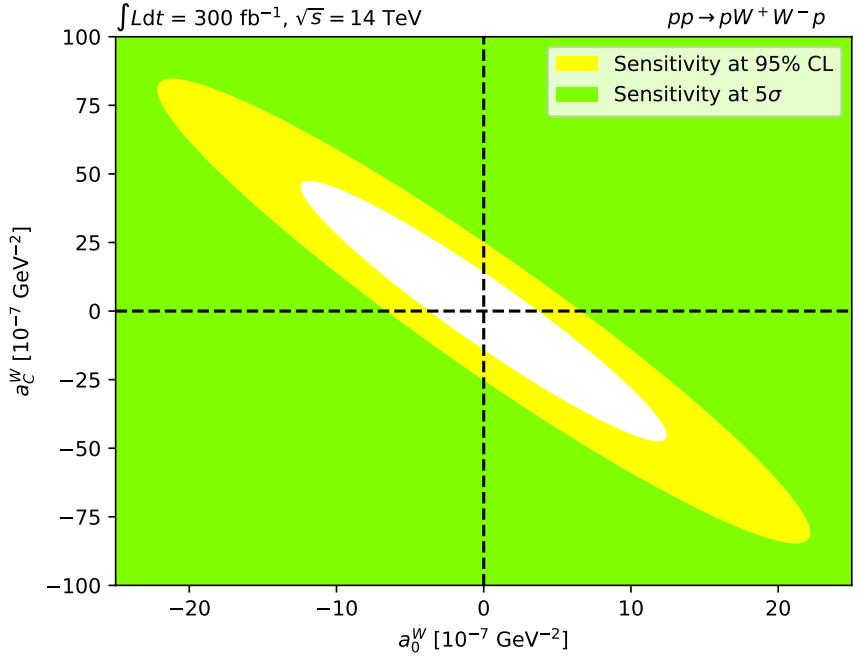

Huge improvement over $W^+W^- \to \ell^+\nu\ell^-\nu$ channel. **Enhanced sensitivity to high-mass new physics.**

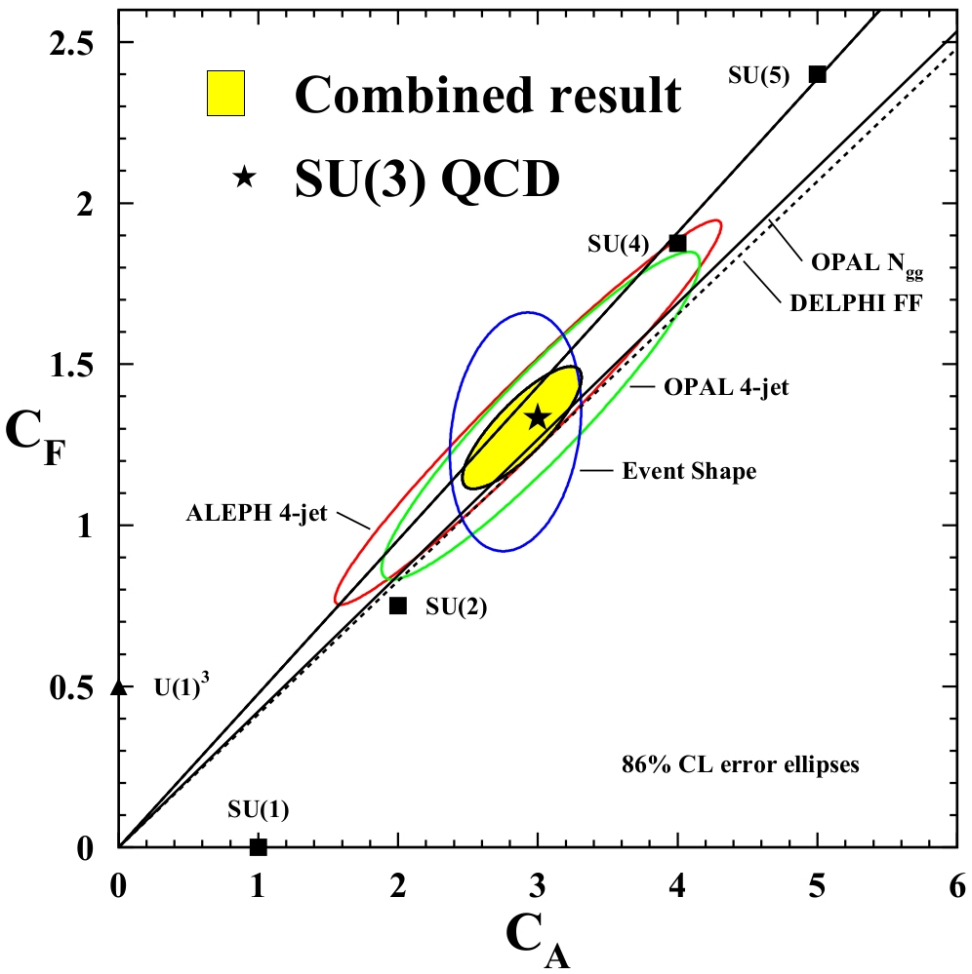

Color factors C_A and C_F from e^+e^- data **strongly favors SU(3) symmetry**.

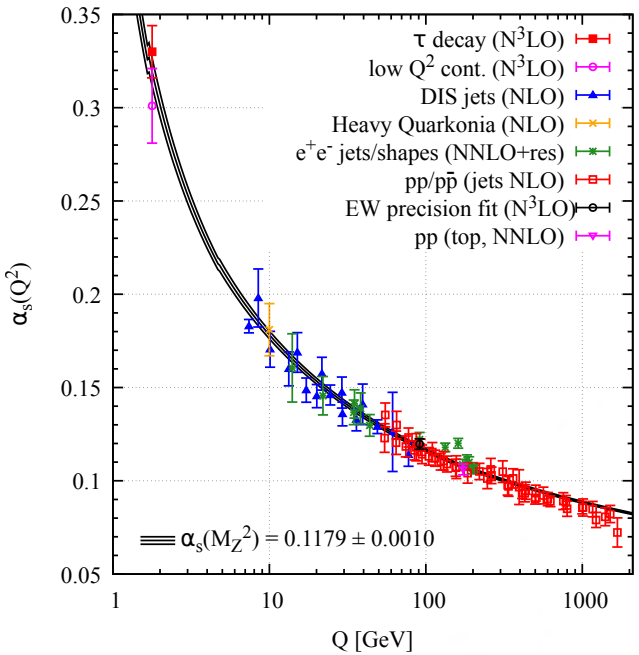

- We think we have the correct theory of the strong interaction (valid to distances as short as 10^{-20} meters).
- Only free parameters to be fit to data are the gauge coupling and quark masses.
- So that is it, *right?*...

The SM is the quantum field theory of elementary interactions.

It describes the strong, weak, and electromagnetic interactions between particles.

The particle content of the SM can be divided into four groups:

- **Quarks:** Spin-1/2 particles that are sensitive to the strong, weak, and electromagnetic interactions.
- **Leptons:** Spin-1/2 particles that are sensitive to the weak and electromagnetic interactions, **but not the strong force.**
- **Gauge vector bosons:** Eight gluons for the strong force, $W^{\pm}$ and Z bosons for the weak interactions, the photon for the electromagnetic interactions.
- **Higgs boson:** The only scalar boson, which appears upon spontaneously breaking the electroweak symmetry $\mathrm{SU}(2)_L \times \mathrm{U}(1)_Y \rightarrow \mathrm{U}(1)_{\mathrm{em}}$, confering mass to all the SM particles.

CMS is a general purpose detector at the LHC ring.

Several subdetector components dedicated to measure **most of the decay debris of proton-proton collisions in a $\approx 4\pi$ solid angle region**.

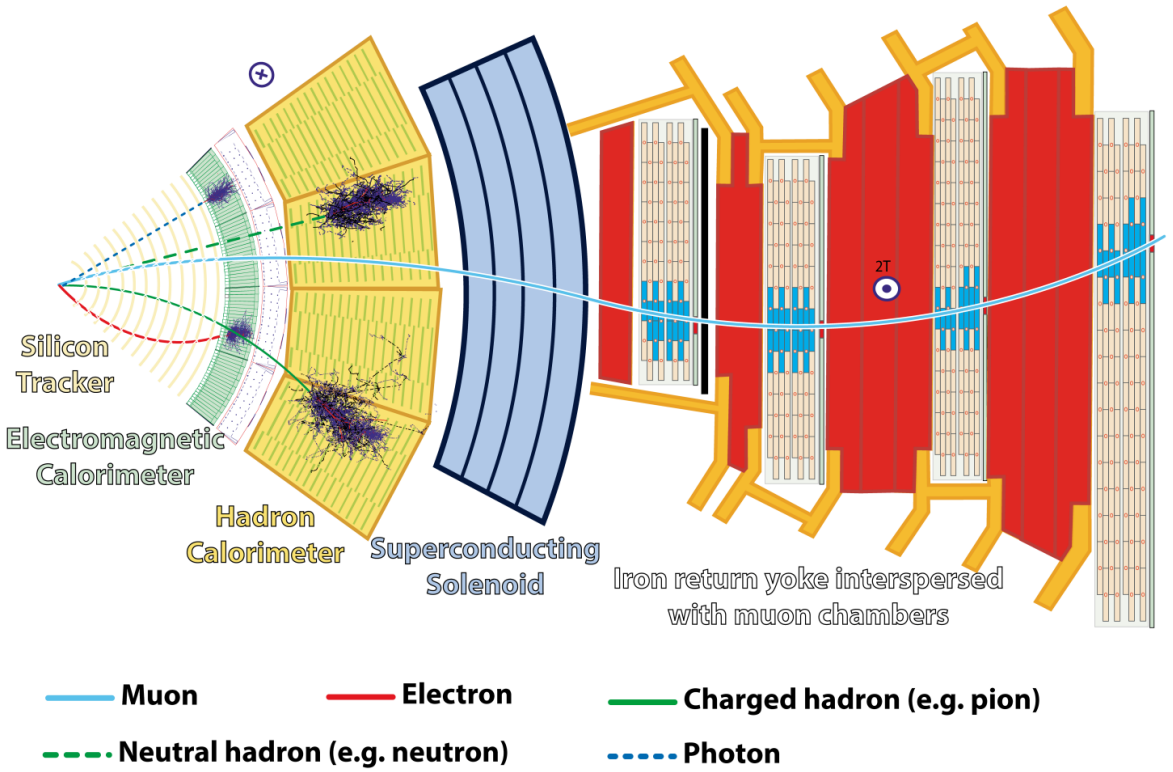

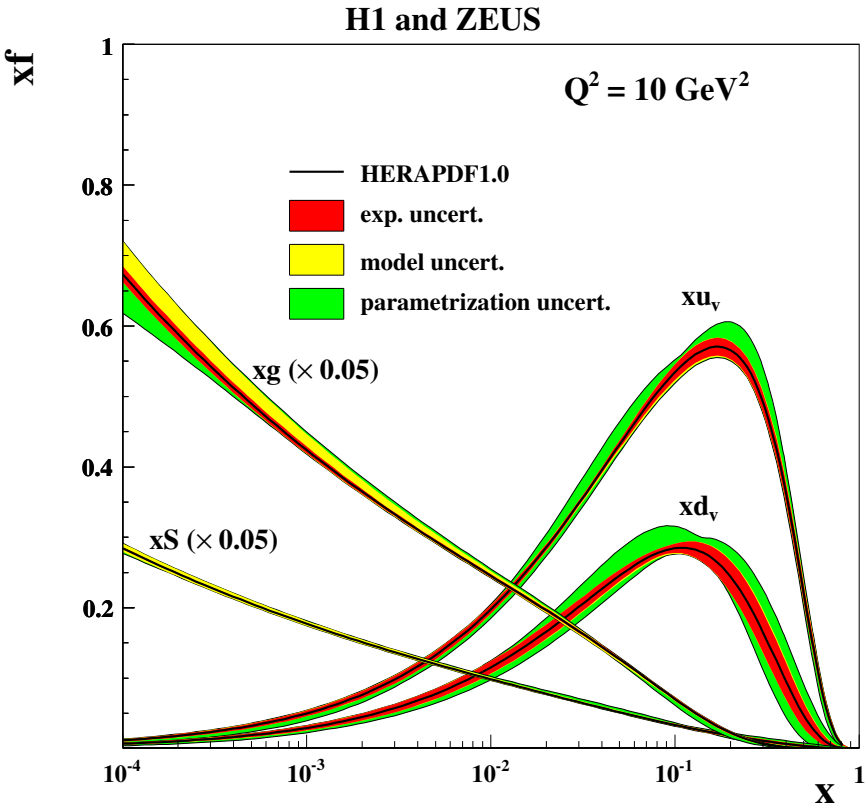

At small-x, small-Q^2, the gluon densities grow rapidly (driven by parton splitting $g \to gg$ or $q \to qg$ at low-x) $\to$ Regime of validity of BFKL evolution.

At very small-x and Q^2, one should expect that not only we have gluon splitting ($g \to gg$), but also gluon recombination ($gg \to g$) to avoid violation of unitarity. This is described by another set of QCD evolution equations (Balitsky-Kovchegov or Jalilian-Marian, Iancu, McLerran, Weigert, Leonidov and Kovner equations).

Charged particle multiplicity between jets + intact proton

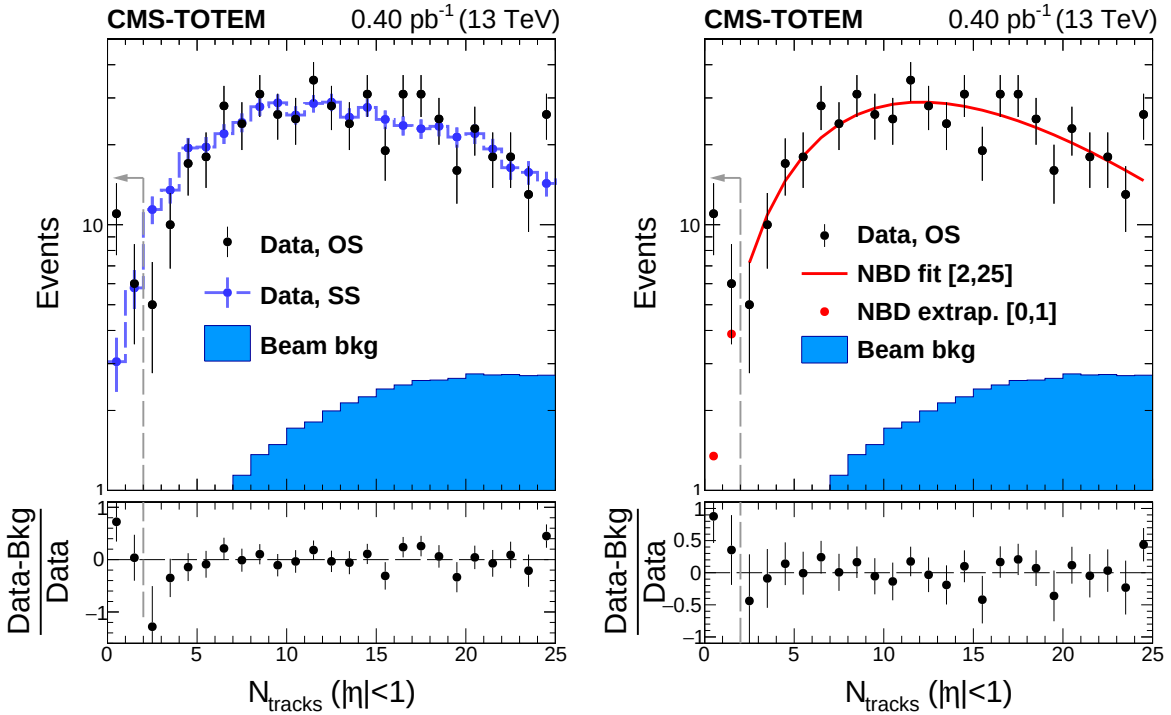

Similar techniques to estimate background from fluctuations in particle multiplicity:

- Orthogonal dijet sample approach: Two jets in same side w.r.t. fixed η region. Interval needs to be adjusted to account for boosts in SD dijet events (0.8 units in η).
- NBD approach: NBD is fit in $2 < N_{\text{tracks}} < 25$, and extrapolated down to $N_{\text{tracks}} = 0$. Different fit range accounts for lower mean N_{tracks} in events with intact protons.

Both approaches lead to an excess of events at low charged particle multiplicities $\rightarrow$ For the first time these events are studied!
Filled histogram represents beam background contribution.

Kinematic properties of jet-gap-jet candidates vs incl. dijet events

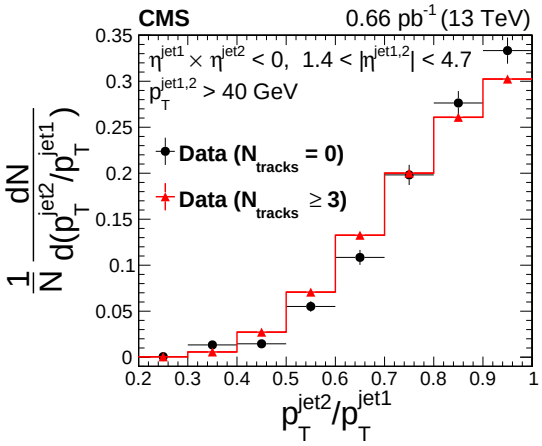

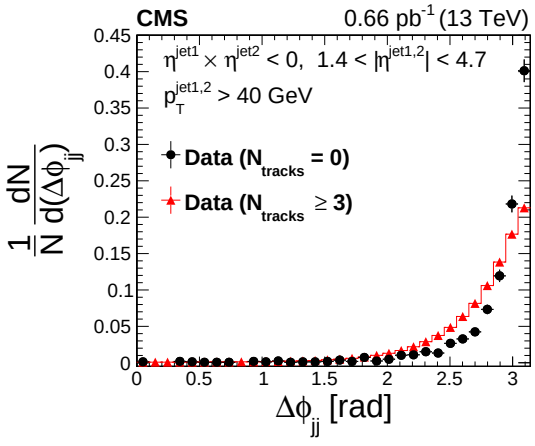

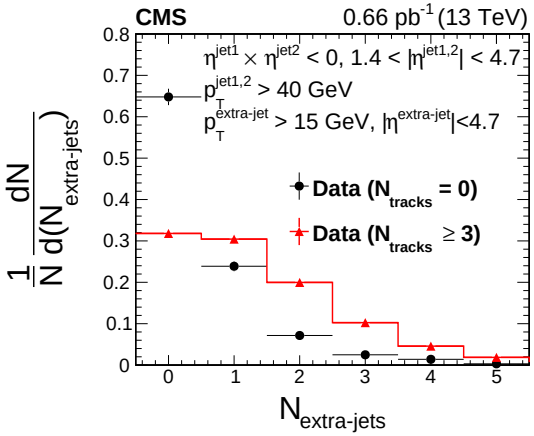

Normalized distributions in:

- p_T^{jet2}/p_T^{jet1}.
- $\Delta\phi_{jj} = |\phi^{jet1} - \phi^{jet2}|$
- Jet multiplicity $N_{extra\text{-}jets}$ for jets with $p_{T,extra\text{-}jet} > 15$ GeV.

Jet-gap-jet candidates with $N_{tracks} = 0$ and events dominated by color-exchange dijet events with $N_{tracks} \geq 3$.

Distributions reflect underlying quasielastic parton-parton scattering process topology.

In the leading logarithm approximation, only diagrams where parton emissions are *strongly ordered in rapidity*, with similar p_T, contribute to the cross section in the high energy limit:

$$y_1 \ll y_2 \ll y_3 \ll \cdots \ll y_{n-2} \ll y_{n-1} \ll y_n$$

$$p_{T,1} \approx p_{T,2} \approx p_{T,3} \approx \cdots p_{T,n-2} \approx p_{T,n-1} \approx p_{T,n} \gg \Lambda_{\mathrm{QCD}}$$

The contributions in the leading logarithm approximation are dominated by gluon branching.

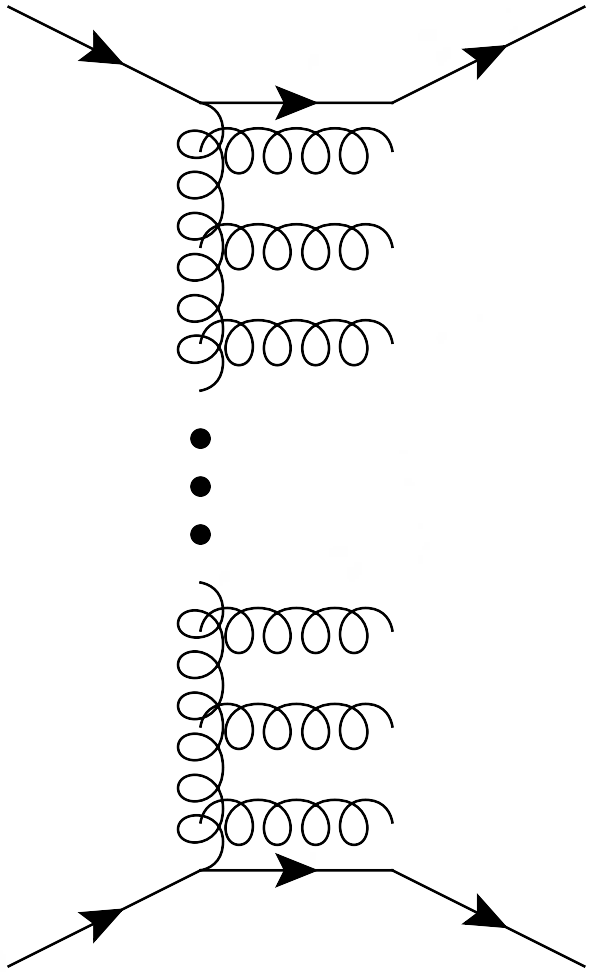

Systematic uncertainty table summary

Source	Jet-gap-jet (%)			Proton-gap-jet-gap-jet (%)
	$\Delta\eta_{jj}$	p_T^{jet2}	$\Delta\phi_{jj}$	
Jet energy scale	1.0–5.0	1.5–6.0	0.5–3.0	0.7
Track quality	6.0–8.0	5.4–8.0	1.5–8.0	8
Charged particle p_T threshold	2.0–5.8	1.6–4.0	1.1–5.8	11
Background subtraction method	4.7–15	2–15	12	28
NBD fit parameters	0.8–2.6	0.6–1.7	0.1–0.6	7.0
Functional form of the fit	2–7.3	1.4–8.0	0.6–7.8	11.5
NBD fit interval	—	—	—	12
Calorimeter energy scale	—	—	—	5.0
Horizontal dispersion	—	—	—	6.0
Fiducial selection requirements	—	—	—	2.6
Total	7–23	9–15	12–18.5	35

Relative systematic uncertainties in percentage on f_{CSE}. Uncertainty range is representative of the variation found in the jet-gap-jet fraction in bins of the kinematic variables of interest.

Although there is a short-distance physics mechanism for gap formation (pomeron exchange), spectator parton activity can destroy the central gap.

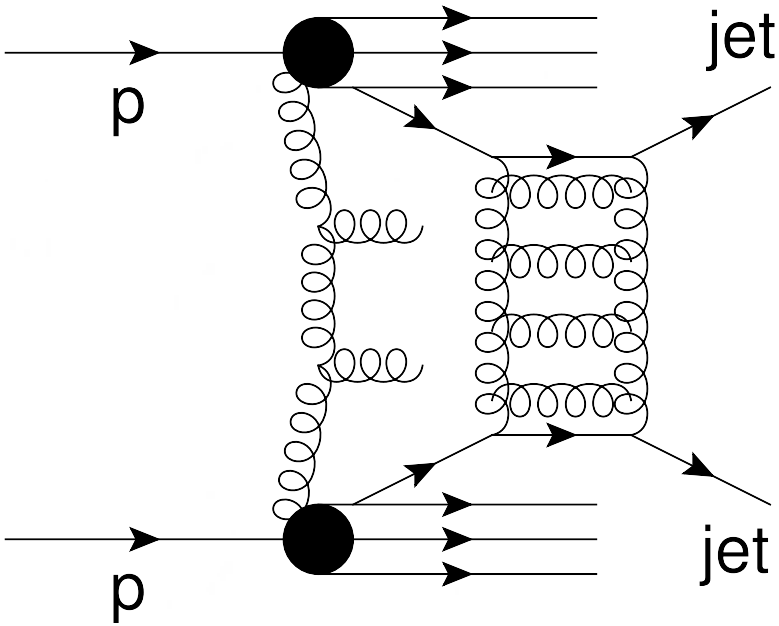

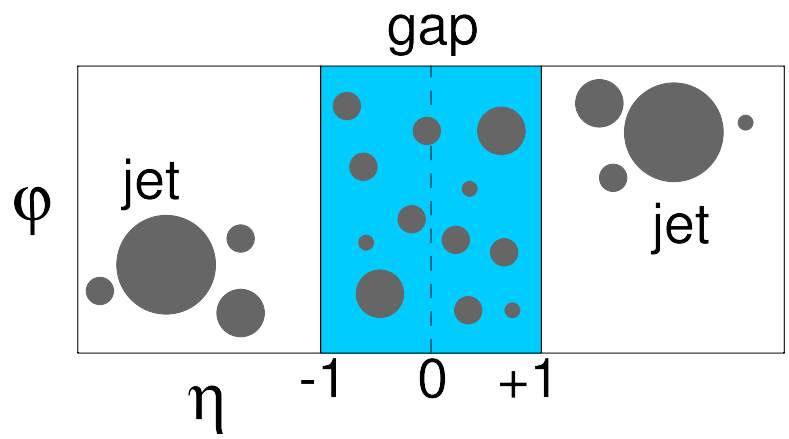

This is parametrized by means of a survival probability, $|\mathcal{S}|^2$, which reduces the visible cross section of jet-gap-jet events. Difficult to understand theoretically. $|\mathcal{S}|^2 = \mathcal{O}(10\%)$ at the LHC

The central η gap signature can be destroyed by multiple-parton interactions or rearrangement of the color field by soft-parton exchanges.

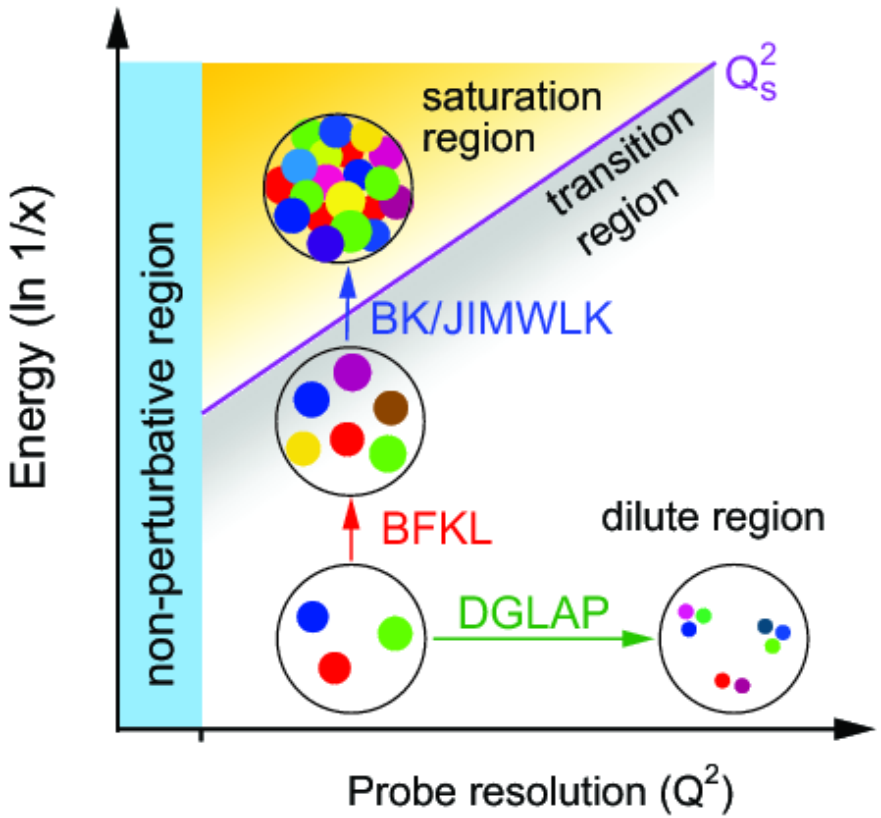

Owing to universality of strong interactions, QCD evolution equations of high-energy scattering arise also in PDF evolution in parton momentum fraction x at hard energy scales Q.

Dokshitzer–Gribov–Lipatov–Altarelli–Parisi (DGLAP): Evolution in Q^2 (resummation of $\alpha_s^n \ln^n(Q^2/Q_0^2)$) $\rightarrow$ Resolving more "smaller" partons with larger Q^2 at fixed x.

BFKL: Evolution in x (resummation of $\alpha_s^n \ln^n(1/x)$) $\rightarrow$ Larger parton densities at smaller x at fixed Q^2.

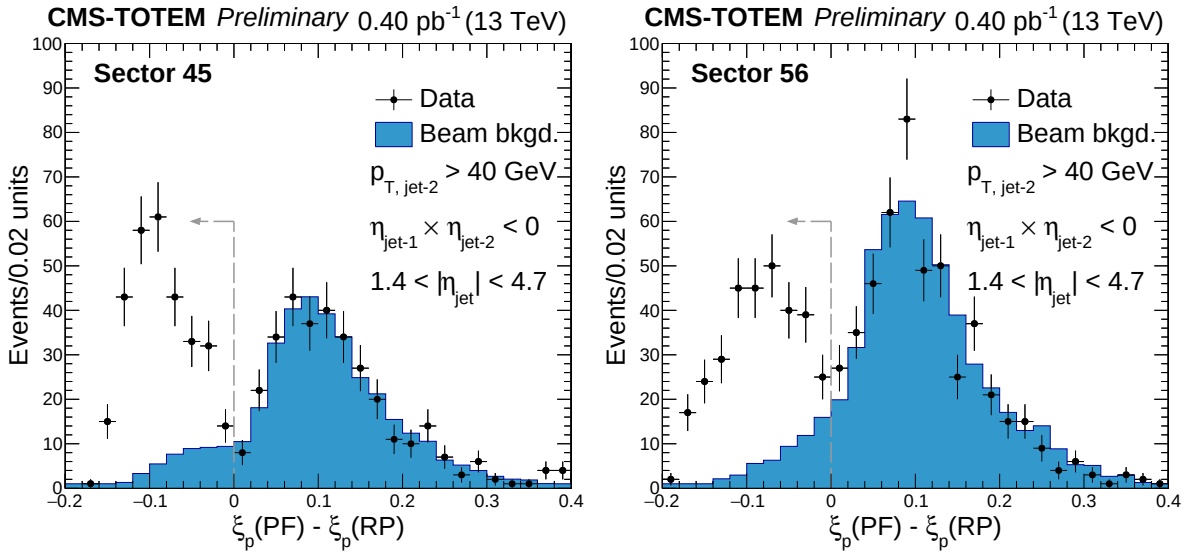

Estimated with event-mixing: inclusive dijet events paired with protons in zero-bias sample.

Requirement $\xi_p(\mathrm{PF}) - \xi_p(\mathrm{RP}) < 0$ indicated by dashed line. Region $\xi_p(\mathrm{PF}) - \xi_p(\mathrm{RP}) > 0$ is dominated by beam bkg contributions $\rightarrow$ Used as control region to estimate residual beam bkg in $\xi_p(\mathrm{PF}) - \xi_p(\mathrm{RP}) < 0$.

Beam background contributes 18.7 and 21.5% for protons in sector 45 and 56 in $\xi_p(\mathrm{PF}) - \xi_p(\mathrm{RP}) < 0$, respectively.

Consistent with other two-rapidity gap topology

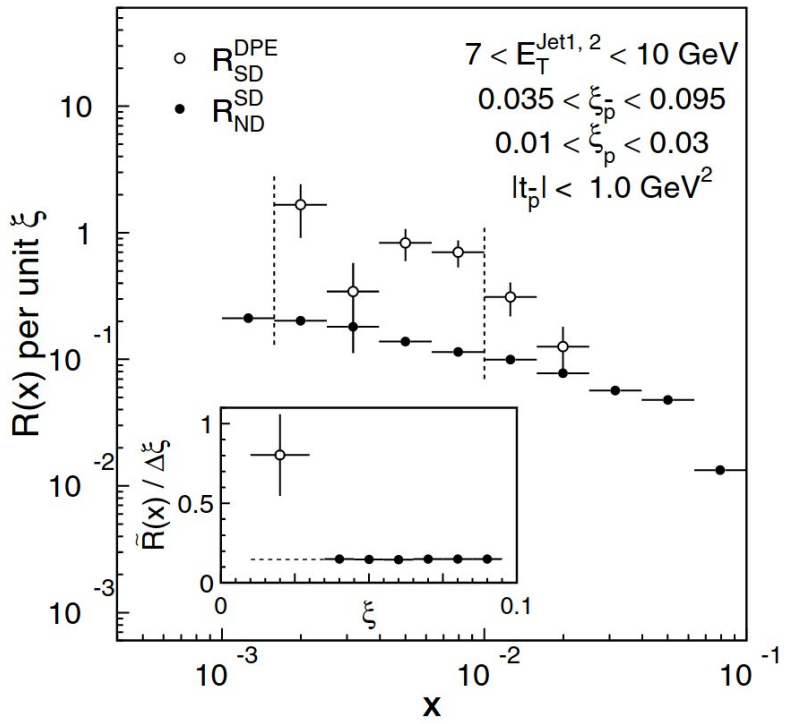

CDF studied double-pomeron exchange/single-diffractive dijet event ratios, compared them to single-diffractive/non-diffractive (**PRL85,4215**):

$\mathcal{R}$ = (DPE/SD) / (SD/ND) = 5.3 ± 1.9, different from factor of 1 expected from factorization. Comparison of gap-jet-jet-gap/gap-jet-jet topology.

Present CMS-TOTEM result finds a similar effect for a different two-gap topology (proton-gap-jet-gap-jet).

Inclusive dijet production + uncorrelated proton from residual pileup or beam halo activity (estimade from data).
Standard diffractive dijet production with no central gap (p-gap-jet-jet topology):

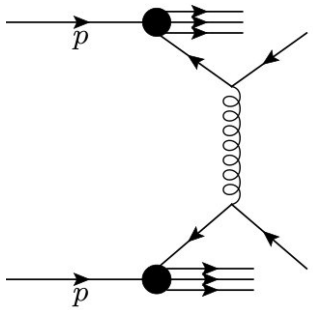

+ uncorrelated forward proton(s)

→ Fluctuations on particle multiplicity can lead to gaps. Needs to be subtracted (NBD and ES methods).

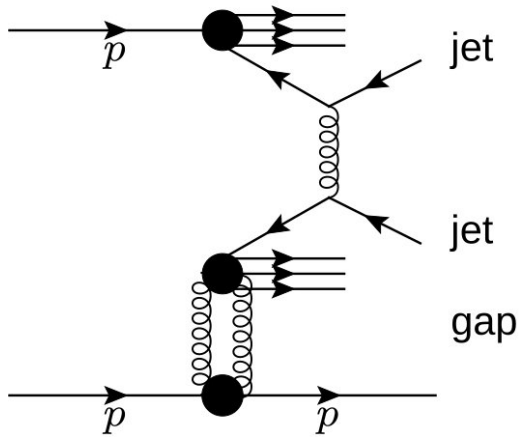

f_{CSE} vs. $\Delta\eta_{jj}$ between 7 and 13 TeV CMS results

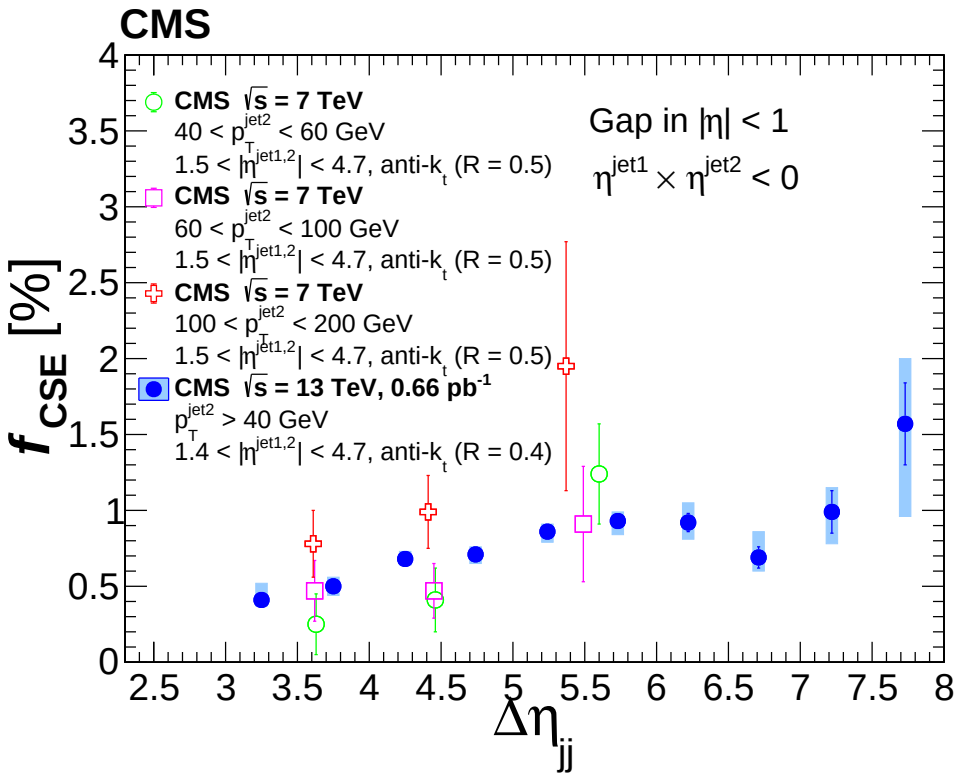

- 7 TeV analysis performed in three bins of $p_{T,\text{jet-2}}$ and three bins of $\Delta\eta_{jj} = 3$–4, 4–5,5–7 (**EPJC**78(2018)242)
- Trend of increasing f_{CSE} with $\Delta\eta_{jj}$ is confirmed with present 13 TeV results with improved precision.
- New results reach previously unexplored values of $\Delta\eta_{jj}$ → Very important to understand hard color singlet exchange.

Food for thought

- **Is it possible that there is something else going on? What other color-singlet exchanges could there be in the SM?**
  $\rightarrow$ t-channel photon, W, or Z boson exchange between quarks also yield the same rapidity gap signature, since they are color singlet.
  ...However, the expected cross sections are too low to explain the observed rates (much smaller than the experimental uncertainties).

- At LO in QCD, the simplest color-singlet exchange is two-gluon exchange. But the rates are too small with this "fixed-order" color-singlet exchange.

- In BFKL, color-singlet exchange cross section is larger in the high energy limit of QCD $\rightarrow$ In principle can explain the global rates, but differential dependence is more difficult to be described.

BFKL color-singlet exchange is the current best candidate to explain the data. Nevertheless, it is extremely challenging to provide a global description of the data.

In pp collisions with intact protons, spectator-parton activity is largely reduced → Central gap more likely to "survive" (Marquet, Royon, Trzebiński, Žlebčík, Phys. Rev. D 87, 034010 (2013)).

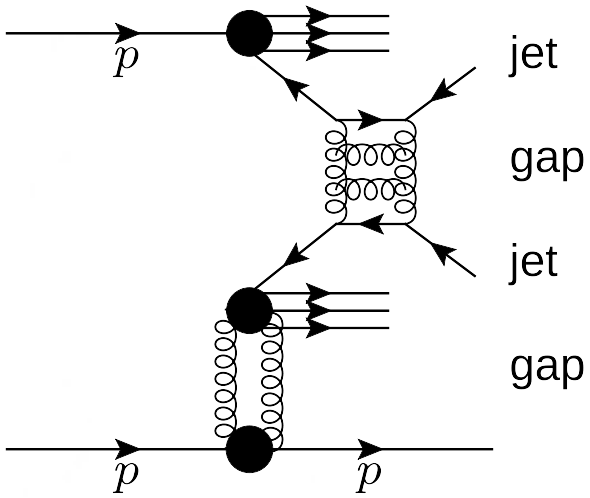

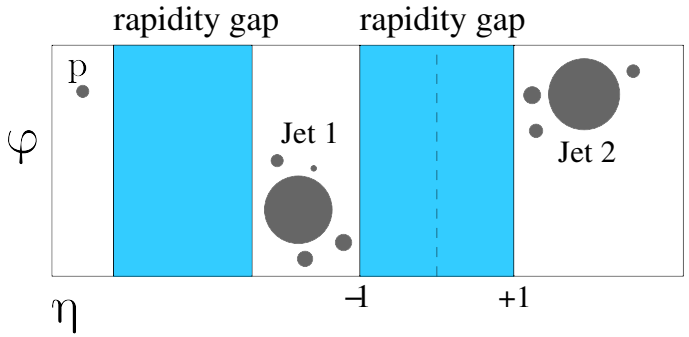

Addressed in study with CMS-TOTEM combined analysis. **First time a proton-gap-jet-gap-jet topology is studied!** Will discuss on second part of this talk.

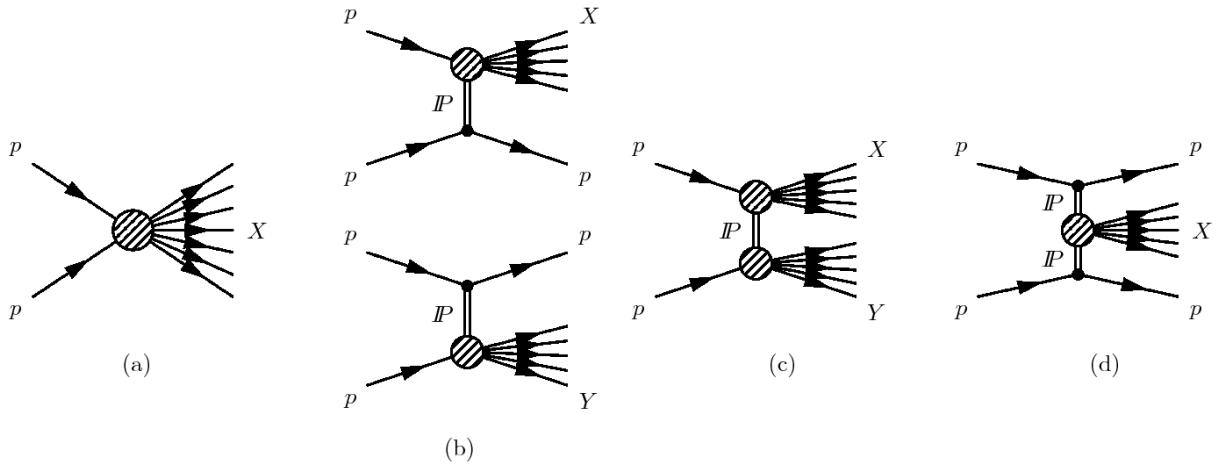

TOTEM shares the same interaction point as CMS (IP5) at the LHC. TOTEM studies a special class of physics, known as diffractive physics:

- Total hadronic cross section measurement, $\sigma_{\mathbf{tot}}$.
- Elastic cross section measurement ($pp \to pp$).
- Single- and central-diffraction $pp \to pX$ and $pp \to pXp$, where X corresponds to many soft particles.

Occassionally, CMS and TOTEM collect data together in dedicated runs to do special physics together (central, harder particles in CMS, and forward, intact protons in TOTEM).

TOTEM Roman pot detectors

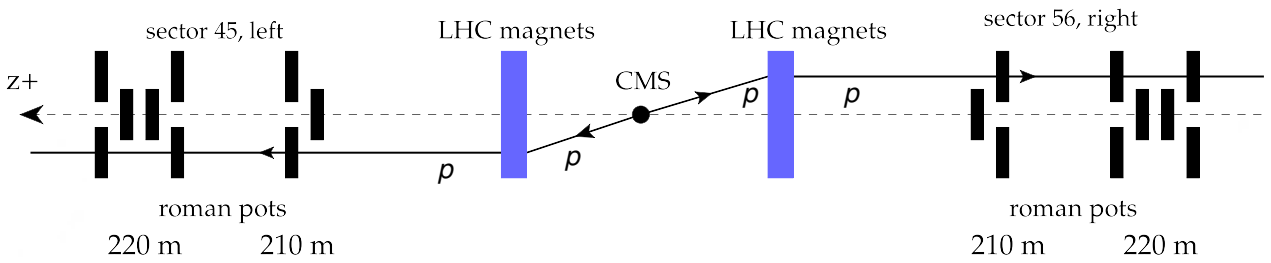

Near-beam (a few mm close to the beam) silicon tracking detectors hosted in vacuum vessels (Roman pots) inserted in the LHC beam pipe. Designed to not disrupt the operation of the LHC.

Accelerator magnetic lattice (magnetic dipoles & quadrupoles), which are designed to manipulate the LHC beam optics, can be also used as an effective proton momentum spectrometer.

Protons that have lost a small fraction of their original beam-momentum will be separated from beam-momentum protons.

Precise knowledge of the magnetic lattice $\rightarrow$ Reconstruction of intact proton kinematics.

Two important kinematic variables:

- Fractional momentum loss of the proton, $\xi = \Delta p/p$.
- Four-momentum transfer square at the proton vertex, $t = (p_f - p_i)^2$.

Projections on a_0^W and a_C^W in all channels at $\sqrt{s} = 14$ TeV with 300 fb^{-1}

W^+W^- decay channel	Hadronic		Semi-leptonic		Leptonic		Combined	
Coupling [10^{-7} GeV^{-2}]	5σ	95% CL	5σ	95% CL	5σ	95% CL	5σ	95% CL
$\lvert a_0^W \rvert$, $a_C^W = 0$ (no form factor)	6.9	3.8	10	4.9	43	24	6.6	3.7
$\lvert a_0^W \rvert$, $a_C^W = 0$ (form factor)	17	9.4	27	13	43	24	16	9.2
$\lvert a_C^W \rvert$, $a_0^W = 0$ (no form factor)	17	9.5	25	12	107	59	16	9
$\lvert a_C^W \rvert$, $a_0^W = 0$ (form factor)	42.0	23	67	33	107	59	41	23

Considering also projections with form factor $a_{0,C}^W \to a_{0,C}^W/(1 + m_{WW}^2/\Lambda_{\text{cutoff}}^2)$, with $\Lambda_{\text{cutoff}} = 2$ TeV.

Projections considering leptonic channel $WW \to \ell^+\nu\ell^-\nu$ for reference.

Large-R jets allow for a better sensitivity to high-mass BSM effects

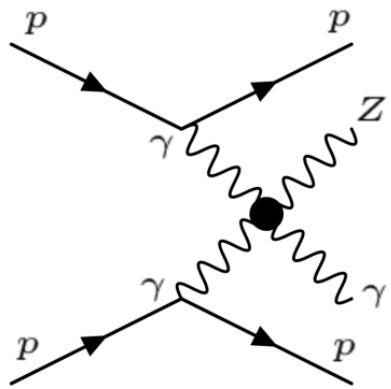

The tree-level $\gamma\gamma\gamma Z$ vertex is absent in the SM. Such an interaction vertex is only induced with virtual box diagrams in the SM.

In high-mass $pp \to p(\gamma\gamma \to \gamma Z)p$, we can search for deviations from the SM expectations ($\sigma^{\mathrm{SM}} \propto \alpha_{\mathrm{em}}^3 \alpha_{\mathrm{ew}} \ll 0.1 fb$).

Assuming that $\sqrt{s_{\gamma Z}} \ll \Lambda_{\text{new physics}}$, we can model the new physics manifestations in an effective field theory formalism,

$$\mathcal{L}_{\gamma\gamma\gamma Z} = \zeta F^{\mu\nu} F_{\mu\nu} F^{\rho\sigma} Z_{\rho\sigma} + \tilde{\zeta} F^{\mu\nu} \tilde{F}_{\mu\nu} F^{\rho\sigma} \tilde{Z}_{\rho\sigma} \tag{4}$$

where $\tilde{F}_{\mu\nu} \equiv \frac{1}{2}\epsilon^{\mu\nu\rho\sigma} F_{\rho\sigma}$ and ζ and $\tilde{\zeta}$ are the anomalous couplings. The quantum numbers and mass of hypotethical new physics particle(s) can be mapped to ζ and $\tilde{\zeta}$ values.

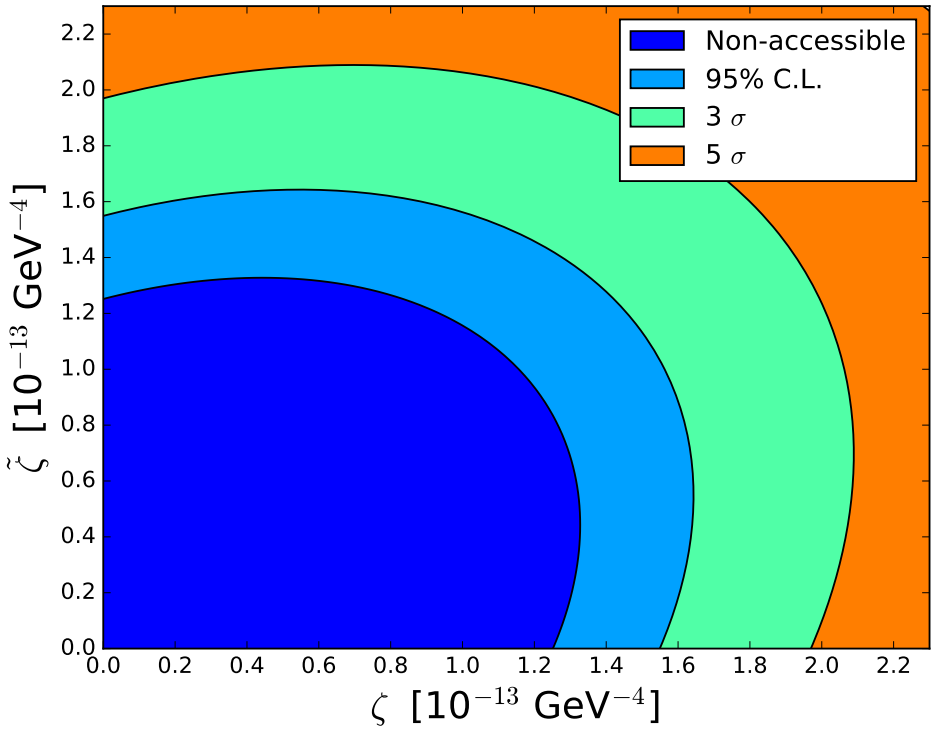

CB, S. Fichet, G. von Gersdorff, C. Royon, JHEP 1706 (2017) 142.

Existing bound at 95%CL set via measurement of $\mathcal{B}(Z \to \gamma\gamma\gamma) < 2.2 \times 10^{-6}$ at 8 TeV by the ATLAS Collaboration Eur. Phys. J. C 76(4), 1-26 (2016). This translates to an upperbound on the $3\gamma Z$ anomalous couplings,

$$\sqrt{\zeta^2 + \tilde{\zeta}^2 - \frac{\tilde{\zeta}\zeta}{2}} < 1.3 \times 10^{-9}\ \text{GeV}^{-4} \text{at 95\% CL} \quad (5)$$

Imagining the measurement is repeated with 300 fb^{-1} of data at $\sqrt{s} = 13$ TeV, the bound on ζ can be improved by about one order of magnitude (ζ, $\tilde{\zeta} < 10^{-10}$ GeV^{-4} at 95% CL).[a]

Our projections based on $pp \to p\gamma Zp$ surpass the existing and expected bounds by about three orders of magnitude.

[a] No updated measurement has been presented yet.

Probing $\gamma\gamma \to WW$ at high-masses

- The $\gamma\gamma \to WW$ process is induced at tree-level in the SM by virtue of γW^+W^- and $\gamma\gamma W^+W^-$ couplings. Can be probed in central exclusive production (E. Chapon, C. Royon, O. Kepka, PRD 81(2010) 074003)
- Typically, searches rely on purely leptonic channel $W^+W^- \to \ell^+\nu\ell^-\nu$.
- Observation at 8.4σ established by the ATLAS experiment at 13 TeV in standard LHC runs (no proton tagging) $\to$ events mostly at low m_{WW}
- **Important to characterize electroweak boson scattering in wide kinematic range, also to enhance sensitivity to BSM effects at high-mass.**

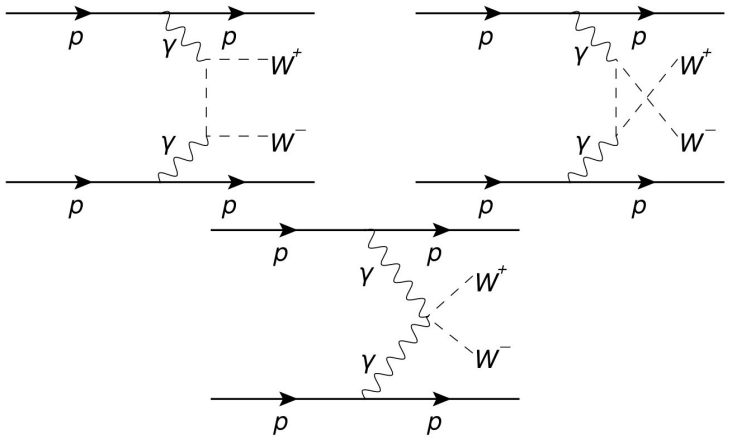

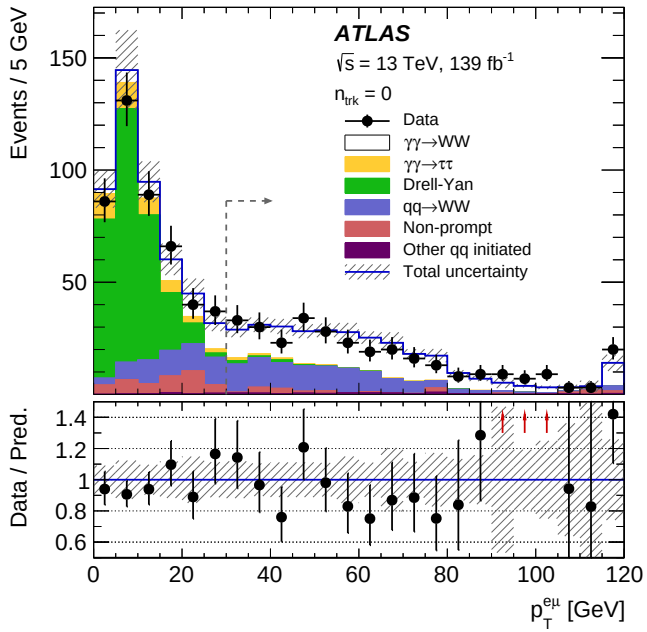

ATLAS, arXiv:2010.04019, PLB 816 (2021) 136190

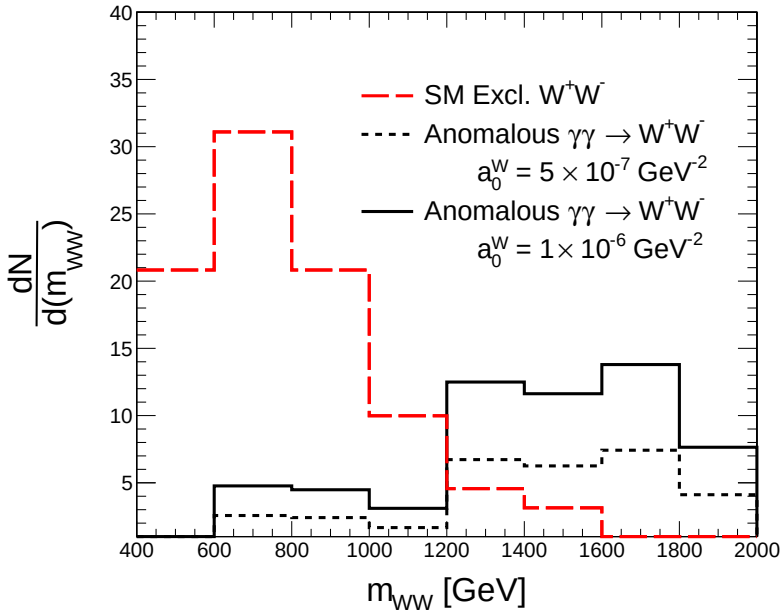

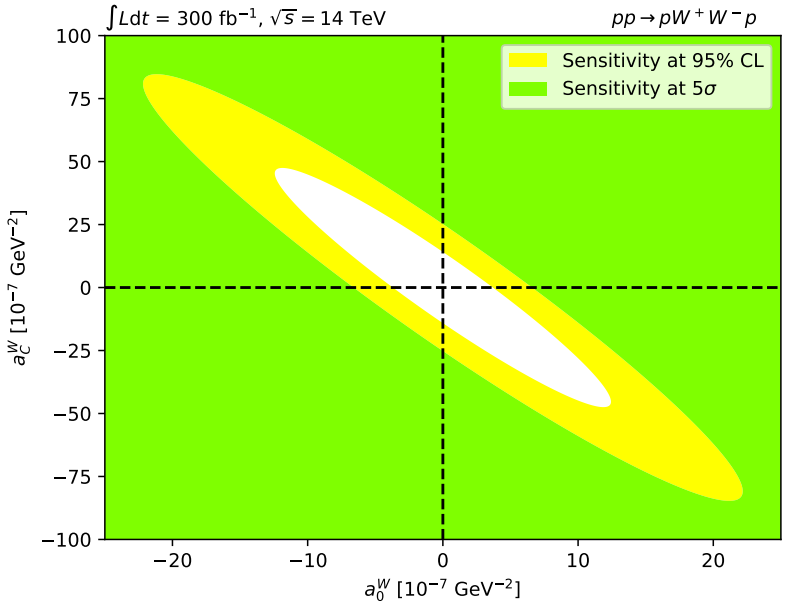

CB, G. Biagi, G. Legras, C. Royon, arXiv:2009.08331, JHEP 12 (2020) 165

Anomalous $\gamma\gamma \to WW$ signal at high-mass m_{WW} and high-p_T^W $\to$ Boosted topologies are favored, more likely to reconstruct W as large-R jets. Projections based on dimension-6 $\gamma\gamma W^+W^-$ effective field theory:

$$\mathcal{L}_6^{\text{eff}} = -\frac{e^2}{8} a_0^W F_{\mu\nu} F^{\mu\nu} W^{+\alpha} W^-_{\alpha} - \frac{e^2}{16} a_C^W F_{\mu\alpha} F^{\mu\beta} \left(W^{+\alpha} W^-_{\beta} + W^{-\alpha} W^+_{\beta} \right) \tag{6}$$

We could probe couplings down to $\{|a_0^W|, |a_C^W|\} = 3.7 \times 10^{-7} (9.2 \times 10^{-7})$ GeV^{-2} at 95% CL with 300 fb^{-1} at $\sqrt{s} = 14$ TeV when combining all decay channels. Existing ATLAS and CMS bounds are of $\{|a_0^W|, |a_C^W|\} = 1 \times 10^{-4} (3.5 \times 10^{-3})$ GeV^{-2}.

F_L is well-fit with NLLx resummation + NNLO DGLAP

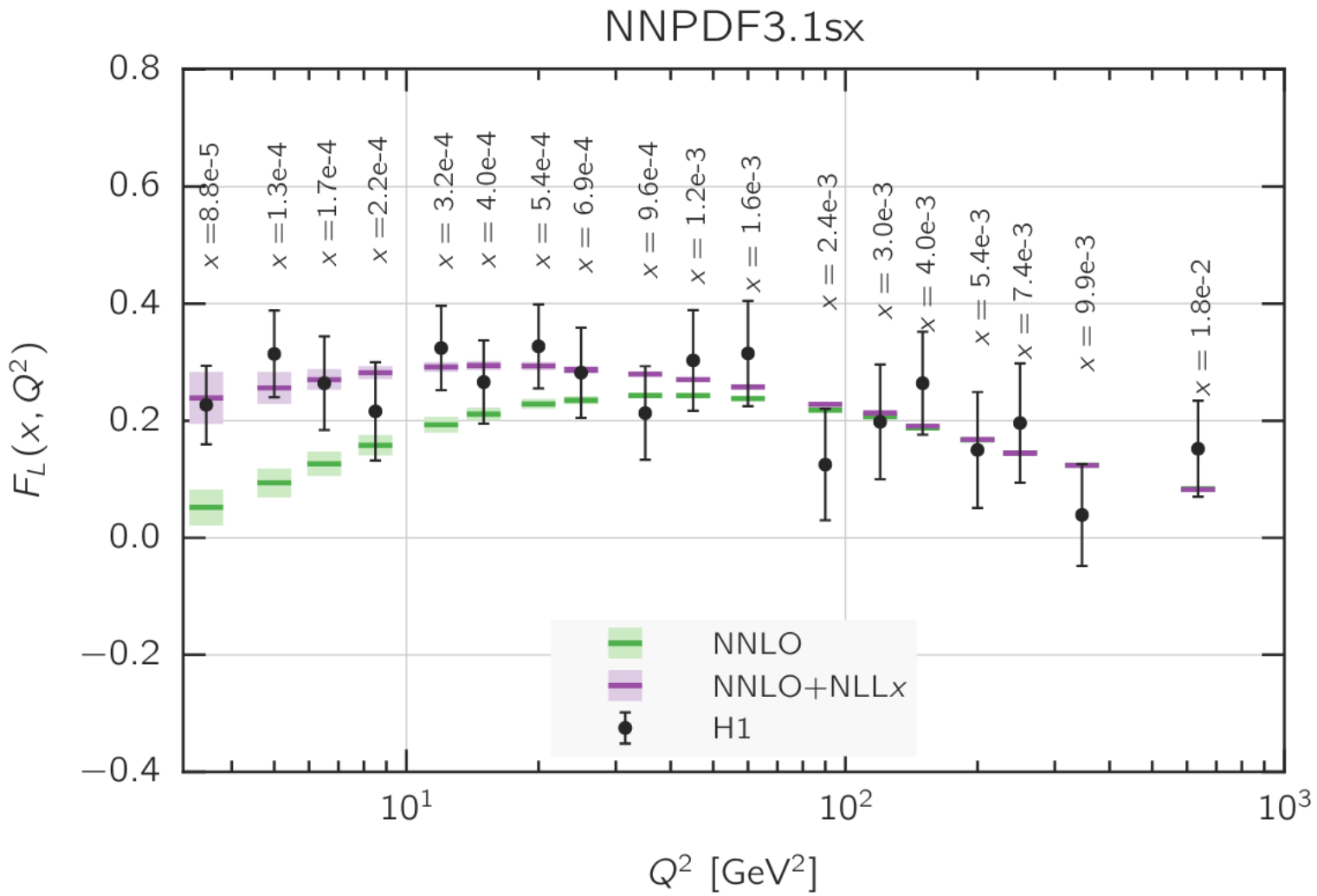

R. D. Ball, V. Bertone, M. Bonvini, S. Marzani, J. Rojo, L. Rottoli, Eur. Phys. J. C (2018) 78:321, arXiv:1710.05935

Most remarkably is the $F_L(x, Q^2)$ function fit at small-x $\rightarrow$ very sensitive to amount of glue in the proton.

Gluon splitting a la BFKL inside the proton

side view

target parton

front view

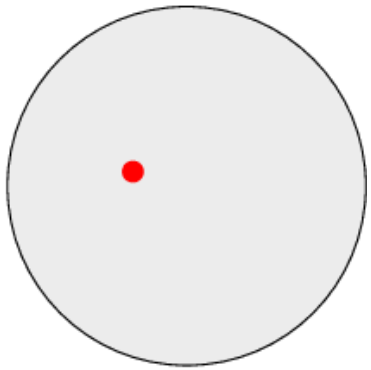

Gluon splitting a la BFKL inside the proton

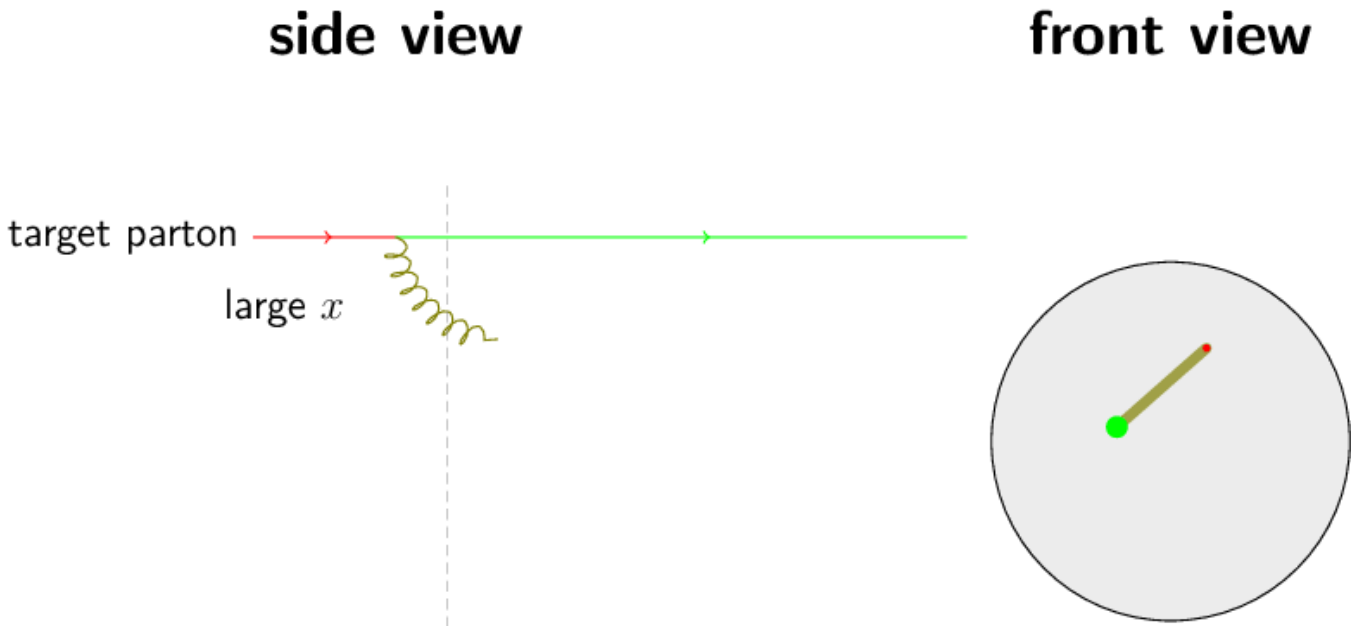

Gluon splitting a la BFKL inside the proton

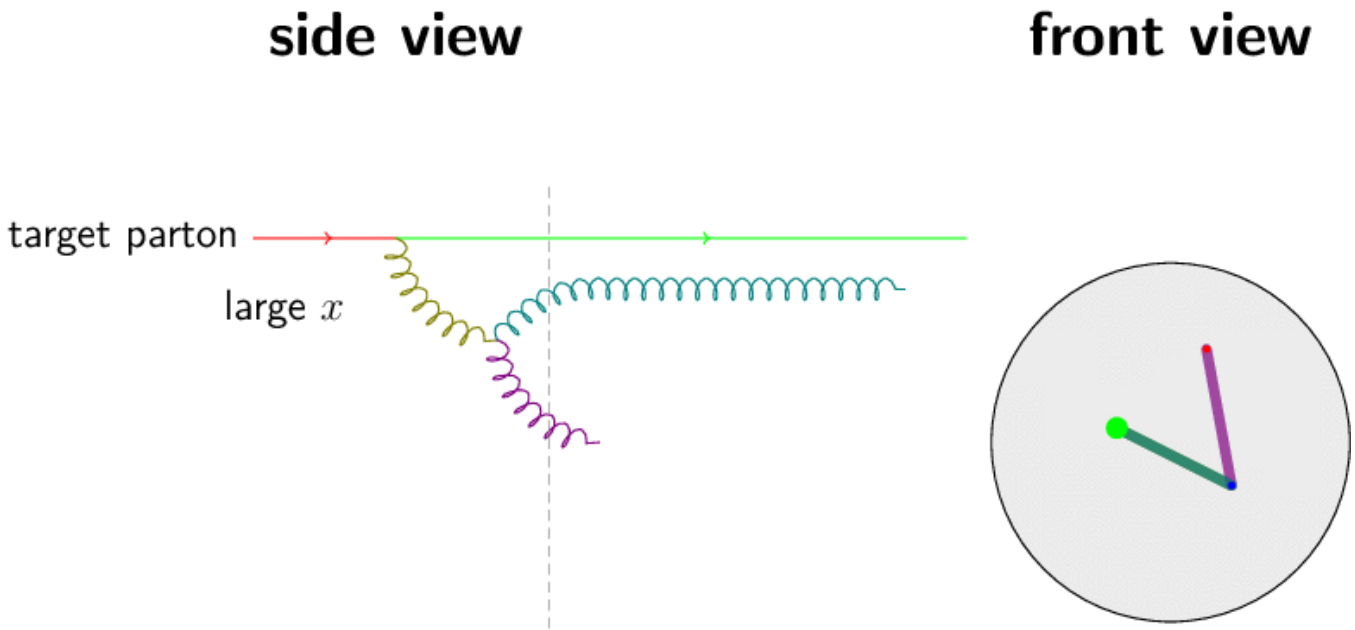

Gluon splitting a la BFKL inside the proton

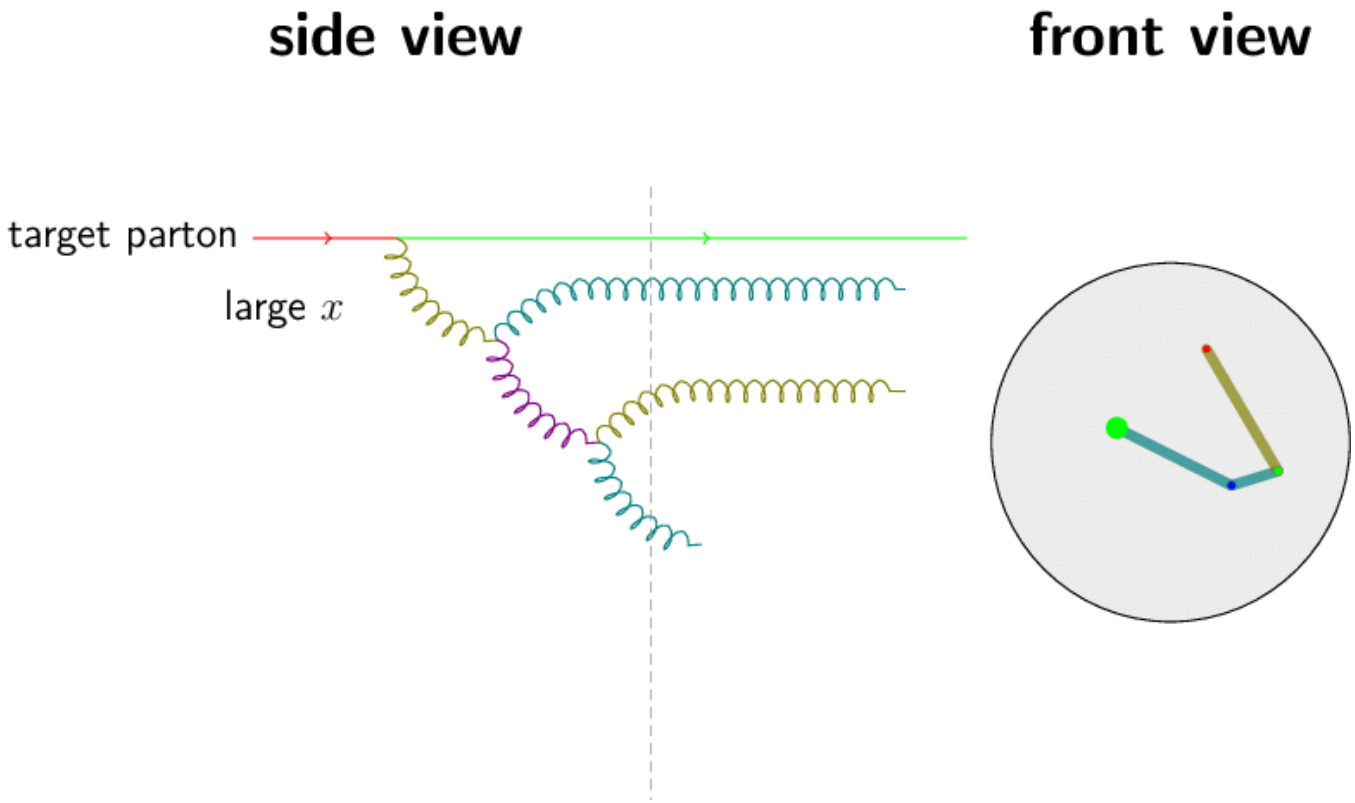

Gluon splitting a la BFKL inside the proton

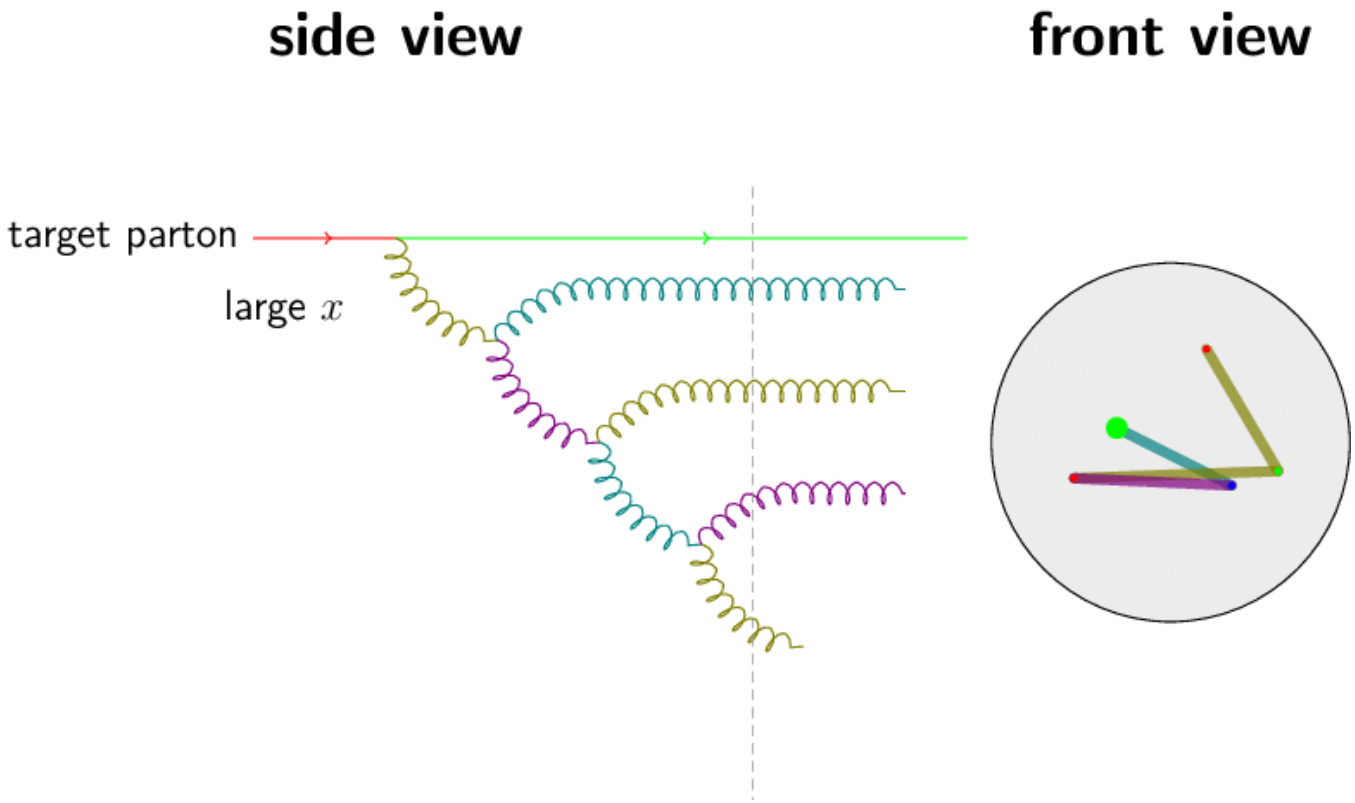

Gluon splitting a la BFKL inside the proton